Innate Immune Responses in Human Oligodendrocytes

by

Leina Bernadette Saito

A thesis submitted in partial fulfillment of the requirements for the degree of

Master of Science
in

Immunology

Department of Medical Microbiology and Immunology
University of Alberta

Abstract

The central nervous system (CNS) is comprised by the brain, spinal cord, and optic nerves, which are vital for normal bodily functions. Microglia and astrocytes are the CNS cells that contribute to homeostasis although excessive immune activation of these cells leads to pathogenic neuroinflammation including inflammasome induction and associated neurodegeneration that are observed in diseases such as multiple sclerosis (MS). Inflammasomes are cytosolic protein complexes that serve as both sensors and effectors of innate immunity through enabling caspase-1 activation with ensuing cytokine release and/or inflammatory programmed cell death, termed pyroptosis. In MS, demyelination and axonal transection occurs in conjunction with glial activation, and infiltrating (and activated) leukocytes. Oligodendrocytes are the myelin-forming cells of the CNS and are injured in MS although their participation in inflammation is uncertain. Nonetheless, oligodendrocytes contain the molecular machinery to respond to proinflammatory stimuli, and because of their central role in MS pathogenesis, it was critical to determine if oligodendrocytes contribute to neuroinflammation. Thus, the capacity of cultured mature and immature human oligodendrocytes to express innate immune molecules and their concurrent vulnerability to injury and cell death were investigated. The ability of *in vivo* oligodendrocytes to respond to inflammation in a toxic model of demyelination in mice was subsequently examined. TNFα exposure induced expression of inflammasome- and Type I interferon (IFN)-associated genes in cultured mature human progenitor-derived oligodendrocytes (PDOs). Type I IFN bioactivity was detected in supernatants, although prototypic inflammasome cytokines IL-1β and IL-18 were not released, from TNFα-exposed or JC virus-infected PDOs. Caspase-1 and

the executioner protein, gasdermin D immunoreactivity were increased in TNFα-exposed mature PDOs. Treatment with the caspase-1 inhibitor, VX-765, suppressed gasdermin D immunoreactivity and prevented pyroptosis in TNFα-exposed PDOs. Demyelination of the corpus callosum with accompanying glial activation and axonal disruption were observed in mice after four and six weeks of cuprizone exposure. Intranasal VX-765 treatment of cuprizone-exposed animals prevented myelin basic protein loss, and both microglial and astrocytic activation in the corpus callosum. While cuprizone-exposed mice displayed gasdermin D immunopositive oligodendrocytes, VX-765 treatment selectively suppressed oligodendrocyte progenitor cell induction in the corpus callosum and prevented axonal injury. Overall, activated human oligodendrocytes displayed innate immune responses in a differentiation-state dependent manner, with evidence of pyroptosis. Caspase-1 and gasdermin D induction was apparent in cuprizone-mediated CNS demyelination. These results demonstrate oligodendrocytes are immunologically active and contribute to CNS innate immunity that could affect cell survival. Intranasal delivery of VX-765 was selectively neuroprotective and highlighted new therapeutic options for inflammatory demyelinating disorders of the CNS such as MS.

Preface

Some of the data described in Chapter 3 of this thesis were made possible by collaborations between the Power Laboratory at the University of Alberta, with Dr. Eugene Major at the National Institutes of Health (NIH)/National Institute of Neurological Disorders and Stroke, and with Dr. Eric Cohen at the Institut de recherches cliniques de Montréal (IRCM). The progenitor-derived oligodendrocytes used in this study were developed by Dr. Maria Chiara Monaco, and I performed the cell culture experiments at the NIH with the assistance of Dr. Monaco. The Type I interferon bioassay was performed by Dr. Meziane at IRCM. All other experiments outlined in Chapter 3 were performed by me at the University of Alberta. The introduction in Chapter 1, the research described in Chapters 4 and 5, and the concluding analysis in Chapter 6 are entirely my work. Additionally, this project received animal research ethics approval from the University of Alberta Health Sciences Animal Care and Use Committee, for the project on Modulation of Demyelination, AUP 00002244.

Some of the results in Chapter 3 of this thesis have been published in McKenzie, B.A., Mamik, M.K., Saito, L.B., Boghozian, R., Monaco, M.C., Major, E.O., Lu, J.Q., Branton, W.G., and Power, C. Caspase-1 inhibition prevents glial inflammasome activation and pyroptosis in models of multiple sclerosis. *Proceedings of the National Academy of Sciences of the United States of America.* 2018 Jun 26; 115(26): E6065–E6074. I was responsible for data collection and analyses, and presentation for experiments involving progenitor-derived oligodendrocytes. Drs. McKenzie and Power were involved with concept development and manuscript composition.

Acknowledgements

I would first like to acknowledge the collaboration between Drs. Power and Major enabled my project. I would like to thank the support and assistance I received from Dr. Monaco with experiments, along with other members of the Major and Jacobson laboratories at NINDS-NIH for making me feel welcome at the NIH and assisting me during my visits.

I am grateful to the Multiple Sclerosis Society of Canada for providing me the necessary financial assistance through the endMS Master's Studentship Award without which I could not have pursued my research.

I would like to thank the members of the Stys lab at the University of Calgary for providing me insights in the cuprizone model of demyelination. I would also like to thank Dr. Cohen and Dr. Meziane for performing the Type I IFN bioassay.

Most importantly, I would like to express my utmost gratitude to Dr. Power, for providing me the opportunity to work in his lab where I have gained invaluable experience. I would also like to thank the current and past Power lab members for supporting me with my project.

And last but not least, I would like to thank my family and friends, especially Ajay, for providing me the emotional support necessary to complete my work.

Table of Contents

List of Tables

List of Figures

Glossary of Terms

ABC	ATP binding cassette
AIM2	absent in melanoma 2
APC	antigen presenting cell
APP	amyloid precursor protein
ASC	apoptosis-associated speck-like protein containing a CARD
ASPA	Aspartoacylase
ATP	adenosine triphosphate
B2M	β2-microglobulin
BBB	blood-brain barrier
BCSFB	blood-CSF barrier
bFGF	basic fibroblast growth factor
BST2	bone narrow stromal cell antigen 2
CASP1	caspase-1
CASP4	caspase-4
CASP6	caspase-6
CASP8	caspase-8
CC	corpus callosum
CCL	C-C motif chemokine ligand
CD	cluster of differentiation
cDNA	complementary deoxyribonucleic acid
CFA	complete Freund’s adjuvant
CNP	2',3'-cyclinc nucleotide 3' phosphodiesterase
CNS	central nervous system
CSF	cerebrospinal fluid
CT	threshold cycle
CV	cresyl violet
CZ	Cuprizone
DAB	3,3'diaminobenzidine

DAMP	damage associated molecular patterns
DDX58	DExD/H-Box Helicase 58
DMT	disease-modifying therapy
EAE	experimental autoimmune encephalomyelitis
EBV	Epstein-Barr virus
ELISA	enzyme-linked immunosorbent assay
FADD	FAS-associated death domain protein
GAPDH	glyceraldehyde 3-phosphate dehydrogenase
GF-	growth factor negative
GF+	growth factor positive
GFAP	glial fibrillary acidic protein
GM-CSF	granulocyte-macrophage colony stimulating factor
GSDMD	gasdermin D
GST-pi	glutathione S-transferase pi
HMGB1	high mobility group protein B1
ICAM-1	intercellular adhesion molecule 1
ICC	Immunocytochemistry
ICW	in-cell Western
IF	Immunofluorescence
IFN	Interferon
IHC	Immunohistochemistry
IL	Interleukin
IRCM	Institut de recherches cliniques de Montréal
IRF1	interferon regulatory factor 1
IRF3	interferon regulatory factor 3
IRF7	interferon regulatory factor 7
ISG	IFN-stimulated gene
JCV	John Cunningham virus
LDH	lactate dehydrogenase
LFB	luxol fast blue
M-CSF	macrophage colony-stimulating factor

MAVS	mitochondrial antiviral-signaling protein
MBP	myelin basic protein
MCT	monocarboxylate transporter
MFI	mean fluorescence intensity
MHC	major histocompatibility complex
MHCV	mouse hepatitis coronavirus
MOI	multiplicity of infection
MOG	myelin oligodendrocyte glycoprotein
mRNA	messenger ribonucleic acid
MS	multiple sclerosis
MYRF	myelin regulatory factor
NAA	*N*-acetyl-l-aspartic acid
NF-κB	nuclear factor kappa-light-chain-enhancer of activated B cells
NG2	neuron/glia antigen 2
NIH	National Institutes of Health
NKX2.2	NK2 Homeobox 2
NLR	NOD-like receptors
NLRP3	NLR Family Pyrin Domain Containing 3
NLRX1	NLR family member X1
NOR	novel object recognition
NT-3	neurotrophin-3
OLIG1	oligodendrocyte transcription factor 1
OLIG2	oligodendrocyte transcription factor 2
OPC	oligodendrocyte progenitor cell
PAMP	pathogen associated molecular patterns
PBS	phosphate-buffered saline
PDGFRα	platelet-derived growth factor receptor alpha
PDL	poly-D-Lysine
PDO	progenitor-derived oligodendrocytes
PLP	proteolipid protein
PML	progressive multifocal leukoencephalopathy

PMS	progressive MS
PPMS	primary progressive MS
PRR	pathogen recognition receptor
qRT-PCR	quantitative real time polymerase chain reaction
RLR	RIG-I-like receptors
RNS	reactive nitrogen species
ROS	reactive oxygen species
RRMS	relapse-remitting MS
SHH	sonic hedgehog
SOCS1	suppressor Of Cytokine Signaling 1
SOX10	SRY-box 10
SPMS	secondary progressive MS
T-Ag	JC virus large T-antigen
T3	Triiodothyronine
TGFβ	transforming growth factor beta
TLR	Toll-like receptor
TMEV	Theiler's murine encephalomyelitis virus
TNFRSF1A	TNF receptor super family member 1A
TNFRSF1B	TNF receptor super family member 1B
TNFα	tumor necrosis factor alpha
TRADD	tumor necrosis factor receptor type 1-associated death domain protein
TRAF2	TNF receptor-associated factor 2
TUNEL	terminal deoxynucleotidyl transferase dUTP nick end labeling
VCAM-1	vascular cell adhesion molecule 1
WB	Western blot

Chapter 1 – Introduction

1.1 Cells of the Central Nervous System (CNS)

The central nervous system (CNS), comprised of the brain, spinal cord, and optic nerves in vertebrates is vital in executing a wide variety of functions necessary for daily life such as movement, knowledge and thought processing, assessing senses, and emotions. These CNS-based tasks are achieved by the integration of activity of neurons and glial cells. Glial cells are a group of non-neuronal cells found in the CNS including microglia, astrocytes, oligodendrocyte progenitor cells (OPCs), ependymal cells, and oligodendrocytes that are necessary for maintaining a healthy CNS environment. Figure 1.1 is a simple illustration of some glial cells and neurons under physiological conditions. In this section, a brief overview of the key CNS cells relevant to my thesis will be discussed.

1.1.1 Neurons

Although not exclusive to the CNS, neurons are most widely recognised cell type found within the CNS. Neurons are the backbone of CNS function within an individual as the key mediator for signal processing and electrical transmission required for bodily functions[1, 2]. These signals are either transmitted along the major neuronal process termed axon as action potentials, or are passed along to nearby neurons in the form of neurotransmitters at points of contact called synapses[1]. In order for efficient signal transmission of the action potential, some axons have an insulating layer along the axon called myelin[3]. Myelin is a lipoprotein layer, synthesised by oligodendrocytes in the CNS, which is wrapped around the axon in multiple layers like a sheath, and enables faster electrical transmission along the axon than in non-myelinated axons. The myelinated and unmyelinated axons can be observed visually in the CNS as white and grey matter, where the former is enriched with myelinated axons, and the latter is mainly enriched with unmyelinated axons and neuronal cell bodies. Although neurons are necessary for CNS function, there are just as many non-neuronal cells, or glial cells that are present within the CNS[4]. These glial cells are just as necessary as neurons to maintain a healthy CNS environment for proper neuronal function, although excessive activation of these cells can exert pathogenic effects causing neuroinflamation[5, 6].

1.1.2 Microglia

Microglia are known as the macrophage-like cells of the brain and represent approximately 10% of total number of CNS cells[7]. These cells are long-lived cells that have capacity for self-renewal[8]. Unlike neurons and other glia that originate from the ectoderm[9], microglia are yolk sac-derived cells. Early in development, yolk sac-derived macrophages traffic into the CNS before blood-brain barrier formation, to complete their final transition into tissue resident cells[10]. Microglia have a role in development by clearing dead neurons that have undergone apoptosis as part of CNS development, and by engaging in synaptic pruning where the microglia eliminate excess neuronal synapses by complement-mediated phagocytosis[11]. Both of these processes are necessary for a healthy CNS development permitting precise signal transmission in the CNS.

Even well after development, microglia continue to have a role in maintaining CNS homeostasis. Microglia release trophic factors necessary to maintain neurons, as well as release growth factors necessary for glial cell differentiation[11]. In addition to releasing trophic factors, microglia are also involved with maintaining neuronal connections in the form of synaptic plasticity, which is required for learning during adult life[8]. As the professional phagocytic cell of the CNS, microglia continue to clear apoptotic cells, and constantly survey the environment. Under this physiological state, microglia display numerous long ramified processes with a small cell body, allowing them to sample the local environment efficiently[11]. Similar to macrophages from other sources, microglia express common cell markers such as major histocompatibility complex (MHC)-II, cluster of differentiation (CD) 68, and Iba-1[11]. The involvement of microglia in innate immune responses will be discussed moving forward.

1.1.3 Astrocytes

Astrocytes are one of the most abundant cell types in the CNS, comprising approximately 20% of the total CNS population[7]. Astrocytes are another cell type that has numerous processes, with the glial fibrillary acidic protein (GFAP) being the most abundant cell marker for astrocytes[12]. Astrocytes are implicated in the maintenance of the blood-brain barrier (BBB) within the CNS[13]. The BBB is not a physiological barrier that separates the CNS from

the rest of the body, but rather a complex system of microvasculature that allows highly controlled movement of certain substances from the blood into the brain, often described as the neurovascular unit[13]. The endothelial cells involved in the BBB have major differences with endothelial cells seen elsewhere in the body. The blood vessels found within the CNS are nonfenestrated, with neighbouring endothelial cells linked with many different tight junction and adherens junction proteins, such as those from the claudin, occludin, and cadherin families[13]. Astrocytes wrap around blood vessels with their end feet processes forming another barrier termed glia limitans[13]. Astrocytes can produce factors such as Sonic Hedgehog (SHH) and retinoic acid that induces tight junction protein expression by endothelial cells, which are necessary for maintaining reduced vascular permeability observed in the BBB[13]. The endothelial cells also express many efflux pumps of the ATP Binding Cassette (ABC) transporter family that actively removes a wide range of substances, such as toxins and xenobiotics that can potentially be harmful if gained entry into the CNS[14]. The multitude of efflux pumps is one reason why drug delivery into the CNS is challenging, as the ABC transporters can also actively remove many drugs[14].

In addition to the close proximity between astrocytes and blood vessels, astrocytes are also in close association with neurons, especially with synapses in order to mediate a crucial role in CNS homeostasis[4]. Astrocytes express many ion channels and transporters to allow potassium ion uptake as well as some neurotransmitter uptake in order to regulate neuronal synaptic activity[15]. The clearing of glutamate, released as a neurotransmitter by neurons, is especially important in order to prevent glutamate-mediated excitotoxicity of neurons under physiological conditions[15].

Astrocytes also support neurons by providing metabolic support to these cells. Due to the regulated transport across the BBB, there is also reduced nutrient transport into the CNS. During times of high neuronal activity, leading to low glucose concentration in the proximity of neurons, astrocytes can provide additional nutrient support to neurons in conjunction with oligodendrocytes[12]. Astrocytes have high glycogen storage that can be broken down during times of need into lactate[12]. Lactate can be transported to neurons along unmyelinated areas through gap junctions as a potential energy source[12].

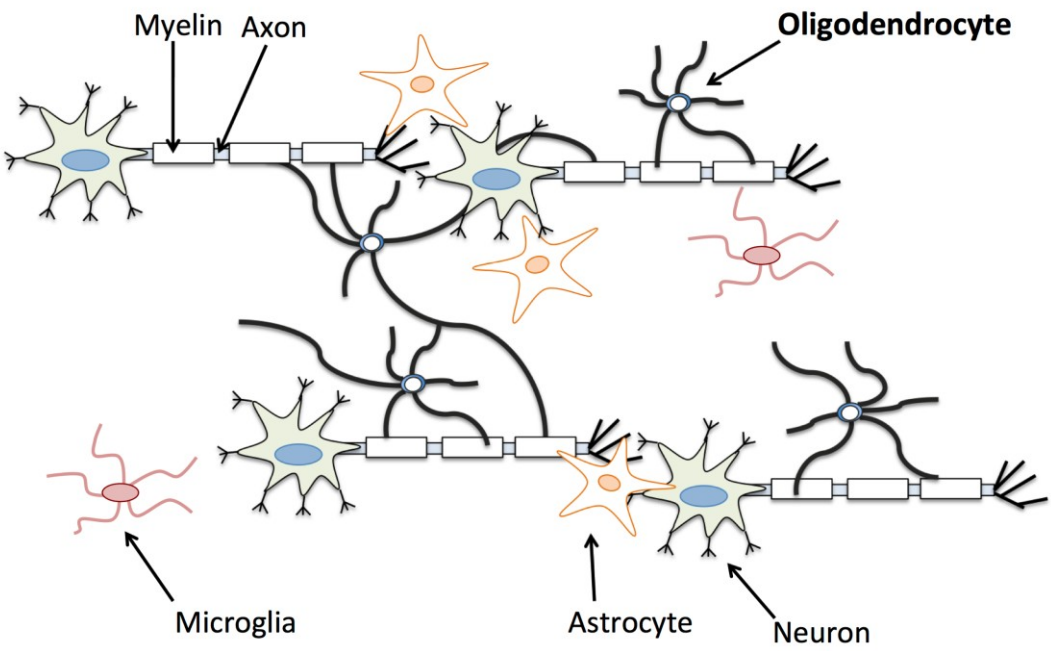

Figure 1.1 Cells of the Central Nervous System (CNS). A schematic of several CNS resident cells relevant to this thesis. Myelin is the lipid rich layer, made by oligodendrocytes, that wraps around neuronal axons. Astrocytes and oligodendrocytes can provide metabolic support to neurons. Microglia are the macrophage-like cells of the CNS vital for debris clearing and maintaining CNS homeostasis.

1.1.4 Oligodendrocyte Progenitor Cells (OPCs)

As suggested by its name, oligodendrocyte progenitor cells (OPCs) are cells that can give rise to oligodendrocytes. OPCs are cells with bipolar morphology that is also known as NG2-glia due to their surface expression of the chondroitin sulphate proteoglycan neuron/glia antigen 2 (NG2), and thus can be used as a cell marker for these cells[16]. The platelet-derived growth factor receptor alpha (PDGFRα) is a receptor that is also highly expressed by OPCs and has importance in oligodendrocyte development. Under physiological conditions, up to 10% of total CNS cells are known to be OPCs[17]. OPCs are highly proliferative cells that are also capable of self-renewal, allowing these cells to exist well into adult life, and differentiate into oligodendrocytes when necessary[18]. Contrary to its name, OPCs are also capable of differentiating into astrocytes during development as demonstrated by fate mapping

experiments performed *in vivo*[19]. However, majority of cells that differentiate from OPCs become into oligodendrocytes in adult life[19].

Although OPCs are largely known as a precursor cell for mature oligodendrocytes, OPCs interestingly share similarities with neurons including their expression of voltage-gated sodium channels, voltage-gated potassium channels, and voltage-gated calcium channels[18]. These voltage-gated channels are only present in the OPC state as expression is lost once OPCs differentiates into oligodendrocytes[18]. The presence of these voltage-gated channels raises the possibility that OPCs are also able to generate action potentials like neurons, however this remains speculative. In addition, there is evidence to suggest OPCs also form synapses with neurons although the main function of these synapses remain largely unknown[18].

1.2 Oligodendrocytes

Oligodendrocytes are the myelin-forming cells in the CNS. As suspected, oligodendrocytes are one of the more abundant glial cells found in the CNS, making up approximately 25% of total CNS cells depending on the brain anatomic site[4]. Oligodendrocytes possess multiple processes, allowing the cells to myelinate multiple axons (up to 50) at once[20]. The myelin generated by oligodendrocytes is absolutely necessary for normal physiological functions. Loss of myelin can lead to pathological outcomes as observed in demyelinating diseases such as multiple sclerosis (MS).

1.2.1 Oligodendrocyte Development

As mentioned previously, oligodendrocytes are derived from OPCs within the CNS. During development or whenever necessary during adult life, once the oligodendrocyte lineage is set, the OPCs are first developed into an immature oligodendrocyte (also known as pre-oligodendrocytes). At this stage, the immature oligodendrocytes cannot myelinate axons but retain some proliferative capacity[21]. The immature oligodendrocyte further develops into mature oligodendrocytes (also known as pre-myelinating oligodendrocyte) that are now able to myelinate axons[22]. As mature oligodendrocytes are terminally differentiated cells, these cells do not proliferate. Although myelination of axons is the end goal of generating mature

oligodendrocytes, if these cells are unable to find naked axons to myelinate these cells eventually undergo apoptosis[23].

The maturation of oligodendrocytes is highly dependent on the environment, as cells of the oligodendrocyte lineage rely on external cues, such as growth factors, to promote the development of oligodendrocyte to the final myelinating state[21, 23]. A wide array of growth factors produced by surrounding microglia and astrocytes has been documented to be involved in oligodendrocyte formation[24]. Growth factors such as PDGF, basic fibroblast growth factor (bFGF), neuregulin, neurotrophin-3 (NT-3), and the thyroid hormone triiodothyronine (T3) has been demonstrated to have importance in promoting the initial development of immature oligodendrocytes from OPCs[21, 24]. PDGF is especially crucial as it can promote OPC proliferation, and it can also stimulate OPC development into immature oligodendrocytes[23]. Due to the mitogenic capabilities of PDGF, immature oligodendrocytes can also proliferate in the presence of PDGF[21]. NT-3 and bFGF is another factor that can induce proliferation, in addition of bFGF being a survival factor for oligodendrocyte lineage cells[21]. T3 has importance in the differentiation process from OPCs to immature oligodendrocytes, as downstream signalling can lead to initiation of myelin protein synthesis and SHH expression[21]. Although growth factors are necessary, the full differentiation into oligodendrocytes requires the removal of highly mitogenic growth factors such as PDGF from the environment[23]. Since mature oligodendrocyte formation is dependent on growth factor availability, oligodendrocytes can be cultured *in vitro* using culture media supplemented with the necessary growth factors[25, 26].

Upon exposure to the necessary growth factors, transcriptional changes can be observed by OPCs to promote oligodendrocyte development and maturation. The SHH protein expression leads to the expression of several transcription factors, such as oligodendrocyte transcription factor 2 (OLIG2), and NK2 Homeobox 2 (NKX2.2), that are dedicated to the differentiation into oligodendrocytes[27]. The co-expression of these two transcription factors can then lead to expression of another lineage specific transcription factors SRY-box 10 (SOX10), which in turn can lead to the expression of another transcription factor, myelin regulatory factor (MYRF)[27]. The production of myelin proteins necessary for differentiation into mature

oligodendrocytes is achieved by the combined activity of these transcription factors[27], with associated morphological changes and downregulation of OPC markers[21].

1.2.2 Oligodendrocyte Function

One of the hallmarks of oligodendrocyte activity is the formation of myelin within the CNS. Myelinated axons are required for efficient physiological function in order to mediate a fast action potential. Comparing two axons with the same diameter, the conduction velocity (the speed in which an action potential travels along an axon) is 100 times faster in myelinated axons compared to unmyelinated counterparts[28]. In addition, having myelin on axons also reduces the area required to maintain a sodium and potassium ion gradient to just at the Nodes of Ranvier, instead of the entire length of axons[28]. This reduces the overall energy and resources required for the axon to readjust back to its resting potential[28].

So, what exactly is myelin? The myelin sheath produced by oligodendrocytes is in essence the plasma membrane of oligodendrocytes that has been tightly wrapped around axons numerous times, and maintained structurally by myelin proteins[3]. Unlike the plasma membrane where the lipid and protein composition is approximately 50% and 40% respectively[29], the myelin membrane is more enriched with lipids, with lipids making up to 70% with a 30% protein content[20, 28], by dry weight. The lipids within the myelin membrane are arranged in a manner that the inner membrane is negatively charged[20]. With regards to protein composition, the myelin basic protein (MBP) and the proteolipid protein (PLP) are the most abundant proteins found within the myelin membrane, making up 30% and 50% of total proteins found within myelin, respectively[20]. Both MBP and PLP are required for cross-linking the myelin membranes in order to compact it[20, 30]. MBP is a cytosolic protein[30], and as suggested by the name, is highly basic[20]. PLP on the other hand is a transmembrane protein[31]. Once sufficient amount of myelin membrane is wrapped around the axon during myelin synthesis, the outer membrane is cross-linked to another outer membrane through PLP interaction, similar to junction proteins[30]. The inner membrane is cross-linked by the attraction of the negatively charged (acidic) inner myelin membrane with the positively charged (basic) MBP[30].

In addition to myelin synthesis, oligodendrocytes also support neurons by transporting metabolites and energy sources. Neurons often rely on external support due to the limited energy stores within neurons, and due to the constant ATP use required for maintaining sodium and potassium ion homeostasis necessary for action potential generation[32]. Oligodendrocytes express monocarboxylate transporter 1 (MCT1), where it can transport metabolites such as lactate down a concentration gradient[32]. As lactate accumulates within oligodendrocytes, as a result of glycolysis, lactate can leave the cell via MCT1, and released into the space between myelin and axon[16, 32]. Lactate can then be transferred into neurons through the MCT2 transporter to be used for subsequent ATP synthesis within neurons[16, 32].

The transport of metabolites between oligodendrocytes and neurons can also be bidirectional. Neurons can produce *N*-acetyl-L-aspartic acid (NAA) as a by-product of the citric acid cycle[33]. The NAA can be transported into oligodendrocytes, possibly through a transporter protein, where it can be cleaved by the aspartoacylase (ASPA)[33]. ASPA is an enzyme that is highly expressed by oligodendrocytes that can cleave the acetate moiety from NAA, which can subsequently be used for fatty acid synthesis[33, 34]. The fatty acids synthesised are then used for generating lipids necessary for myelin synthesis[33, 34].

1.3 Immunity in the CNS

The immune responses observed within the CNS are unique and different from the immune responses observed in other external tissues. For the longest time the CNS has been described as an "immunologically privileged" site based on previous observations regarding absence of graft rejection responses within the CNS[35]. However, describing the brain as immunologically privileged can be misleading. Under physiological conditions, immune surveillance of the CNS by infiltrating leukocytes, such as T-cells, is indeed limited compared to the rest of the body, but it is not absent[35]. In addition, CNS resident cells are by no means immunologically silent. It has been demonstrated that glial cells are fully capable in generating a plethora of innate immune responses by cytokine/chemokine release, release of reactive oxygen species (ROS), inflammasome activation, and phagocytosis and subsequent antigen presentation in response to CNS pathogens[36]. It is because of their ability to generate innate immune responses that glial cells are implicated in disease mechanisms

underlying neuroinflammatory diseases such as MS[37]. The immune responses observed under physiological conditions within the CNS will be briefly discussed, focusing on the innate immune responses.

1.3.1 CNS Barriers – The First Line of Defence

Although immune responses can be mounted within the CNS, there is benefit in restricting immune cell access into the CNS. The CNS is vital yet fragile, stemming from the limited regenerative capacity observed by neurons. Neuronal injury can be detrimental as it can severely impact normal bodily functions, as in the case of neurodegenerative conditions such as Alzheimer's disease and Parkinson's disease[37, 38]. One way to prevent potential neuronal injury is by limiting what can enter the CNS including immune cells and pathogens alike. Pathogens can potentially invade the CNS through the choroid plexus[2, 39], by traversing the coverings of the CNS (meninges)[2, 39], and by breaching the BBB[2, 39]; all three of these points of entry have barriers that can reduce the efficacy of infection or injury within the CNS proper[35].

1.3.1.1 Choroid Plexus

The choroid plexus is a group of cells and capillary network found within the brain ventricles, a connected series of hollow areas found within the brain[35, 40]. The epithelium cells in the choroid plexus are responsible in generating most of the cerebrospinal fluid (CSF) that circulates within the CNS. Unlike the BBB, the capillaries found within the choroid plexus are fenestrated, and have limited barrier function[35]. Instead, barriers are created by the CSF-producing epithelial cells forming a blood-CSF barrier (BCSFB)[35]. These epithelial cells are linked to one another by claudin-enriched tight junction complexes, and can limit paracellular pathogen entry into the brain parenchyma via the CSF[2]. Furthermore, tissue-resident antigen presenting cells (APCs), largely bone marrow-derived macrophages, are also found within the choroid plexus, which can also aid in the immunosurveillance[35].

The choroid plexus is also highly immunomodulatory, and able to restrict unnecessary immune activation. The choroid plexus epithelial cells express intercellular adhesion molecule 1 (ICAM-1) and vascular cell adhesion molecule 1 (VCAM-1), both of which are

required for immune cell extravasation[35]. However, both of these adhesion molecules are solely expressed on the apical surface of the epithelial cells[35]. As the apical surface of the epithelial cells face outwards towards the CSF-filled ventricles, immune cells can only interact with the basolateral surface of the epithelial cells. This can limit the capacity of immune cells to exit the choroid plexus under physiological conditions[35]. Furthermore, the epithelial cells of the choroid plexus can skew the local macrophage populations to adopt an anti-inflammatory phenotype by releasing interleukin (IL) 4, IL-13, and macrophage colony-stimulating factor (M-CSF)[41]. The anti-inflammatory environment is further supported by the transforming growth factor β (TGFβ) released by the endothelial cells of the choroid plexus[41].

1.3.1.2 Meninges

The meninges is a highly vascularised three-layered membranous covering that encases the brain and spinal cord on the outer surface[42]. Starting with the outermost layer, the meninges are comprised of the dura mater, the arachnoid mater, and the pia mater[42]. Right below the pia mater lies the edge of the CNS termed glia limitans, similar to the BBB[42]. Each layer of the meninges constitutes a unique barrier that contributes to the overall protection of the CNS[35]. The dura mater of the meninges is not recognised as an immune privileged site, stemming from the fact that its blood vessels are fenestrated, and are accompanied by a wide range of resident immune cells such as mast cells, dendritic cells, and lymphocytes[35, 42]. The arachnoid mater forms an impermeable barrier similar to a BBB, aligned with cells expressing efflux pumps and tight junctions[42]. The space between the arachnoid mater and the pia mater is termed subarachnoid space[42]. The subarachnoid space is a CSF filled space, with nonfenestrated blood vessels[42]. A limited diversity of immune cells, compared to the dura mater, can also be found[42]. Finally, the single-layered pia mater and the glia limitans form the last barrier before the CNS, and both are permeable to solutes and small molecules[42]. Pathogen entry into the CNS through the multi-layered meninges can be challenging, as it requires traversing an impermeable membrane as well as evading an arsenal of immune cells. In addition to limiting pathogen entry to the CNS, T-cell entry is also limited at the meninges[42]. Under physiological conditions, activated CD4+ and CD8+ T-cells can readily traffic into the subarachnoid space or into the subpial space (space between the pia mater and glia limitans) mediated by P-selectin adhesion molecules that are consecutively expressed by

meningeal blood vessels[43]. Nonetheless, the activated T-cells are unable to cross the glia limitans without re-activation by local APCs expressing their corresponding cognate antigen[35]. Without this re-activation, the T-cells cannot enter the CNS, and may undergo apoptosis or leave the meninges entirely[35].

1.3.1.3 Blood-Brain Barrier

As mentioned previously, movement across the BBB is restricted by the expression of a wide range of junction proteins and efflux pumps[44]. The tight junction proteins that link brain endothelial cells prevent paracellular transport of materials, thus pathogen entry through this mechanism can be restricted[14]. Immune cell trafficking through the BBB is also limited, primarily because of the low levels of selectin molecules that are constitutively expressed by the BBB endothelial cells[41]. Similar to the meningeal barriers, under homeostatic conditions activated T-cells are capable in leaving the CNS blood vessels, but will not be able to cross the glia limitans unless it is re-stimulated by perivascular APCs expressing their cognate antigen[35]. Without this re-stimulation, the T-cells may undergo eventual apoptosis within the space between the endothelial cells and glia limitans (termed perivascular space), or it may leave the CNS altogether[35]. In addition to restricting activated T-cells from gaining entry into the CNS, the pericytes, another type of cells that support endothelial function, found in the BBB also produce TGFβ, which may promote the generation of regulatory T-cells (T_{Regs})[40]. Overall, this is another mechanism to restrict immune cell access to prevent any unwanted access of immune cells.

1.3.2 Players in CNS Immune Responses

Although CNS barriers can prevent potential pathogens from gaining access into the CNS, these are by no means a complete barrier, as evidenced by the many neurotropic viruses that are fully capable infecting immunocompetent individuals[2, 39]. As there are limited immune cells that reside within the CNS, the first group of cells that mount an immune response are the glial cells[37]. The type of responses observed by glial cells will now be discussed.

1.3.2.1 Microglia

As the chief macrophage-like cell found within the CNS, microglia have a pivotal role in mediating innate immune responses within the CNS. Under physiological conditions, the local environment is continuously sampled by microglia to assess any presence of pathogens or cellular damage by detecting pathogen-associated molecular patterns (PAMPs) and or damage-associated molecular patterns (DAMPs)[36]. The detection of PAMPs and DAMPs are mediated by signalling through pathogen recognition receptors (PRRs), such as toll-like receptors (TLRs), RIG-I-like receptors (RLRs), and NOD-like receptors (NLRs) that are expressed by microglia[36]. Depending on the type of PRRs that have been engaged, downstream signalling can mediate the innate immune activation within the microglia. Immunologically activated microglia can secrete chemokines such as C-C motif chemokine ligand (CCL) 2 (CCL2/MCP-1), CCL3 (MIP-1α), and CCL5 (RANTES) to promote recruitment of traditional immune cells into the CNS[36, 37]. Microglia can also release a wide range of cytokines, such as IL-1β, IL-6, 1L-12, IL-23, IL-33, tumour necrosis factor α (TNFα), interferon β (IFNβ), and TGFβ[36, 37]. Microglia can also induce expression of MHC-I, MHC-II and co-stimulatory molecules necessary for T-cell activation, such as CD40, CD80, and CD86[37]. Depending on the cytokine profile of the CNS, the infiltrated CD4+ T-cells can become a T_H1 cell that can then produce IFNγ[37]. This situation can further skew the microglia (as well as infiltrating monocytes) population into an inflammatory phenotype, leading to the production and release of ROS[36, 37] and reactive nitrogen species (RNS)[39], that can be beneficial for clearing extracellular pathogens. Although microglia can mediate inflammation in the brain in response to CNS injury, it can also mediate tissue repair by phagocytosis of debris, and by production and release of cytokines, such as IL-4 and IL-10 that can promote tissue repair[36].

1.3.2.2 Astrocytes

Astrocytes are also known to express some PRRs such as TLR2, TLR3, TLR4, TLR9, RIG-I, and NLRP2 that is involved with the NLRP2 inflammasome[45]. Similar to microglia, downstream signalling of PRRs can lead to production of variety of cytokines and chemokines by astrocytes such as IL-1β[36, 45], IL-6[39], IL-8[39], IL-10[39], IFNα[39], IFNβ[39], TNFα[39], TGFβ[36], CCL2[39], and CCL5[39]. Astrocytes can express and release several complement

proteins such as C3 and C5A[46]. The anti-viral response mediated by type I IFNs is particularly important in astrocytes via the IFNα/β receptor (IFNAR)[39]. IFNAR signalling in astrocytes can lead to the tightening of the BBB by astrocyte-endothelial cross talk, and this in turn can reduce some viral entry into the brain parenchyma[39]. Astrocytes can also rapidly proliferate at the site of injury or infection, forming a glial scar in order to block off the section of the brain with the pathogen to prevent the infection from spreading[2]. The formation of glial scars is pivotal to preventing widespread disease because it can focus the inflammation to a specific region within the CNS and reduces the amount of infiltrating leukocytes, thus leading to less BBB breakdown and less bystander killing mediated by trafficking immune cells[2, 47].

1.3.2.3 Neurons

Neuronal death can lead to irrecoverable damage and disability, but these cells also do not appear to be immunologically silent. Although limited, PRR expression has been documented in neurons[36]. In addition to expressing PRRs, neurons also appear to be involved with antiviral responses. Depending on the brain anatomic site, mice neurons express a baseline level of IFNβ[2], and thus have baseline expression of some IFN-stimulated gene (ISG) proteins[39], thus can limit replication of some viruses. Neurons can also recruit other immune cells by releasing several chemokines such as CCL2, and CCL5[2]. Additionally, neurons are also reported to undergo inflammasome activation involving in the NLRP1, and absent in melanoma 2 (AIM2) inflammasome activation[45]. However, inflammasome activation within neurons is associated more with severe neuronal damage and CNS injury[45].

1.3.2.4 Oligodendrocytes

Oligodendrocyte is another CNS cell type that has been assumed to be immunologically silent. This assumption stems from the fact that oligodendrocytes are the myelin-forming cells of the CNS, and are crucial in maintaining neuronal health, thus any immunological activity by oligodendrocytes might have pathological outcomes. Nonetheless, there is increasing evidence that suggests oligodendrocytes might also be involved in local inflammation. Oligodendrocytes have been demonstrated to express TLR2[48], TLR3[48] and TLR4[49], where TLR2 signalling has been implicated in protection in murine stroke models[50],

TLR3 signalling has been associated with rat oligodendrocyte death[48], and TLR4 has been associated with demyelination in rats[49]. Studies in mice have revealed very modest production of Type I IFNs by oligodendrocytes in response to infection with a neurotropic hepatitis virus, but also demonstrate the ability of oligodendrocytes to generate ISGs in response to external sources of Type I IFNs[51]. There is also evidence of NLRP3 inflammasome-associated protein expression in mouse oligodendrocytes[52], and rodent oligodendrocytes have been reported to express IL-1 receptors[53]. Oligodendrocytes have also been reported to produce multiple cytokines and chemokines[54]. Additionally, recent findings have demonstrated murine oligodendrocytes to express MHC-I and MHC-II[55]. Although there is increasing evidence to suggest oligodendrocytes have the machinery necessary to mount an immune response, more work is necessary to fully elucidate the complete role of oligodendrocytes with respect to inflammation and immunity, and the potential consequences it may have.

1.3.2.5 Trafficking Leukocytes

Leukocyte trafficking, specifically T-cell trafficking into the CNS, under physiological conditions are limited due to the existence of CNS barriers but are not completely absent under physiological conditions[35]. The importance of baseline T-cell trafficking into the CNS can be highlighted from the increased frequency of opportunistic infections such as progressive multifocal leukoencephalopathy (PML) in severely immunosuppressed individuals[56]. PML is a potentially lethal infection of the brain caused by John Cunningham (JC) virus. JC virus is a ubiquitous neurotropic virus that predominantly infects oligodendrocytes, with more than half of the general human population being latently infected[56]. The reactivation of JC virus and subsequent PML development is suggested to be due to the reduced T-cell trafficking into the CNS[56], as evidenced by the increased risk of developing PML in MS patients who are treated with natalizumab[57]. Natalizumab is a monoclonal antibody that inhibits α4β7 integrins that are necessary for T-cell adhesion to endothelial cells for local tissue extravasation[56]. As natalizumab reduces T-cell trafficking into the CNS, these patients have an increased risk in developing PML[57] Although T-cell trafficking into the CNS appears to be necessary to keep latent viruses in check, the route T-cells take to accomplish this task has not been elucidated yet[35].

1.4 Multiple Sclerosis (MS)

MS is a chronic demyelinating disease of the CNS, characterised by the presence of pathologic neuroinflammation and neurodegeneration. Canada has one of the highest incidences of MS across the globe, with approximately 100,000 individuals currently living with MS[58]. The diagnosis of MS is often made after manifestation of the first clinical symptoms, with accompanying magnetic resonance imaging (MRI) confirming the diagnosis based on the presence of lesions in the brain or spinal cord[5]. The usual age of onset for MS ranges between 20-40 years, corresponding to what would normally be an individual's most productive years of their life[5]. Because of this, MS can be highly debilitating for patients as it can influence every aspect of daily life. Progress made in understanding MS development, leading to the discoveries of several disease-modifying therapies (DMTs)[59]. Currently there are 14 DMTs available for use for MS patients in Canada[60]. There have been increasing understanding of potential risk factors with MS development[61, 62]. Yet, despite all the progress made, the cause for MS remains unknown, along with the lack of definitive cure[62]. The current understanding of different forms of MS, symptoms, and disease pathogenesis will be briefly discussed.

1.4.1 Different Forms of MS

MS can be grouped in two major groups, relapse-remitting MS (RRMS) and progressive MS (PMS). The disease manifestation can be different between RRMS and PMS, ranging from disease pathology, affected demographic, as well as treatment options.

1.4.1.1 Relapse-Remitting MS (RRMS)

RRMS is the most common form of MS that is observed, covering approximately 85% of the total MS patient population[63]. RRMS as the name suggests is characterised by the presence of relapses (an acute attack involving neurologic symptoms) followed by remission (complete or partial recovery of symptoms). There is often no immediately obvious progression of disease between relapses once remission is reached[64]. However, since full recovery is not achieved after every remission, disability can accumulate leading to worsening of function over long periods of time[65]. The time between relapses is not predictable[5]. Patients often experience approximately 1 relapse a year, although the

frequency of relapse appears to go down with age and increasing disability[5]. RRMS disease development has an autoimmune component involving autoreactive "encephalitogenic" T-cells[62]. A female bias observed in autoimmune diseases[66] is also observed in RRMS, with females being 2-3 times more likely to develop RRMS than males[62, 65]. Female patients also have more frequent relapses, with greater inflammatory activity associated than male patients[67]. Because there is a strong adaptive immune component to RRMS, there are several immunomodulatory therapeutic agents available for RRMS[59]. All of the DMTs available in Canada are approved for RRMS patients[60]. Although DMTs have been beneficial in reducing the frequency of relapses in patients, it is still not a cure for the disease, and unfortunately the vast majority of patients will go on to develop secondary progressive MS[5, 59].

1.4.1.2 Progressive MS (PMS)

Unlike RRMS, the disease course of PMS does not involve relapses and remission. Instead there is a slow progression of disease with increase in disability overtime, without any major improvements[65]. Approximately 10-15% of patients develop progressive disease without any prior relapse-remitting disease, classified as primary PMS (PPMS)[65]. Up to 80% of RRMS patients can also develop progressive disease, although the time it takes to transition into progressive disease can vary greatly, classified as secondary PMS (SPMS)[68]. Unlike RRMS, PPMS appears to affect males and females equally, but there is evidence to suggest male patients to have more aggressive disease progression than female patients[67, 69]. In addition, PPMS has a reduced adaptive immune component for disease manifestation[5], thus most DMTs available for RRMS patients are not effective[59]. Currently ocrelizumab, an anti-CD20 monoclonal antibody, is the only approved DMT available for PPMS patients in Canada[60]. There are currently no DMTs approved for SPMS patients[60].

1.4.2 Common MS Symptoms

The "sclerosis" in MS is a Greek word meaning scars. The disease name for MS comes from the presence of multiple lesions, or scars observed along the CNS of affected individuals[5]. There are many symptoms that are attributed with MS, but heterogeneity in patient population is observed as the symptoms experienced from one individual can vary greatly from another[70]. Patients can experience any one of physical, psychological, and cognitive

symptoms associated with MS[71]. Common physical symptoms include reduced mobility, weakness, ataxia (reduced coordination of muscle movements), spasticity (muscle stiffness), and bladder and bowel dysfunction[70, 72]. Patients also often experience fatigue, chronic pain, and vision impairments[70]. Additionally, patients can also develop cognitive impairments such as language deficits, memory decline, reduced attention span, and behaviour changes[73]. Major depressive disorder can also develop in some patients because of MS disease, although it can also develop as a comorbidity of MS[74]. DMTs are beneficial in reducing relapse rate in RRMS patients, but it does not appear to be beneficial in symptom management[59]. MS truly is a debilitating disease for the patient and for their families and caregivers as all of these symptoms can be taxing for everyone.

1.4.3 Major Cellular Players of MS Pathogenesis

Although the cause of MS is still unknown, there is increasing understanding of the cells involved with the tissue damages observed. The demyelination and neurodegeneration observed in MS are due to orchestrated events involving CNS resident glial cells as well as infiltrating immune cells[5, 68]. The disease pathology differs between early stages of MS compared to later stages of MS, which may reflect why immunomodulatory therapies are only beneficial in RRMS patients[5, 68]. A simplified illustration of the cells involved in MS pathogenesis can be found on Fig. 1.2.

1.4.3.1 Early MS Disease Development (RRMS)

Infiltration of activated leukocytes, especially activated T-cells into the CNS is one of the key observations made during relapses or early MS disease[5]. The initial triggering event that leads to the activation of CNS-reactive T-cells remains elusive[68]. It is unclear whether the MS disease reaction starts within the CNS or within secondary lymphoid organs[68]. There is a correlation between Epstein-Barr virus (EBV) infection and MS development[61], suggesting MS pathogenesis may be due to a molecular mimicry response after EBV infection[5, 68]. Furthermore, the specific antigen recognised by autoreactive T-cells in MS also remains unclear due to the lack of a dominant T-cell antigen[68]. Myelin proteins has been thought to be the primary target of autoreactive T-cells, although myelin responsive T-cells and B-cells have also been detected from healthy individuals[68]. Whatever the cause may be, activated T-

cells are being trafficked into the CNS where they are reactivated by local APCs, such as microglia[5, 68]. The T-cell-APC interaction can further activate local APCs leading to the secretion of multiple cytokines including IL-1β that can promote BBB breakdown, allowing more immune cells to traffic into the CNS[5]. BBB breakdown is also mediated by the production of matrix metalloproteinases by astrocyte[75], microglia[76], and T-cells[77].

T_H1 and T_H17 cells are the most common helper T-cells observed in MS[68]. Both helper T-cells are capable in contributing in generating a pro-inflammatory environment by secreting pro-inflammatory cytokines such as IL-12, TNFα, IFNγ by T_H1 cells and IL-17A by T_H17 cells[59]. An influx of CD8+ T-cells into the CNS is also observed in MS, that may target oligodendrocytes and neurons directly[59]. B-cells can also contribute to MS by presenting antigen to T-cells and promoting T_H1 and T_H17 differentiation of CD4+ cells[5]. Autoantibodies are also frequently detected in CSF from MS patients, although it is suggested that these autoantibodies may not directly contribute towards MS relapses[5]. A reduction of T_{Reg} function are also observed in MS patients that may contribute to the aberrant influx and activation of autoreactive T-cells into the CNS[5, 68]. Infiltrating macrophages, microglia, and astrocyte can contribute in disease pathogenesis by secretion of a variety of proinflammatory cytokines that can contribute to oligodendrocyte injury, as well as secretion of chemokines required for recruitment of cells involved in inflammation[5, 68]. Overall, the contribution from all of these cells can lead to the inflammation and ultimately demyelination observed in early MS disease.

1.4.3.2 Late MS Disease Development (PMS)

Unlike early MS disease, the inflammation observed in late MS disease, or in PMS, is mediated largely by glial cells and not by the adaptive immune system[68]. Immune cell trafficking into the CNS is reduced, however formation of tertiary lymphoid structure along the meninges has been observed in SPMS patients[68]. These tertiary lymphoid structures are generated from the clustering of T-cells, B-cells, and dendritic cells[68]. Although there is reduced adaptive immune cell trafficking into the CNS, cells from the tertiary lymphoid structures can contribute to the chronic inflammation by promoting astrocyte dysfunction and glia limitans disruption[68]. Astrocytes can influence demyelination by limiting differentiation

of OPCs necessary for remyelination[5]. Glial scar formation by astrocytes can also contribute to the lack of remyelination observed[69]. Astrocytes can release CCL2 and granulocyte-macrophage colony stimulating factor (GM-CSF), which recruit microglia to the site of injury[69]. Microglia can perpetuate chronic inflammation by the release ROS and RNS[69]. Additionally, activated microglia can stimulate astrocyte activation, which can continue to support further microglial activation[68]. The constant inflammation leads to demyelination, which ultimately leads to axonal loss that contributes to neurodegeneration[69].

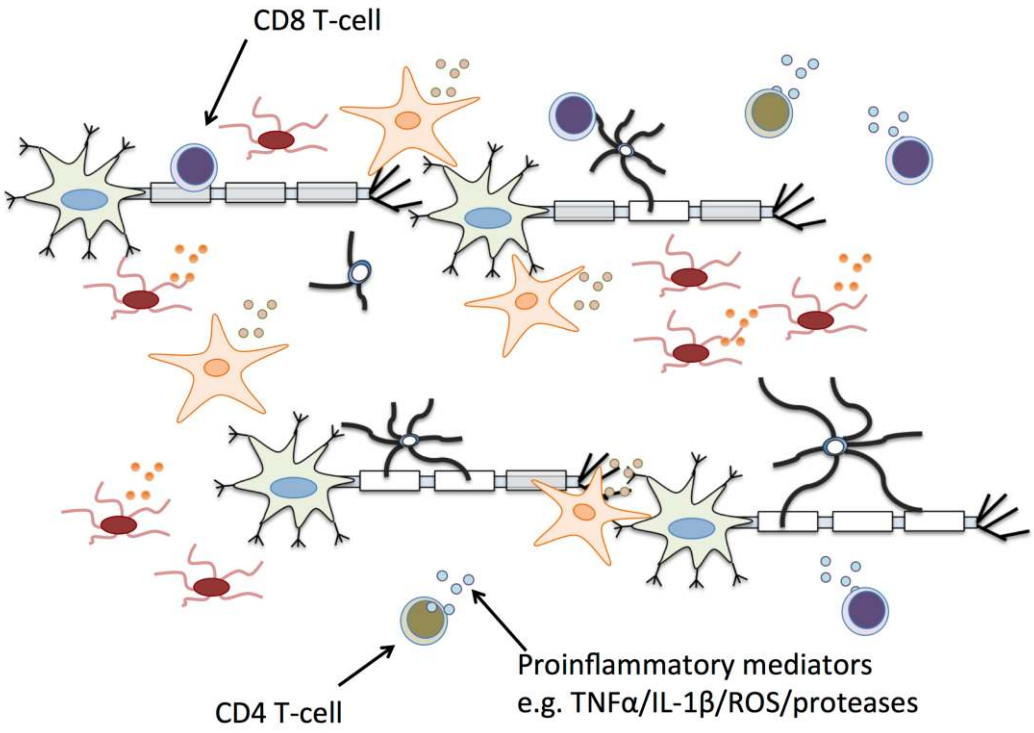

Figure 1.2 Cells involved with CNS inflammation in MS. A schematic of some cells involved with MS pathogenesis. Aberrant activation of microglia and astrocytes leads to production of proinflammatory mediators, such as proinflammatory cytokines, reactive oxygen species, and matrix metalloproteinases (MMP), and contribute to neuroinflammation and demyelination. Adaptive immune cells and innate immune cells (not shown) infiltrate the CNS in MS brains. CD4 T-cells can contribute to MS pathogenesis by cytokine and protease (e.g., MMP) release. CD8 T-cells can target myelin and oligodendrocytes directly, inducing demyelination.

1.4.4 Inflammasomes and MS

Inflammasomes are a multiprotein complexes found in the cytosol that enable the activation of inflammatory caspases such as caspase-1[78]. Activation of the inflammasome has a crucial role in MS disease development. The canonical activation of inflammasome complex involving caspase-1 activation typically leads to the cleavage and ensuing release of IL-1β and IL-18 production[64], of which IL-1β is required for the differentiation of T_H17 cells that is highly expressed in MS patients[5]. Within the CNS, IL-1β can be released by activated microglia, infiltrating macrophages, as well as astrocytes[79]. IL-1β release can also promote leukocyte entry into the CNS by increasing adhesion molecules expression by endothelial cells, and by promoting BBB breakdown by reducing tight junction protein expression[64]. Increased IL-18 levels are also observed in serum and CSF from MS patients, and together with IL-1β can contribute to maintain neuroinflammation within the CNS[64].

Inflammasomes are activated by the detection of PAMPs or DAMPs by the cytosolic NLRs[80]. TNFα signalling can induce nuclear factor kappa-light-chain-enhancer of activated B cells (NF-κB) activity[81], leading to transcriptional induction of several inflammasome related proteins such as pro-IL-1β, pro-IL-18, pro-caspase-1, and NLRP3[80]. In MS, ATP is one of the DAMPs that may be detected by cells expressing NLRP3, such as microglia[64, 79]. Detection of DAMPs can initiate the oligomerization of the NLRP3 receptors, followed by the incorporation of the adaptor protein associated speck-like protein (ASC), and pro-caspase-1[64]. This complex then catalyzes the autoproteolytic cleavage of pro-caspase-1 to bioactive caspase-1[64]. Activated caspase-1 can then cleave substrates such as pro-IL-1β, and pro-IL-18 into its bioactive form[64]. Active caspase-1 can also cleave and activate gasdermin D[82, 83]. Gasdermin D is a pore-forming protein that can be oligomerized and incorporated into the plasma membrane to mediate IL-1β release[82, 83]. Additionally, cleaved gasdermin D can mediate an inflammatory lytic form of cell death termed pyroptosis[82, 83]. A cell undergoing pyroptosis can further support local inflammation by the release of DAMPs and inflammatory mediators[83].

1.4.4.1 Pyroptosis

Pyroptosis is an inflammatory, lytic form of programmed cell death that was initially described as a caspase-1 dependent cell death mechanism in monocytes and neutrophils upon exposure to intracellular bacterial insult[84, 85]. Recently, gasdermin D has been identified to be the key executioner protein for mediating pyroptosis[86, 87]. The gasdermin D protein is a pore-forming protein that can be cleaved by activated caspase-1[84, 88] as a result of canonical inflammasome activation[64], or cleaved by caspase-4/5 (in humans) or caspase-11 (in mice)[84, 88] as a result of non-canonical inflammasome activation[89]. Once cleaved, the N-terminal fragment can oligomerize and insert into the plasma membrane, leading to the generation of a pore with a diameter or approximately 12nm in the plasma membrane[84]. These gasdermin D pores can instigate leakage of cytosolic contents, which can disrupt the osmotic balance of the cell, causing eventual lysis and death of the cell[84]. Because of the lytic nature of pyroptosis, it can lead to release of DAMPs, which can promote inflammation in nearby cells[88]. Additionally, gasdermin D pores have also been demonstrated to mediate IL-1β release[82, 83], thus pyroptosis can often coincide with IL-1β release. Although pyroptosis is best described in context of caspase-1 activation, because caspase-4/5 or caspse-11, can also cleave gasdermin D without cleaving pro-IL-1β, pyroptosis can take place without IL-1β release[85]. Additionally, caspase-1 mediated pyroptosis without IL-1β release has also been demonstrated[90, 91]. Thus, the best marker for pyroptosis is the detection of cleaved gasdermin D (33 kDa), in combination with measuring loss of cytosolic contents.

1.4.5 Consequence of Oligodendrocyte Injury in MS

Oligodendrocyte injury resulting in demyelination is one of the main outcomes of CNS inflammation observed in MS. The loss of myelin on myelinated axons can be detrimental, as the axon can no longer generate efficient action potentials[92]. Remyelination can be observed in MS brains, however the remyelination process is often incomplete[93]. The incomplete, or lack of remyelination can lead to damaged axons, which then causes neurodegeneration, resulting in permanent disability in patients[93].

1.4.5.1 Oligodendrocyte Injury and Demyelination in MS

Demyelination is the active loss of myelin sheath, either by direct damage to myelin, or by the stress or death of oligodendrocytes that make and maintain myelin[5]. Injury to oligodendrocytes can be mediated by multiple ways in MS. Oligodendrocytes[94] and myelin[5] can be direct targets of cytotoxic CD8+ T-cells. Oligodendrocyte death can also be influenced by the release of toxic proinflammatory cytokines, such as TNFα produced by activated microglia, astrocytes, and by infiltrating leukocytes[5, 75]. During chronic inflammation, oligodendrocyte death can be mediated by oxidative injury[5, 95]. ROS released by microglia can induce lipid peroxidation (oxidative degeneration of lipids), and contribute to direct myelin loss[95]. ROS can also induce oligodendrocyte and neuronal death by accumulation of damaged DNA with accompanying oxidative damage within the cell[75]. Irrespective of how myelin loss was brought about, demyelination causes the axons to be bare. Denuded axons can no longer generate an efficient action potential due to poorer conductance arising from the uneven distribution of voltage-gated sodium and potassium channels that otherwise would not have been an issue with intact myelin[92]. Conduction of action potentials can be improved without remyelination as neurons can reorganise the arrangement of voltage-gated ion channels along its axon[92]. Nonetheless, the lack of myelin leads to the increased energy consumption by neurons in order to meet the energy demands required to generate an action potential[92]. With the loss of oligodendrocytes neurons also lose the metabolic support that it received from oligodendrocytes[92]. Once the metabolic burden becomes too great, axonal degeneration can take place, leading to disability[92, 93].

1.4.5.2 Failure of Remyelination in MS

After a demyelinating event, axons can be remyelinated in order to preserve the demyelinated axon[92, 93]. Remyelination is achieved mainly by OPC differentiation into new oligodendrocytes with *de novo* myelin synthesis[93]. There is limited evidence of previously myelinating oligodendrocytes to be able to remyelinate after a demyelinating event[93, 96]. Thus, OPC proliferation and recruitment to the lesion site, followed by differentiation into mature oligodendrocytes is necessary for remyelination to take place[92, 93]. Partial remyelination of axons can be observed in MS patients, termed shadow plaques, but it is variable within the patient population and likely age-related[92]. Indeed, remyelination failure is more common in

older individuals[92]. One reason for remyelination failure is from the reduced ability to clear myelin debris[92]. The ability of phagocytic cells to undergo phagocytosis also wanes with increased age[92]. Remyelination can be stalled with the reduced clearing of myelin debris generated from the previous demyelinating event[92]. The reduced differentiation of OPCs into mature oligodendrocytes is another suggested reason for remyelination failure[92]. Chronic MS lesions have reduced number of oligodendrocytes[92]. Some OPCs can differentiate into pre-myelinating oligodendrocytes, but the maturation does not progress resulting in the failure of efficient remyelination of denuded axons[92]. The lack of myelination is due to in part the lack of axonal activity, which is necessary for efficient myelination, and by the expression of inhibitory molecules on axons that prohibits myelination[92].

1.5 Animal Models of MS

Investigations using animal models have been used to decipher the immunopathology involved in MS, as well as testing therapeutic agents that are currently available for patients today[97]. There are several animal models of MS available, however not one animal model can fully recapitulate the heterogeneous aspects of MS observed in human patients[98]. Despite the lack of a perfect model for MS, each model has its own strengths that have contributed to a better understanding of MS disease mechanisms[98]. Some of the most common *in vivo* models will be discussed.

1.5.1 Experimental Autoimmune Encephalomyelitis (EAE)

EAE is probably the most common animal models used to study MS. The EAE model involves immunisation of an animal with a CNS antigen with a strong adjuvant, such as complete Freund's adjuvant (CFA)[98, 99]. Typically, a strong T-cell disease with neuroinflammation is observed in immunised animals[99]. This model can be fairly versatile, as it can be induced in several different species of animals such as rats, guinea pigs, and non-human primates although the model is most frequently performed in C57BL/6 or SJL mice strains[99]. The outcome of the disease model can vary depending on the type of antigen used, and on the background of the animal[99]. This model has been primarily used as a model for RRMS[99] and has been used to test many DMTs available today[97]. Although EAE can be performed on animals other than mice, mice are the most commonly used animals for EAE

induction due to the ease of handling and the large number of transgenic animals available[100]. Here two of the most common EAE types (active and passive EAE) will be discussed.

1.5.1.1 Active EAE

Active EAE involves the direct sensitisation of the animal with a specific CNS antigen with CFA[99]. The specific antigen required to induce EAE depends on the background of the animal used[99]. The C57BL/6 mice immunised with myelin oligodendrocyte glycoprotein (MOG) peptide from amino acid 35-55 (MOG_{35-55}) is the most frequently used model[97]. When the model is performed in mice, additional injection of pertussis toxin is often necessary to facilitate EAE disease[99]. The pertussis toxin is suggested to induce the trafficking of T-cells across the BBB[99]. Onset of disease is often observed within 10 days after immunisation[101]. Depending on the specific immunisation protocol and animals strain used, EAE induction leads to the generation of an acute or a chronic inflammatory disease, mediated mainly by autoreactive CD4+ T-cells[99]. EAE induction in mice leads mainly to a spinal cord disease with ascending paralysis, where as in MS patients the disease often involves the brain[98]. The types of lesions observed in mice also differ from those observed from MS patients[99]. EAE induced on non-human primates, guinea pigs, or rats resemble disease more similar to MS involving generation of lesions similar to those observed from MS patients[99]. An antibody response is also observed in these models in addition to the generation of autoreactive CD4+ T-cells[99].

1.5.1.2 Passive EAE

Another common method to induce EAE is by the adoptive transfer of encephalitogenic CD4+ T-cells[99]. This model involves the removal of T-cells from an animal approximately 7-10 days after immunised with a myelin protein[98]. The T-cells removed from the animal is expanded *in vitro* before adoptively transferring into naïve mice[98]. The disease observed in recipient mice is similar to active EAE, involving spinal cord disease[99]. This model has been beneficial in studying T-cell trafficking into the CNS, and involvement of T-cells in inflammation[99]. Since disease is development is mediated by the action of transferred T-cells, one of the shortfalls of this model is the limited involvement of other immune cells and glial cells, which are highly involve in MS patients[99].

1.5.2 Viral Models of Inflammatory Demyelination

There is epidemiological evidence that suggest EBV infection can increase risk of developing MS[61]. To address this, several models of demyelination have been developed involving neurovirulent viruses[98, 99]. These models have been used to study propagation of inflammation and demyelination within the brain and spinal cord[98, 99]. However, the viral models of demyelination are also challenging due to the confounding antiviral response generated in the animals[98, 99]. Additionally, the viral models of demyelination can only be performed on mice due to the species selectivity of the virus used[98, 99].

1.5.2.1 Theiler's Murine Encephalomyelitis Virus (TMEV) induced Demyelination

TMEV is a non-enveloped, single strand, positive sense RNA virus[98]. The model involves an intracerebral injection of the virus, causing acute encephalitic phase, followed by a chronic disease with demyelination mainly observed in the spinal cord[99]. The disease severity is dictated by the virulence of the specific viral strain used[99]. TMEV can infect neurons during the acute phase of disease, causing neuronal stress, which can trigger the immune cell recruitment leading to demyelination[98, 99, 101]. During chronic disease, persistent infection in microglia, macrophages, astrocytes, and oligodendrocytes are observed[98]. This models share some similarities with MS such as the site of active demyelination being observed at site of microglia and macrophage activation[98]. However, one of the major shortfalls of this model is the persistent infection observed in this model, which has not been demonstrated in MS patients[98].

1.5.2.2 Mouse Hepatitis Coronavirus (MHCV) induced Demyelination

Another murine virus that can induce demyelination is MHCV. MHCV is a coronavirus that was initially isolated from the brain of a paralysed mouse with disseminated disease with demyelination[98]. MHCV can infect a variety of organs such as those of the enteric, respiratory, and nervous systems, causing disease depending on the strain of virus used[101]. MHCV delivery is performed either by intracranial injection or by nasal infection of the virus[99]. Similar to TMEV, disease is development takes place in two stages. The first stage involves panencephalitis within couple of days post infection[99]. MHCV is usually cleared after the first stage of infection[99]. Approximately 4 weeks after recovery from the

panencephalitis, the mice develop chronic disease with inflammatory demyelination involving paralysis[99]. This model involves generation of autoreactive T-cells against myelin proteins such as PLP and MBP[99]. The demyelination observed in the chronic stage is mediated by the killing of oligodendrocytes by CD8+ T-cells either directly or by bystander effect[99, 101]. The inflammation in this model also has profound glial involvement with microglial activation in the brain and spinal cord with ROS production at lesions, and dysfunctional astrocytes[102].

1.5.3 Toxic Models of Demyelination

The EAE and virus-induced demyelination models both induce demyelination with inflammation involving infiltrating adaptive immune cells. However, there can be variability between experiments with regard to disease onset and severity in both models[99]. Additionally, the location and age of demyelinating lesions can differ from mouse to mouse, making it challenging to assess the extent of demyelination and remyelination[98]. To overcome these challenges, toxin-mediated models of demyelination can be used[103]. Toxin-induced demyelination can be performed either by the injection of lysolecithin, or by oral exposure to cuprizone. Both models lead to predictable demyelination in specific regions within the CNS, making it desirable to study the influence of demyelination[103].

1.5.3.1 Lysolecithin Induced Demyelination

This model involves the direct injection of lysolecithin, an activator of phospholipase A2, into white matter tracts of the CNS[103]. Rapid demyelination is induced after lysolecithin injection into the CNS due to its detergent properties of the chemical directly affecting myelin[98]. Demyelination is only observed at site of injection, as the chemical does not cause direct cytotoxicity of nearby cells other than oligodendrocytes[103]. After the demyelinating event, an acute inflammation involving recruited immune cells, microglia and astrocytes is induced[98, 103]. The remyelination process starts after the injection, with complete remyelination observed within 6-weeks post lysolecithin injection[98]. The recruited immune cells may also contribute to remyelination, as cells such as T-cells can produce growth factors to support remyelination[98]. Phagocytosis of myelin debris is also necessary for

efficient remyelination[92]. This model can be performed in several species including mice, rats, rabbits, and cats[98].

1.5.3.2 Cuprizone Induced Demyelination

Cuprizone (bis-cyclohexanone-oxaldihydrazone) is a copper chelator that can induce spontaneous demyelination in mice, rats, guinea pigs or hamsters[99] by administration of the toxin in the diet of animals, although the model is most commonly performed on mice[103]. Demyelination is partially induced by selective oligodendrocyte injury, possibly through mitochondrial dysfunction, although the specific mechanism targeting oligodendrocytes has not been fully determined[103]. Cuprizone feeding of mice leads to notable demyelination at the corpus callosum, as well as the hippocampus[103]. Complete demyelination in the corpus callosum can be observed within 6 weeks of constant exposure to cuprizone[101, 103]. Spontaneous remyelination of demyelinated regions can be observed once mice are switched back to standard diet[98].

It is recently recognised that cuprizone-mediated demyelination requires local CNS inflammation mediated by astrocytes, microglia and or macrophages, infiltrating neutrophils but not adaptive immune cells[103, 104, 105]. Previous experiments involving *in vitro* exposure of cuprizone only to oligodendrocytes did not lead to reduced viability[106]. However, reduction in viability was observed when there was a combined exposure of TNFα and or IFNγ with cuprizone[106]. This suggested that inflammatory mediators produced by microglia and astrocytes are necessary to mediate complete demyelination in the cuprizone model[106].

1.6 Limitations of Current Understanding on Oligodendrocytes

There has been extensive research performed on the consequences of myelin loss and oligodendrocyte death in the context of MS disease. However, there is little information on the capacity of oligodendrocytes to actively participate in CNS inflammation, especially human oligodendrocytes. Past studies involving *in vitro* oligodendrocyte exposure to inflammatory cytokines and *in vivo* animal models of MS have relied on assessing oligodendrocyte death by visual assessment[107] or by measuring terminal deoxynucleotidyl transferase dUTP nick end labeling (TUNEL) staining[108, 109], and determining cells were

undergoing apoptosis. With the recent discovery of inflammatory forms of cell death, such as pyroptosis[110], there is implicit value in re-assessing whether oligodendrocytes are merely just the targets of neuroinflammation, or act as inflammatory effectors. Furthermore, oligodendrocytes have been demonstrated to express TLRs[49] and other proteins associated with immune responses[52, 54], although defined roles of oligodendrocytes have not been fully elucidated. Importantly, the vast majority of *in vitro* studies assessing immune protein were performed on rodent oligodendrocytes[51, 53, 54], thus the extent of human oligodendrocytes to participate in CNS inflammation is poorly understood. As oligodendrocytes are one of the main target cells in inflammatory diseases such as MS, there is a possibility that oligodendrocytes may actively participate in neuroinflammation.

1.7 Objectives and Hypothesis

This thesis has two main objectives.

Objective 1: To determine the capacity of differentiated and undifferentiated human oligodendrocytes to generate innate immune responses including induction of inflammation, as well as inflammatory cell death upon exposure to proinflammatory stimuli *in vitro* using primary cultured human oligodendrocytes.

Hypothesis 1: Human oligodendrocytes are capable of expressing innate immune genes that are involved in CNS inflammation.

As part of this thesis, I assessed the induction of innate immune genes in cultured human oligodendrocytes after *in vitro* exposure of MS-relevant stimuli. The expression of select innate immune proteins involved in inflammatory cell death pathways were subsequently assessed, demonstrating oligodendrocytes are not immunologically silent but nonetheless able to undergo pyroptosis.

Objective 2: To investigate how *in vivo* oligodendrocytes respond to and participate in CNS inflammatory responses using the cuprizone model of demyelination.

Hypothesis 2: *In vivo* induction of demyelination observed in the cuprizone model in mice required activation of innate immune mechanisms including inflammasome pathways in oligodendrocytes.

Within this objective the cuprizone model of demyelination was initially optimised before assessing the presence of inflammatory oligodendrocytes. I examined the effects of intranasal treatment with VX-765, a caspase-1 inhibitor, on neurobehavioural deficits caused by cuprizone exposure, neuroinflammation, and associated demyelination.

Chapter 2 – Materials and Methods

2.1 Experiments Involving Progenitor Derived Oligodendrocytes (PDOs)

All PDO cultures and experiments were performed at our collaborators' laboratory at National Institutes of Health (NIH), Maryland, USA, with the assistance from Dr. Maria Chiara Monaco, and Dr. Eugene Major. PDO characterisation and culturing methods have been described previously[26].

2.1.1 Culturing PDOs

The PDOs used for this study was initially characterised by Dr. Monaco[26]. Progenitor-derived oligodendrocytes, as the name suggest, are cells that were differentiated into oligodendrocytes from neural progenitor cells *in vitro.* The neural progenitor cells were initially harvested from 8-week gestation age foetal brain[26]. Growing neural progenitor cells in a media enriched with growth factors (GF+ medium) leads to differentiation of an immature form of oligodendrocytes, termed GF+ PDOs. The GF+ PDOs can be further differentiated into GF- PDOs, that represents a more mature form of oligodendrocyte, by culturing in media lacking growth factors (GF- media). The GF- PDOs express prototypical oligodendrocytes markers such as myelin basic protein (MBP) that is not detectable in GF+ PDOs[26].

2.1.1.1 Coating with Poly-D-Lysine (PDL)

All culturing and experiments involving PDOs used poly-D-Lysine (PDL, Sigma, Cat: P6407) coated flasks or plates. All coating procedures were performed under a biosafety cabinet. A PDL (50µg/ml) solution prepared in distilled water was used to coat surfaces. The PDL solution was used to cover the entire base surface of flasks or plates, and incubated for 90 minutes at room temperature, in dark. The PDL solution was removed, and coated surfaces were washed once with distilled water. Coated flasks and plates were air-dried before use. Unused coated flasks and plates were stored in dark in a box. Excess PDL solution was stored at -20ºC and was thawed before use for coating in the future.

2.1.1.2 Culturing GF+ PDOs

The GF+ media contained the following components: 1X DMEM/HAMS-F12 1:1 media (Omega Scientific, Cat: DM-251), 1% bovine serum albumin (Sigma, Cat: A9418), 2mM L-glutamine (Quality Biologicals, Cat: 118-084-061), 50µg/ml gentamicin (Quality Biologicals, Cat: 120-098-031), 1% N2 components (Gibco BRL, Cat: 17502), 20ng/ml basic fibroblast growth factor (PeproTech, Cat: 100-18B), 10ng/ml platelet-derived growth factor-AA (PeproTech, Cat: 100-13A), 2ng/ml sonic hedgehog (R&D Systems, Cat: 1314-SH/CF), 3nM triiodothyronine (Sigma, Cat: T2877), and 2ng/ml neurotrophic factor-3 (PeproTech, Cat: 450-03). Since GF+ PDOs are immature oligodendrocytes, these cells can proliferate in culture for up to 11 passages[26]. GF+ PDOs were maintained on GF+ media, in a humidified incubator at 37ºC with 5% CO_2 atmosphere. Half media exchange was performed every few days until cells reached 95% confluency. For passaging cells, cells were trypsinised using 0.05% trypsin-EDTA. Trypsin was quenched using GF+ media. Cells were centrifuged at 1200rpm for 7 minutes. Cells were re-suspended in GF+ media, and $2.5x10^6$ cells were seeded in a PDL coated T75 flask.

2.1.1.3 Culturing GF- PDOs

Switching the culture media from GF+ media to GF- media is sufficient to differentiate GF+ PDOs to GF- PDOs[26]. The GF- media has the same components as GF+ media except it lacked neurotrophic factor-3, sonic hedgehog, basic fibroblast growth factor, and platelet-derived growth factor-AA. Since GF- PDOs are terminally differentiated the cells do not propagate, and thus cannot be maintained in culture for more than 14 days post differentiation. Therefore, the differentiation of GF+ PDOs to GF- PDOs was only performed on PDL coated plates prior to scheduled experiments. To promote differentiation of cells, GF+ PDOs were trypsinised, and centrifuged at 1200 rpm for 7 minutes. Cells were re-suspended in GF- media, and appropriate amount of cells were plated onto plates, depending on the experiment. For most experiments, cells were differentiated for 3-7 days.

2.1.2 Cytokine Exposure Experiments Using PDOs

$2.5x10^5$ cells were plated on PDL coated 12-well plates, or $5x10^4$ cells were plated on ibidi µ-Slide 8 Well plates (ibidi, Cat: 80826). Half of all cells had GF+ media for GF+ PDOs, and

the other half had GF- media to promote GF- PDO differentiation. All plated cells were left in the incubator for 3-7 days to allow time for GF- PDO differentiation.

GF+ and GF- PDOs were stimulated with 0, 5, 25, or 50ng/ml of human recombinant TNFα (R&D Systems, Cat: 210-TA) or with human recombinant 20ng/ml of IL-1β (R&D Systems, Cat: 201-LB) for 24 hours. For a subset of TNFα stimulated cells, cells were pre-exposed to 50μM VX-765 (InvivoGen, Cat: inh-vx765-1) for 4 hours before TNFα exposure. After 24 hours of cytokine exposure, cells plated on ibidi μ-Slide 8 Well plates were fixed with 4% paraformaldehyde solution (PFA) for immunofluorescence analysis, and cells plated on 12-well plates were treated with TRIzol (ThermoFisher, Cat: 15596018) for RNA extraction and subsequent qRT-PCR analysis. Supernatants were collected for ELISA and lactate dehydrogenase (LDH) assays. Analyses of PDO-derived samples after sample collection post cytokine exposure were performed in the Power lab.

2.1.3 JC virus infection experiments using PDOs

$5x10^5$ PDOs were plated on PDL coated 12-well plates. Half of all cells had GF+ media for GF+ PDOs, and the other half had GF- media to promote GF- PDO differentiation.
GF+ and GF- PDOs were infected with 1 multiplicity of infection (MOI) of JC virus (Mad-4 strain)[111, 112]. To induce viral attachment, virus was diluted in minimum volume necessary to cover the well (500μl) for 90 minutes, and then the media was added up to 1000μl per well. After a 3-day infection, cells were treated with TRIzol for RNA extraction and subsequent qRT-PCR analysis. Supernatants were collected for Type I IFN bioassay. Analyses of PDO-derived samples after sample collection post cytokine exposure were performed in the Power lab.

2.1.4 PDO RNA Isolation and cDNA Synthesis

TRIzol samples of PDOs were stored at -80ºC until use. Total RNA was harvested using RNeasy Mini Kit (Qiagen, Cat: 74106), following manufacturer's instructions. Total RNA from PDO samples was measured using NanoDrop Spectrophotometer. cDNA synthesis was performed with at least 100ng of RNA. RNA samples were DNase I (Promega, Cat: M610A) treated for 60 minutes, followed by a 5-minute incubation with random primers (Sigma-

Aldrich, Cat: 11034731001) before undergoing reverse transcription reaction at 50ºC for 90 minutes using Superscript III reverse transcriptase (ThermoFisher, Cat: 18080-044). The reaction was inactivated by a 15-minute incubation at 70ºC. After completion of cDNA synthesis, 100µl of nuclease-free water (ThermoFisher, Cat: 10977-015) was added to each sample. Samples were stored at -20ºC until use for qRT-PCR analysis.

2.1.5 Quantitative Real-Time Polymerase Chain Reaction (qRT-PCR) on PDO samples

Specific genes of interests were quantified by performing a 3-step qRT-PCR using the i-Cycler IQ5 system (Bio-Rad, Cat: 170-9780)[113]. The threshold cycle (CT) values for each gene of interest was measured using i-Cycler IQ5 system by detecting the increase of fluorescence of SYBR Green dye (Bio-Rad, Cat: 1708880) in real time using the following program: Cycle 1 (initial cDNA denaturation and DNA polymerase activation) 95ºC for 5 minutes, Cycle 2 (for 45 cycles), Step 1 (cDNA denaturation) 95ºC for 30 seconds, Step 2 (annealing) 60ºC for 30 seconds, Step 3 (extension) 72ºC for 30 seconds, Cycle 3 (final extension) 72ºC for 5 minutes, Cycle 4 (melt curve analysis) 10 seconds for 35 cycles, starting from 65ºC with 1ºC increase per cycle. All primers used in this thesis are listed on Table 2.1 (page 35). Data for each gene of interest was expressed as a relative fold change (RFC) compared to untreated GF+ PDOs. RFC values were calculated using the ΔΔCT method using *GAPDH* as an endogenous reference gene.

2.1.6 IL-1β and IL-18 ELISA

Supernatant samples were thawed slowly on ice just before use. IL-1β ELISA was performed using the Human IL-1β DuoSet ELISA kit (R&D Systems, Cat: DY201)[114]. The IL-18 ELISA was performed using the ThermoFisher IL-18 Human Instant ELISA kit (ThermoFisher, Cat: BMS267INST). ELISAs were performed according to manufacturer's instructions. Absorbances were measured using a BioTek Synergy HT plate reader.

2.1.7 Interferon Bioassay

Assessment of type I IFN activity in supernatants from treated PDOs were performed by Dr. Meziane from the Cohen lab at IRCM. The Type I IFN bioassay was conducted by incubating the PDO supernatant samples with a reporter cell line HEK-Blue IFN-α/β cells

(InvivoGen, Cat: hkb-ifnab)[115]. This reporter cell line expresses a reporter gene for secreted embryonic alkaline phosphatase (SEAP) under the interferon stimulated gene (ISG) 54 promoter, which is inducible upon IFNα/β signalling. The SEAP released was detected based on manufacturer's instructions. The concentration of the Type I IFN release was determined by comparing to the standard curve generated from exposing the HEK-Blue IFN-α/β cells with known values of Type I IFNs.

2.1.8 Lactate Dehydrogenase (LDH) Release Assay

Supernatant samples were thawed slowly on ice just before use. LDH release in supernatant was measured using the LDH-Cytotoxicity Assay Kit II (Abcam, Cat: ab65393). Manufacturer's instructions were followed for the assays. Absorbances were measured using the BioTek plate reader. % LDH release was calculated by normalising all results to untreated controls.

2.1.9 Cell Culture Immunofluorescence (Immunocytochemistry, ICC)

Cell culture immunofluorescence was performed to identify whether PDOs expressed caspase-1 and gasdermin D proteins after TNFα exposure. The morphological changes in PDOs following TNFα exposure were also investigated.

2.1.9.1 Immunofluorescence analysis of PDO samples

GF+ and GF- PDOs were cultured on PDL coated 180µm thick polymer coverslip ibidi µ-Slide 8 Well plates. After exposing cells to TNFα for 24 hours, cells were fixed with 4% PFA. Cells were permeabilized with 0.1% Triton X-100 in PBS and blocked with Odyssey blocking buffer (Li-Cor, Cat: 927-40000) for 2 hours. Cells were incubated with primary antibodies, diluted in Odyssey blocking buffer, overnight at 4ºC. Cells were washed three times manually with Odyssey blocking buffer. Cells were incubated with fluorescent secondary antibodies, diluted in Odyssey blocking buffer, at room temperature for 2 hours in dark. All antibodies used in this thesis are outlined on Table 2.2 (page 36) and Table 2.3 (page 37). Cells were washed again three times with Odyssey blocking buffer. F-actin was labeled with Antigreed 488 ReadyProbe reagent (ThermoFisher, Cat: R37110) according to manufacturer's instructions. Cellular DNA was stained with DAPI solution (6µg/ml) and

incubated for 10 minutes in dark, followed by another three washes with Odyssey blocking buffer. Cells were mounted using Prolong Gold antifade reagent (ThermoFisher, Cat: P36934).

Table 2.1 List of all primers used in the qRT-PCR analysis on PDO samples.

Gene Name	Forward Primer	Reverse Primer
MAVS	CAGGAGCAGGACACAGAAC	AGGAGACAGATGGAGACACAG
DDX58	AAACCAGAATTATCCCAACCGA	TGATCTGAGAAGGCATTCCAC
SOCS1	ACTACCTGAGCTCCTTCCC	CAAAATAACACGGCATCCCAG
IRF1	TGCCTCCTGGGAAGATGA	CCTGGGATTGGTGTTATGC
IRF3	GCACAGCAGGAGGATTTCG	AGCCGCTTCAGTGGGTTC
IRF7	TACCATCTACCTGGGCTTCG	AGGGTTCCAGCTTCACCA
IFNB	CAT CTA GCA CTG GCT GGA ATG	ACTCCTTGGCCTTCAGGTAATG
MX1	GAAGATAAGTGGAGAGGCAAGG	CTCCAGGGTGATTAGCTCATG
BST2	CCTGCTCGGCTTTTCGCTTGAACAT	CGGAGGGAGGCTCTGGAGGGAGAC
CASP1	TCCAATAATGGACAAGTCAAGCC	GCTGTACCCCAGATTTTGTAGCA
GSDMD	TGTGTCAACCTGTCTATCAAGG	GATCTTTGCCTGTCCTGGG
NLRP3	GATCTTCGCTGCGATCAACAG	CGTGCATTATCTGAACCCCAC
IL1B	CCAAAGAAGAAGATGGAAAAG	GGTGCTGATGTACCAGTTGGG
CASP4	CAAGAGAAGCAACGTATGGCA	AGGCAGATGGTCAAACTCTGTA
CASP6	CCATGGCGAAGGCAATCA	CTCCAGCAGGCAGCGTGTAA
ASC	GCCTGCACTTTATAGACCAGC	GCTTCCGCATCTTGCTTGG
NLRX1	AACGGTGCAGGTGACACA	GCTCAGCTCATTGAAGTAGA
OLIG1	CTAAAATAGGTAACCAGGCGTCTCA	CCCGGTACTCCTGCGTGTT
PLP	CTTTGGAGCGGGTGTGTACTT	CAACGGTCAGGGCATAGGTG
NG2	GAGCCCAGGCACGAAAAATG	GTATGTTTGGCCCCTCCGAA
CNP	TGGAGTTAAGCGAGCAGCAA	CTAAGAGGTCAAGGCCCGTC
B2M	TCTCACTCCCACTATTACCCCT	AGGCCCTTTACACTGTGAGC
TNFRSF1A	CCAAATGGGGGAGTGAGAGG	ATTCCCACCAACAGCTCCAG
TNFRSF1B	GCACCGCCTCCAAATGCTAA	AGTGCGTTATCTTGCCCAGG
CASP8	AGTAAGCAACAAGGATGACAAGA	ATCAATCAGAAGGGAAGACAAGTT
FADD	TCTCCTCTCTGAGACTGCTAAG	AGAGAGTGCTGTGTGTCAATC
TRAF2	CACACCTGTCCCTCTTCTTTG	CCTGAAGGCGTCAATCACGTG
TRADD	GCTGTTTGAGTTGCATCCTAGC	CCGCACTTCAGATTTCGCA
JCV T-Ag	AGTGTTGGGATCCTGTGTTTTCA	GTGGGATGAAGACCTGTTTTGC
HMGB1	ACCCAGATGCTTCAGTCAAC	GGCGATACTCAGAGCAGAAG
GAPDH	AGCCTTCTCCATGGTGGTGAAGAC	CGGAGTCAACGGATTTGGTCG

Table 2.2 List of all primary antibodies used in this thesis. IHC immunohistochemistry, IF immunofluorescence, ICC immunocytochemistry, WB western blot, ICW in-cell Western. Antibodies used for PDO immunofluorescence analysis is labelled as ICC. Antibodies used for tissue immunofluorescence analysis is labelled as IF.

Target Protein	Host Species	Used In	Dilution	Product Catalogue
AIM2	Rabbit IgG	IHC	1:200	Abcam, ab93015
APP	Rabbit IgG	IF	1:200	Abcam, ab241592
ASPA	Rabbit IgG	IHC, IF	1:500	Abcam, ab97454
Caspase-1	Rabbit IgG	ICC, IF	1:200	Santa Cruz, sc-514
Gasdermin D	Mouse IgG	ICC	1:200	Abcam, ab57785
Gasdermin D	Mouse IgG	IHC, IF, WB	1:200 IHC/IF, 1:1000 WB	Sigma-Aldrich, WH0079792M1
GFAP	Rabbit IgG	IHC, IF	1:500	Dako, Z0334
GST-pi	Goat IgG	IHC, IF	1:500 IHC, 1:200 IF	Abcam, ab53943
HRP conjugated β-Actin	Mouse IgG	WB	1:1000	Santa Cruz, sc-47778HRP
Iba-1	Rabbit IgG	IHC, IF	1:200	Wako, 019-19741
IL-18	Rabbit IgG	IHC	1:200	Santa Cruz, E-8
IL-1b	Rabbit IgG	IHC	1:200	Santa Cruz, sc-7884
MBP (QD-9)	Mouse IgG	IHC, IF	1:500	Abnova, MAB8817
MBP (SMI94)	Mouse IgG	ICW, WB	1:200 ICW, 1:1000 WB	Covance, SMI-94R
NG2	Rabbit IgG	IHC	1:200	Abcam, ab129051
NLRX1	Rabbit IgG	IHC	1:200	Abcam, ab1007611

2.1.9.2 Confocal Microscopy and Quantification of PDO samples

Cells were imaged using the Wave FX1 Spinning Disc confocal microscope (Zeiss) at 20X or 40X using the Volocity 6.3 Acquisition software (PerkinElmer). Images were analysed using Volocity 6.3 Analysis software (PerkinElmer). To quantify the Cy5 and Cy3 fluorescence intensity (for gasdermin D and caspase-1 quantification, respectively), cell bodies of PDOs were first selected using the *Freehand ROI tool*. The MFI value of each fluorescent channel was obtained under the *Measurements* tab on Volocity. The MFI of secondary antibody only

control cells was also obtained, and the average MFI values were used as a background measurement, which was subtracted out from all tested samples. Fluorescently labelled F-actin was used to quantify PDO processes. To measure the length of processes, individual processes were carefully traced and length in µm calculated by using the *Line tool* on Volocity. All processes present on a single PDO with positive nuclear staining were measured. The number of processes a single PDO had was also measured. For both measurements, PDOs without processes (with distinct nuclear staining) were included for analysis. Finally, the proportion of PDOs that lacked processes was calculated by counting the number of PDOs without processes as well as the total number of PDOs in each condition. For all quantification procedures, at least 100 cells from each condition were quantified.

Table 2.3 List of all secondary antibodies used in this study. IHC immunohistochemistry, IF immunofluorescence, ICW in-cell Western, WB Western blot.

Secondary Antibody Name	Used in	Dilution	Product Catalogue
Biotinylated Goat anti-Mouse IgG	IHC	1:500	Vector Laboratories, BA-9200
Biotinylated Goat anti-Rabbit IgG	IHC	1:500	Vector Laboratories, BA-1000
Biotinylated Rabbit anti-Goat IgG	IHC	1:500	Vector Laboratories, BA-5000
Donkey anti-Goat IgG Cy5	IF	1:800	Abcam, ab6566
Goat anti-Mouse IgG Alexa Fluor 488	IF	1:500	Abcam, ab150117
Goat anti-Mouse IgG Alexa Fluor 568	IF	1:500	Abcam, ab175473
Goat anti-Mouse IgG Alexa Fluor 647	IF	1:800	Abcam, ab150115
Goat anti-Rabbit IgG Alexa Fluor 488	IF	1:500	Abcam, ab150077
IRDye 800C Goat anti-Mouse IgG Secondary Antibody	ICW	1:800	Li-Cor, 926-32210
Peroxidase AffiniPure Goat anti-Mouse IgG	WB	1:10000	Jackson Immuno Research, 115-035-003

2.2 Cuprizone Model of Toxic Demyelination

2.2.1 Animal Ethics

All animal experiments were performed according to the Canadian Council on Animal Care and approved by the University of Alberta Health Sciences Animal Care and Use Committee (AUP 00002244).

2.2.2 Pre-experimental Set up

9-week old female or male C57BL/6J mice from Jackson Laboratories were used for my studies. Mice were housed in new cages upon arrival to the Health Sciences Laboratory Animals Service (HSLAS) facility, with three similar-weighted, same sexed mice per cage. Mice were acclimated for approximately one week before commencing cuprizone diet, during this time mice were fed with standard rodent chow (LabDiet, Cat: 5L0D) provided by HSLAS.

2.2.2.1 Preparation of Food

Food containing cuprizone was prepared by mixing 0.3% or 0.5% cuprizone (Sigma-Aldrich, Cat: 14690)) with Neutra-Gel diet (BioServ, Cat: F4798-KIT) (weight/dry food weight). The powdered food containing cuprizone was reconstituted with 1.5X warm Milli-Q water, and then chilled to form gel-food cubes, as per BioServ's instructions. The final cuprizone content after reconstitution was calculated to be 0.13% and 0.22%, respectively. The same Neutra-Gel diet without cuprizone was used for control diet. The control food, 0.3% cuprizone food, and 0.5% cuprizone food was stored in separate containers at 4ºC until feeding. Food was prepared on a weekly basis to maintain freshness of food.

2.2.2.2 Experimental Design

Cages were assigned randomly for each type of diet. At the first day of experiment, the standard chow was removed and one cube of 0.3%- or 0.5%-cuprizone diet, or control diet was placed in each cage to allow feeding *ad libtum*. The mice were fed on the assigned diet for the duration of the experiment. Gel-food cubes in cages were replaced every other day. Housing cages for mice was replaced once every 2 weeks. Experiments were terminated at 2,

4, or 6 weeks post commencement of cuprizone diet. Weights of mice were monitored on a weekly basis.

2.2.2.3 Intranasal Drug Treatment of the Caspase-1 Inhibitor VX-765

Drug treatment of female C57BL/6J mice started after 2-weeks of feeding on 0.5 % cuprizone diet. VX-765 dissolved in 1:1 PBS:DMSO (10mg/kg) was administered daily by intranasal delivery (n=12), while maintaining 0.5% cuprizone diet. Control mice (n=12) and a subset of 0.5% cuprizone-fed mice (n=12) received vehicle (1:1 PBS DMSO mixture) intranasally as well. Each experiment was terminated after 4 weeks of drug treatment.

2.2.3 Behaviour Analyses

2.2.3.1 Open Field Test

The open field test was performed at 6-weeks post commencement of 0.3% or 0.5% cuprizone diet. An open field bin was prepared using an opaque bin (w=44cm, l=36cm, h=12.5cm) with green tape taped on the bottom of the bin. The tape was used to mark all quadrants of the bin (by taping the width and the length of the bin so it overlaps at the middle), as well as to create a 13cm by 16cm rectangle in the middle of the bin. A 3cm square was also taped on the underside of the bin in the middle of one of the quadrants. The inside of the bin was decontaminated using 1% Virkon.

Mice were tested individually. A mouse was removed from its home cage and placed in the bin on the 3cm square and was allowed to move freely around the open field bin for 5 minutes. During this time, the time spent in the centre, the number of crosses, and the number of rearings was counted. The time spent in the centre was defined as the total time a mouse spent inside of the 13cm x 16cm rectangle and was measured using a stopwatch. Both hindlimbs of the mouse had to be inside the 13cm x 16cm rectangle to qualify as being in the centre. The number of crosses was defined as the number of times the mouse moved from one quadrant to another. The number of rearings was defined as a position where the mouse is standing on its hindlimb while touching the walls of the bin with its forelimbs. After 5 minutes, the mouse was placed back into the home cage, and bin surfaces were decontaminated using 1% Virkon.

2.2.3.2. Novel Object Recognition Test

Female C57BL/6J mice to be trained were removed from the housing area to the procedure room. The Novel Object Recognition test was conducted at 2-, 4-, or 6-weeks post commencement of 0.5% cuprizone diet. Mice were trained and tested one at a time and were trained and tested only once. During training, a mouse was placed in an open field bin (w=44cm, l=36cm, h=12.5cm) with two identical objects (sample collection containers) for 5 minutes. Each mouse was placed in the bin from the same location, on the opposite side of the two identical objects, facing the objects. The mouse was free to move around the bin and investigate the two objects for the 5 minutes. After the allocated time, the mouse was placed back to its home cage. The open field bin and the objects were thoroughly cleaned with 1% Virkon before training the next mouse. All mice were placed back to the housing area after completion of training and left undisturbed for 6 hours.

For testing, a mouse was placed in the same open field bin with the familiar object from the training session, with one of the familiar objects replaced with a novel object (Lego block figure). The mouse was free to investigate for 5 minutes, similar to the training session. During this time, the time spent by the mouse interacting with the novel object and old object was recorded using a stopwatch. A mouse was considered to be interacting with an object if it touched, licked, bit, or sniffed the object, but not if it climbed on top of the object. After the 5 minutes, the mouse was placed back into its home cage, and the surfaces of open field bin and objects were decontaminated with 1% Virkon. Mice were tested in the same order as it was trained.

2.2.4 Mouse Brain Dissections and Sample Collection

Mice were euthanized at the end of the experiment after 2-, 4-, or 6-weeks of feeding on specialised diet, and brains were collected by cervical dislocation. All brain dissections were performed on ice-filled petri dish, one at a time. Surgical instruments were disinfected with 70% ethanol between samples.

2.2.4.1 Harvesting the Cerebellum, Parietal Lobe, and Brainstem

The cerebellum was first removed from all mouse brains by gently scraping the cerebellum off from the hindbrain with a razor, while holding the brain with surgical tweezers. The cerebellum was collected in a 1.5ml tube or in a lysing matrix tubes (MP, Cat: 6913-500), and snap frozen in liquid nitrogen. After removing the cerebellum, the parietal lobe and the brainstem was collected from a subset of control mice and 0.3% cuprizone-fed mice. The brain stem was removed from the brain by resecting it with a razor. The parietal lobe was isolated by dissecting the brain coronally at a point right below bregma with a razor. The parietal lobe and brainstem were collected in separate 1.5ml tubes and were snap frozen in liquid nitrogen.

2.2.4.2 Dissections for Histology Purposes and Slide Preparations

For the subset of mice brains where the parietal lobe and brainstem was removed, the remaining forebrain was fixed in 4% PFA pH6.0 and stored at 4ºC until processing for paraffin embedding. For the rest of mice brains, after removing the cerebellum, the whole brain was fixed in 4% PFA pH6.0 and stored at 4ºC for two days. After fixing the brain for two days, each brain was cut coronally with a razor at approximately 1cm from the olfactory bulb. The forebrain was placed back into fixative and was stored at 4ºC until processing for paraffin embedding. After paraffin embedding, samples were sectioned into 10µm thickness onto glass sides and used for immunohistochemical and immunofluorescence analysis. All paraffin embedding and sectioning was performed by the Alberta Diabetes Institute Histology Core.

2.2.4.3 Isolation of the Corpus Callosum

The corpus callosum was dissected from a subset of mice. After removing the cerebellum, the brain was further chilled with ice-cold PBS. The brain was cut coronally approximately 2mm above and below bregma. The brain section was re-chilled with ice-cold PBS, and placed on top of a filter paper, cut side up. While observing the brain under a dissection microscope, the cortex and striatum (grey matter above and below the corpus callosum) were removed as much as possible with a razor. After removing as much grey matter, the corpus callosum was collected in 1.5ml tubes and was snap frozen in liquid nitrogen.

2.3 Brain Tissue Analysis of Cuprizone-fed Mice

2.3.1 Histochemical and Immunohistochemical Analysis

2.3.1.1 Luxol Fast Blue (LFB) Staining of Brain Tissue

Tissue sections were deparaffinized by incubating slides at 60ºC for 1 hour, followed by immersing slides in two toluene baths at room temperature for 5 minutes each. Slides were hydrated by immersing slides in two 100% ethanol baths, and two 95% ethanol baths, with 5-minute incubation per bath. Slides were incubated in 0.1% LFB solution (Solvent Blue 38, Sigma-Alderich, Cat: S-3382) overnight at 56ºC. LFB solution was then washed off in 95% ethanol, and slides were rinsed multiple times in Milli-Q water. Slides were incubated in 0.05% lithium carbonate solution for maximum of 30 seconds, followed by an immediate incubation in 70% ethanol for maximum of 30 seconds, and rinsed thoroughly with Milli-Q water. LFB staining of the white matter was confirmed microscopically. If slides had excessive staining, the entire batch was incubated in 0.1% lithium carbonate solution and 70% ethanol again. After confirming proper LFB staining, slides were incubated in 95% ethanol for 5 minutes, followed by dehydration in two 100% ethanol baths, and in two toluene baths, with 5-minute incubation per bath. Slides were mounted using Acrytol Mounting Medium (Surgipath, Cat: 01720).

2.3.1.2 Cresyl Violet Staining of Brain Tissue

Tissue sections were deparaffinized by incubating slides at 60ºC for 1 hour, followed by immersing slides in two toluene baths at room temperature for 5 minutes each. Slides were hydrated by immersing slides in two 100% ethanol baths, and two 95% ethanol baths, with 5-minute incubation each bath. Slides were then incubated in 0.22µm-filtered 0.1% cresyl violet solution (Cresyl Violet Acetate, Sigma-Aldrich, Cat: C5042) for 3 minutes, and rinsed in Milli-Q water. Cresyl violet staining of neuron cell bodies was confirmed microscopically. After confirming proper cresyl violet staining, slides were incubated in 95% ethanol for 5 minutes, followed by dehydration in two 100% ethanol baths, and in two toluene baths, with 5-minute incubation per bath. Slides were mounted using Acrytol Mounting Medium. A subset of LFB stained slides were counterstained with cresyl violet. After confirming LFB

staining, slides were incubated in 0.22µm-filtered 0.1% cresyl violet solution for 3 minutes and rinsed in Milli-Q water. The cresyl violet staining protocol was followed from this point.

2.3.1.3 Immunohistochemistry of Brain Tissue

Tissue sections were deparaffinized by incubating slides at 60ºC for 1 hour, followed by immersing slides in two toluene baths at room temperature for 5 minutes each. Immersing slides in two 100% ethanol baths, two 95% ethanol baths, two 70% ethanol baths, and two Milli-Q water baths, for 5 minutes per bath, hydrated tissue sections. Slides were then boiled in 0.01M sodium citrate buffer (pH 6.0) for 10 minutes in the microwave for tissue antigen retrieval. Slides were left to cool at room temperature. Humidified slide chambers were prepared by filling up an empty micropipette tip box with ~100ml of distilled water and placing a moist paper towel that covered the entire surface area of the tip holder of the box. All following incubation steps used this humidified slide chamber by placing slides on top of the paper towel (tissue side up), with the box lid closed, unless otherwise stated. Precautions were made to not let the tissue sections dry out. Tissue sections were marked around with a hydrophobic pen (Super PAP Pen, ThermoFisher, Cat: 008899), to allow liquid reagents to stay within the marked area when slides are placed within a humidified slide chamber. Endogenous peroxidases were inactivated with 0.3% hydrogen peroxide solution, with 200µl per slide, for 20 minutes. Each tissue sections were blocked with excess Odyssey blocking buffer for 3 hours at room temperature. Slides were incubated with primary antibody solution diluted in Odyssey blocking buffer, with 150µl of antibody per slide, overnight at 4ºC. Slides were washed by placing slides in a PBS-filled Coplin jar and placing it on an orbital shaker at medium speed for 5 minutes. The wash was repeated two more times, with PBS exchanged between washes. After the final wash, the slides were incubated with biotinylated secondary antibody diluted in Odyssey blocking buffer, with 150µl of antibody per slide, for 2 hours at room temperature. Refer to Table 2.2 (page 36) and Table 2.3 (page 37) on antibodies used in this analysis. Slides were washed three times in PBS as stated above, and then incubated in Vectastain Elite HRP ABC kit reagent (Vector Laboratories, Cat: PK-6100) diluted in PBS, with ~200µl per slide, for 2 hours at room temperature. Slides were washed again three times in PBS as mentioned previously. Slides were incubated with DAB reagent (Vector Laboratories, Cat: SK-4100), with ~200µl per slide, at room temperature until slides turned

brown, or for a maximum of 10 minutes. Slides were then incubated in Milli-Q water bath at room temperature for 10 minutes, before dehydrating tissue sections in two 70% ethanol baths, two 95% ethanol baths, two 100% ethanol baths and two toluene baths, for 3 minutes per bath. Slides were mounted using Acrytol Mounting Medium. For a subset of slides, LFB was co-stained on the same slide after DAB staining. After dehydrating slides in two 70% ethanol baths, slides were immersed in a Coplin jar filled with 0.1% LFB solution. The LFB methods outlined on section 2.3.1.1. were followed from this point.

2.3.1.4 Quantification of Histochemical and Immunohistochemical Images

Histological and immunohistochemical slides were imaged using Zeiss Axioskop 2 microscope (Zeiss) in conjunction with QC Capture Pro 6.0 software. Using this software, the white background levels and colour contrast of images were adjusted based on unstained tissue-free areas of the slide. After adjusting for background and colour contrast, the same light and software settings were used to image slides that were stained in the same batch. Images of the corpus callosum located right below the sagittal sinus were taken at 10X, 20X, or 40X. The Ammon's horn of the hippocampus was also imaged and captured at 10X.

All histological and immunohistochemical images were analysed using the ImageJ Fiji program. To quantify LFB stained areas of the corpus callosum, the blue-coloured areas of the entire image was first selected. Using the *Color Threshold* tab, the blue colour spectrum was selected by setting the lower hue at 120, and the upper hue at 180. The saturation and brightness were then adjusted to select out non-specific artefacts, such as dirt, followed by converting the image type to 16-bit. The corpus callosum within the image was selected using the *Freehand selections* tool. The *Threshold* maximum and minimum values were then set to 85, which generated a % LFB stained area within the selected corpus callosum.

To quantify DAB stained areas of the corpus callosum on immunohistochemical slides, the corpus callosum within the image was first selected using the *Freehand selections* tool, and the selected area was measured using the *Measure* tab. The *Color Threshold* tab was used to select total DAB immunopositive areas within the corpus callosum. Selections of positively stained areas were adjusted based on hue, saturation, and brightness. Non-specific artefacts

were excluded from the selection process. The total area of immunopositive area was measured using the *Measure* tab. The percent DAB immunopositive area was calculated by taking in consideration of the total area of the corpus callosum measured initially. This method of quantification was only performed on same batch samples since DAB stain intensity of the same protein of interest can vary from batch to batch. The *Colour Threshold* settings used to select DAB immunopositive areas remained consistent throughout each batch. For counting DAB immunopositive cell bodies within the corpus callosum, the area of the corpus callosum was measured as mentioned above. Positively stained cells were then counted using the *Multi-point* tool.

2.3.2 Fluorescence and Immunofluorescence Analysis

2.3.2.1 Nile Red Staining of Brain Tissue

For Nile Red staining of lipids, tissue sections were deparaffinized by incubating slides at 60ºC for 1 hour, followed by immersing slides in three toluene baths at room temperature; 10 minutes for the first bath and 5 minutes for the second and third baths. Slides were hydrated by incubating in 100% and 95% ethanol baths for 5 minutes each. Slides were then immersed in 10µM Nile Red solution diluted in PBS (Sigma-Alderich, Cat: 72485) for 10 minutes in dark, by covering slides with an ice bucket. Slides were washed three times with PBS in dark. Each wash was performed in a PBS-filled Coplin jar placed on an orbital shaker at medium speed for 5 minutes, with an ice bucket overtop. The PBS was replaced between washes. Slides were mounted with Prolong Gold antifade reagent.

2.3.2.2 Brain Tissue Immunofluorescence

Tissue sections were deparaffinized by incubating slides at 60ºC for 1 hour, followed by immersing slides in three toluene baths at room temperature; 10 minutes for the first bath and 5 minutes for the second and third baths. Slides were hydrated by incubating in 100% and 95% ethanol baths for 5 minutes each, followed by a 5 minutes Slides were washed with running distilled water for 5 minutes, and then boiled at 95ºC in 0.01M sodium citrate buffer (pH 6.0) for 1 hour for tissue antigen retrieval.

Humidified slide chambers were prepared in the same manner as mentioned in section 2.3.1.3. All incubation steps were performed using the humidified slides chambers as mentioned previously, and precautions were made to keep the tissues moist. Once slides were cooled after boiling, tissue sections were marked around with a hydrophobic pen, and was blocked with excess HHFH buffer (1mM HEPES buffer, 2% horse serum, 5% foetal bovine serum, 0.1% sodium azide, 1X Hanks' balanced salt solution) for 3 hours at room temperature. Slides were incubated with primary antibodies diluted in HHFH buffer overnight at 4ºC, with 150µl of antibody per slide. Slides were washed three times with PBS as mentioned in section 2.3.1.3. Background autofluorescence was quenched by incubating slides with freshly 0.22µm-filtered 1X True Black Autofluorescence Quencher (Biotium, Cat: 23007) solution for 3 minutes, with ~100µl per slide, at room temperature. Slides were washed three more times in PBS as described previously. Slides were incubated with fluorescent secondary antibodies at room temperature for 2 hours in dark. Cellular DNA were stained by incubating slides with ~100µl per slide of 6µg/ml DAPI solution diluted in PBS for 10 minutes in dark. Slides were washed four times with PBS in dark and were mounted using Prolong Gold antifade reagent. Slides were stored at dark at all times.

2.3.2.3 Confocal Microscopy and Quantification

Fluorescence-stained slides were imaged using Wave FX1 Spinning Disc confocal microscope (Zeiss). All fluorescence slides were imaged in z-stacks using the Volocity Acquisition software (PerkinElmer), and all images were analysed using Volocity Analysis software (PerkinElmer).

For Nile Red stained slides, the Texas Red laser was used to image slides. Images of the central corpus callosum located below the sagittal sinus, and the corpus callosum located below the right and left cingulum were taken at 10X. To quantify Nile Red staining intensity of the corpus callosum, the corpus callosum and the cortex of any given image was selected using the *Freehand ROI tool*. The fluorescence measurement of the cortex was used as a background staining measurement. The *Volume* and *Sum* of fluorescence (ROI) values of the corpus callosum and cortex selected, found under the *Measuments* tab, was recorded. The total fluorescence ROI of the corpus callosum (CC ROI) was calculated as ("Volume of

corpus callosum"/"Sum of fluorescence of corpus callosum") – ("Volume of cortex"/"Sum of fluorescence of cortex"). To calculate % demyelination, the CC ROI for the corresponding control mice were set at 100%.

For immunofluorescence slides, 20X or 40X images of the central corpus callosum in the area below the sagittal sinus were imaged. The Cy5, Cy3, FITC, and DAPI lasers were used to image each slide, depending on the secondary antibodies used. Cells with intact nuclei staining were considered positive if signal for a particular fluorescence channel was three times higher than background. Positive cells were counted using the *Point tool*. Axonal blebs were quantified digitally by counting APP immunopositive particles that were larger than $20\mu m^3$. The number of axonal blebs per mouse were summarised as per field of view, averaged over 10 different fields of view.

2.3.3 Western Blot Analysis

2.3.3.1 Protein Isolation from the Corpus Callosum

Dissected out corpus callosum samples were stored at -80ºC until protein isolation. Corpus callosum samples were kept on ice. Each corpus callosum samples were weighed and transferred into individual lysing matrix tubes. 10µl of cold 1X RIPA buffer (Abcam, Cat: ab156034)) with protease inhibitors was added for every mg of tissue. The tissue was homogenised for 20 seconds using a Fast-Prep 24 homogenizer and centrifuged at 12,000 RCF for 15 minutes at 4ºC. The supernatant was collected into a fresh 1.5ml tubes. Isolated protein samples were flash frozen in liquid nitrogen before storing at -20ºC.

2.3.3.2 Protein Quantification

Protein samples were quantified using Bio-Rad DC Protein Assay kit (Bio-Rad, Cat: 500-0116) and performed according to manufacturer's instructions. Absorbances were measured using a BioTek plate reader.

2.3.3.3 SDS-PAGE

15-30µg of protein was used for gel electrophoresis. Proteins samples were prepared by mixing with 4X lammeli buffer (Bio-Rad, Cat: 161-0747) and 10% B2-mercaptoethanol, and

boiled at 97ºC for 10 minutes. 4-20% pre-cast gels from Bio-Rad (Cat: 456-1094) were used for gel electrophoresis in SDS running buffer (25mM Tris-Base, 192mM glycine, 3.77mM SDS in Milli-Q water) for 85 minutes at 100V. Gels were then transferred onto a 0.2µm-nitrocellulose membrane (Bio-Rad, Cat: 1620112) for 50 minutes at 0.10A in cold transfer buffer (20% methanol, 25mM Tris-Base, 192mM glycine, in Milli-Q water). Membrane was blocked for 1 hour at room temperature in Odyssey blocking buffer. Membranes were incubated with primary antibody diluted in Odyssey buffer overnight at 4ºC. Membranes were washed with PBS-T (0.1% Tween-20 in PBS), followed by a 1-hour incubation of secondary HRP-conjugated antibody, diluted in 5% skim milk, for 1 hour at room temperature. Blots were developed using Pierce kit (ThermoFisher, Cat: 32132), with the ECL substrate diluted 1:4 in Milli-Q water and applied to blots for 7 minutes. Blots were imaged using GE health sciences biomolecular imager in the Cy2 channel.

2.3.3.4 Quantification of Western Blots

The Image Studio Lite software (Li-Cor) was used to quantify protein bands from Western blots. Individual protein bands of interest were selected, and the maximum signal intensities were recorded. These values were normalised to corresponding β-actin values bands that were analysed in the same manner.

2.4 Statistical Analysis

Parametric statistical analyses were performed for analysis all data using GraphPad Prism software Version 8, except for the χ^2-test used to assess the number of pyroptotic cells. Tests were considered significant with a p-value lower than 0.05.

Chapter 3 – *In vitro* results: Oligodendrocytes are capable in generating an innate immune response *in vitro*

To investigate whether oligodendrocytes are capable in generating innate immune molecules, experiments were conducted on growth factor GF+ and GF- progenitor-derived oligodendrocytes (PDOs). The GF+ PDOs represent an immature form of oligodendrocytes, and the GF- PDOs represents a more mature form of oligodendrocytes. The *CASP1*, *GSDMD*, *CASP8*, *FADD*, *TRADD*, *TRAF2*, and *IL1B* qRT-PCR results (Fig. 3.3, 3.7), the LDH assay results from GF- PDOs (Fig. 3.10) and the graphical results from immunocytochemistry analyses (Fig. 3.11-3.13, but not the images) from TNFα stimulated PDOs presented in this chapter have been published as part of McKenzie, B.A., Mamik, M.K., Saito, L.B., Boghozian, R., Monaco, M.C., Major, E.O., Lu, J.Q., Branton, W.G., and Power, C. Caspase-1 inhibition prevents glial inflammasome activation and pyroptosis in models of multiple sclerosis. *Proceedings of the National Academy of Sciences of the United States of America.* 2018 Jun 26; 115(26): E6065–E6074[116]. All experimental analyses were performed by myself except for the Type I IFN bioassay (Fig. A.3), which was performed by Dr. Meziane.

3.1 TNFα exposure reduces oligodendrocyte cell marker expression in PDOs

To confirm oligodendrocyte stress can be observed *in vitro*, PDOs were stimulated with increasing concentrations of TNFα, a cytokine that is highly expressed in MS brains[5]. After a 24-hour exposure, cells were collected, and transcriptional changes in oligodendrocyte cell markers, *OLIG1*, *PLP*, *NG2*, and *CNP*, were first assessed by qRT-PCR (Fig. 3.1). TNFα exposure led to transcript reduction in *OLIG1* (Fig. 3.1A), a gene encoding an oligodendrocyte specific transcription factor, and *PLP* (Fig. 3.1B), a gene encoding the most abundant myelin protein expressed in the CNS, in GF- PDOs. In contrast, GF+ PDOs displayed an increase in *NG2* transcript levels (Fig. 3.1C), a proteoglycan gene enriched in OPCs, at low TNFα concentrations. *CNP*, a gene for a myelin-associated enzyme, did not show reduced transcriptional activity in PDOs stimulated with TNFα (Fig. 3.1D). In addition to assessing oligodendrocyte associated transcriptional changes in TNFα exposed PDOs, the changes in MBP protein expression was also assessed by in-cell Western analysis (Fig. 3.2).

Approximately three-fold reduction in MBP protein levels were observed in GF- PDOs (Fig. 3.2B), whereas no changes were observed in GF+ PDOs (Fig. 3.2A). The reduction in *OLIG1* and *PLP* transcript, along with reduction in MBP protein expression in GF- PDOs demonstrated the sensitive nature of these cells towards TNFα. The increase in *NG2* transcript at low TNFα concentrations in GF+ PDOs might suggest these cells could be reverting to a more OPC like phenotype. Collectively these results show oligodendrocyte injury, as determined by altered oligodendrocyte associated transcript and protein expression, can be observed *in vitro* using PDOs.

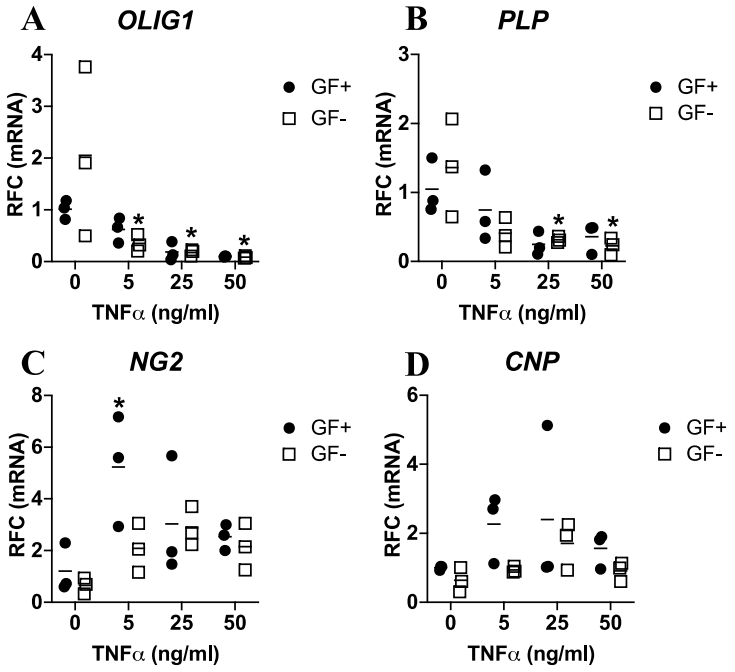

Figure 3.1 TNFα exposure leads to reduction of oligodendrocyte associated transcripts in GF- PDOs. qRT-PCR analysis of oligodendrocyte markers, *OLIG1* (A), *PLP* (B), *NG2* (C), and *CNP* (D), were performed on GF+ (black circles) and GF- (white squares) PDOs exposed to increasing concentrations of TNFα for 24 hours (n = 3). TNFα exposure led to down regulation of *OLIG1* and *PLP* in GF- PDOs, whereas low concentration of TNFα GF induced *NG2* expression in GF+ PDOs. *p-value<0.05 by two-way ANOVA with Tukey's multiple comparison analysis. Asterisks indicate significant values when compared to corresponding controls.

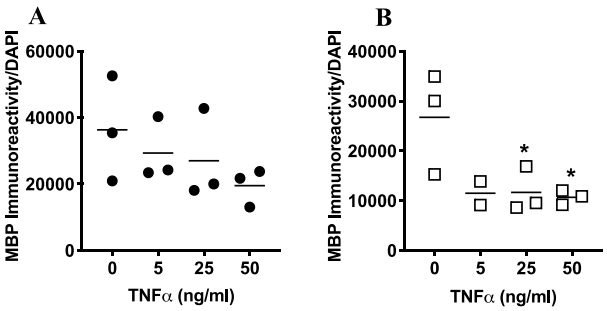

Figure 3.2 TNFα exposure reduces myelin basic protein (MBP) expression in GF- PDOs. In-cell Western analysis of MBP immuoreactivity was performed on GF+ (A), and GF- (B) PDOs exposed to increasing concentrations of TNFα for 24 hours (n = 3). MBP immunoreactivity was normalized to corresponding cellular DNA staining (DAPI). Higher TNFα concentrations induced lower MBP expression only in GF- PDOs. *p-value<0.05 by one-way ANOVA with Tukey's multiple comparison analysis. Asterisks indicate significant values when compared to corresponding controls.

3.2 TNFα exposure induces transcriptional changes of innate immune genes in PDOs. As myelinating cells of CNS, there are very few studies reporting the involvement of human oligodendrocytes in innate immune responses and inflammation. To determine if any transcriptional changes in innate immune genes were induced, qRT-PCR analysis on TNFα-exposed GF+ and GF- PDOs were conducted on a variety of inflammasome-related (Fig. 3.3) and Type I IFN-related (Fig 3.4) genes. More than a 100-fold increase in *CASP1* transcript (Fig. 3.2A) and a 30-fold increase in *GSDMD* transcript (Fig. 3.2B) was observed in GF- PDOs exposed to TNFα. No other prominent inflammasome genes were found to be induced in GF- PDOs, such as *NLRP3* (Fig. 3.2C), *IL1B* (Fig. 3.2D) and *ASC* (Fig. 3.2G), which all are well known for its role in mediating the canonical inflammasome activation[82]. On the other hand, TNFα exposure reduced *CASP6* transcript in GF+ PDOs (Fig. 3.2F). With regards to Type I IFN-related genes, a significant induction of *IFNB* (Fig. 3.4A), *MX1* (Fig. 3.4B), *BST2* (Fig. 3.4C), *IRF1* (Fig. 3.4D), *IRF3* (Fig. 3.4E), and *IRF7* (Fig. 3.4F) transcripts were observed in GF- PDOs that were exposed to higher concentrations of TNFα. Only *BST2* was inducible in exposed GF+ PDOs. In combination with results observed in Fig. 3.1 and

Fig 3.2, there is a clear maturation-state dependent response in PDOs when stimulated with TNFα. TNFα exposed GF- PDOs displayed a reduction in oligodendrocyte-associated gene transcripts together with induction of innate immune gene transcripts, whereas only a limited response was observed in TNFα exposed GF+ PDOs. These results suggest mature, potentially myelinating oligodendrocytes might be more sensitive to proinflammatory environments that are present in diseases such as MS, compared to its immature counterparts.

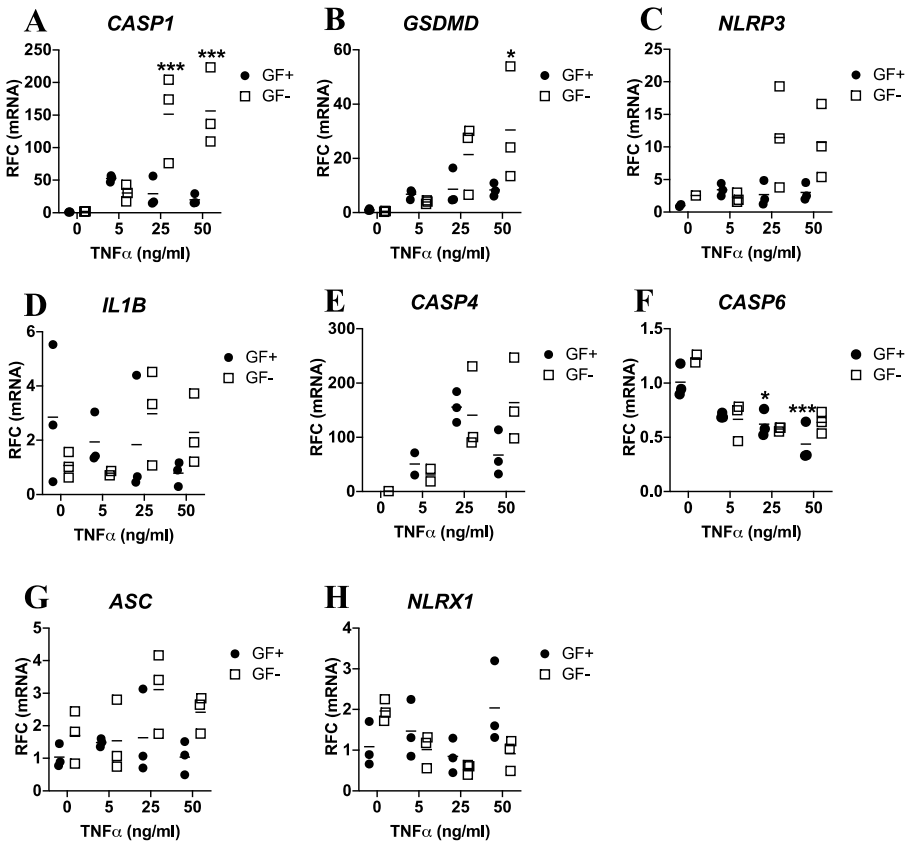

Figure 3.3 TNFα exposure leads to altered inflammasome-related gene expression in GF- PDOs. qRT-PCR analysis of inflammasome associated genes, *CASP1* (A), *GSDMD* (B), *NLRP3* (C), *IL1B* (D), *CASP4* (E), *CASP6* (F), *ASC* (G), and *NLRX1* (H) were performed on GF+ (black circles) and GF- (white squares) PDOs exposed to increasing concentrations of TNFα for 24 hours ($n = 3$). *CASP1* and *GSDMD* were highly induced in GF- PDOs after TNFα exposure. *p-value<0.05, ***p-value<0.001 by two-way ANOVA with Tukey's multiple comparison analysis. Asterisks indicate significant values when compared to corresponding controls.

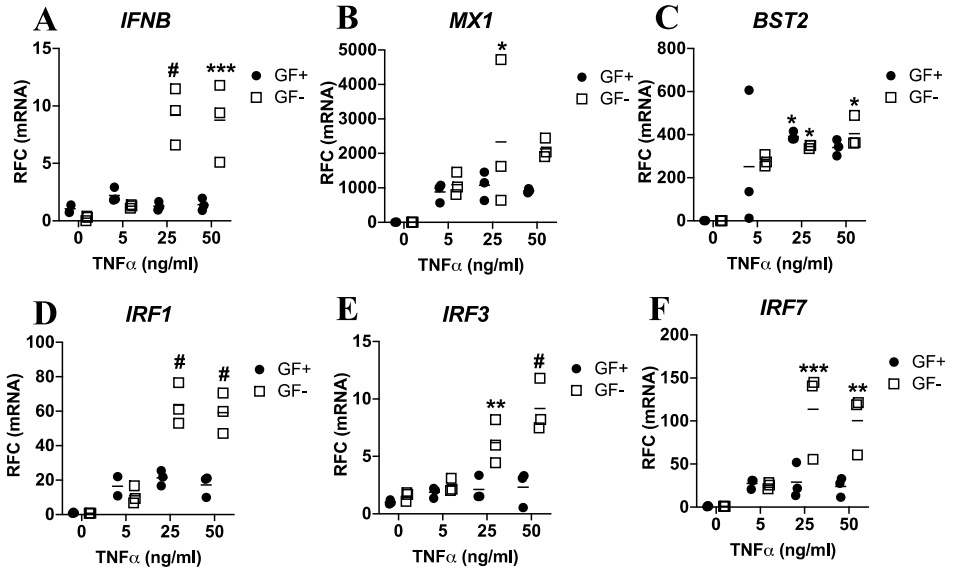

Figure 3.4 TNFα exposure leads to induction of Type I IFN-related genes in GF- PDOs. qRT-PCR analysis of Type I IFN associated genes, *IFNB* (A), *MX1* (B), *BST2* (C), *IIRF1* (D), *IRF3* (E), and *IRF7* (F) were performed on GF+ (black circles) and GF- (white squares) PDOs exposed to increasing concentrations of TNFα for 24 hours (n = 3). Several Type I IFN-related genes were highly induced, such as *IFNB*, *IRF1*and *IRF3* in GF- PDOs, but not in GF+ PDOs. *p-value<0.05, **p- value<0.01, ***p-value<0.001, #p-value<0.0001 by two-way ANOVA with Tukey's multiple comparison analysis. Asterisks indicate significant values when compared to corresponding controls.

3.3 Innate immune gene transcriptional changes observed in GF- PDOs are dependent on stimulant.

To assess whether the induction of innate immune genes observed in GF- PDOs were specific to TNFα exposure, PDOs were infected with Mad-4 strain of JC virus (MOI of 1) for 3 days, or stimulated with IL-1β (20ng/ml) for 24 hours. Innate immune gene transcript induction was then assessed by qRT-PCR. The JC virus infection was performed because JC virus has tropism for glial cells, mainly oligodendrocytes and astrocytes[117]. IL-1β is a proinflammatory cytokine that is often induced in MS brains[5]. JC virus infection of PDOs was confirmed by detection of T-Ag transcript by qRT-PCR (Fig. A.1, page 132). As JC virus is a DNA virus, any residual viral genomic DNA in the cellular RNA samples would be

disintegrated by DNase I treatment that is performed prior to cDNA synthesis. Given this assumption, a reduction in T-Ag Ct values by qRT-PCR in infected PDO samples relative to uninfected PDOs was suggestive of JC virus infection of these cells. Similar to TNFα exposed PDOs, a range of antiviral genes (Fig. 3.5) and inflammasome-related genes (Fig. 3.6) transcript induction was assessed. Out of all antiviral genes assessed in JC virus infected PDOs, *IRF7* was the only inducible gene in GF- PDOs (Fig. 3.5E). Among the inflammasome-related genes, *IL1B* (Fig. 3.6 C) and *CASP6* (Fig. 3.6E) transcript levels were induced in infected GF- PDOs, unlike genes such as *CASP1* (Fig. 3.2A) that was highly upregulated in TNFα exposed GF- cells. With JC virus infection, only a handful of genes were upregulated in GF- PDOs, and the magnitude of response was also limited, ranging from 1.5 to 2.5-fold induction. However, the limited response observed by infected PDOs might have been due to analysing the cells at 3 days post infection. The cellular response might have been different at 24 hours post infection compared to 3 days post infection. It is possible the initial transcriptional induction might have resolved by day 3-post infection. Additionally, the low innate immune transcript induction may also be contributed by the low input infectivity of JC virus[118].

Unlike TNFα exposed and JC virus infected cells, PDOs that were exposed to IL-1β did not show any transcriptional changes in innate immune genes observed (Fig. A.2, page 133). Overall, the innate immune gene transcriptional response observed in PDOs differed depending on the specific stimulus. Since greatest transcriptional changes were observed in TNFα exposed cells, subsequent studies were focused on TNFα stimulated cells.

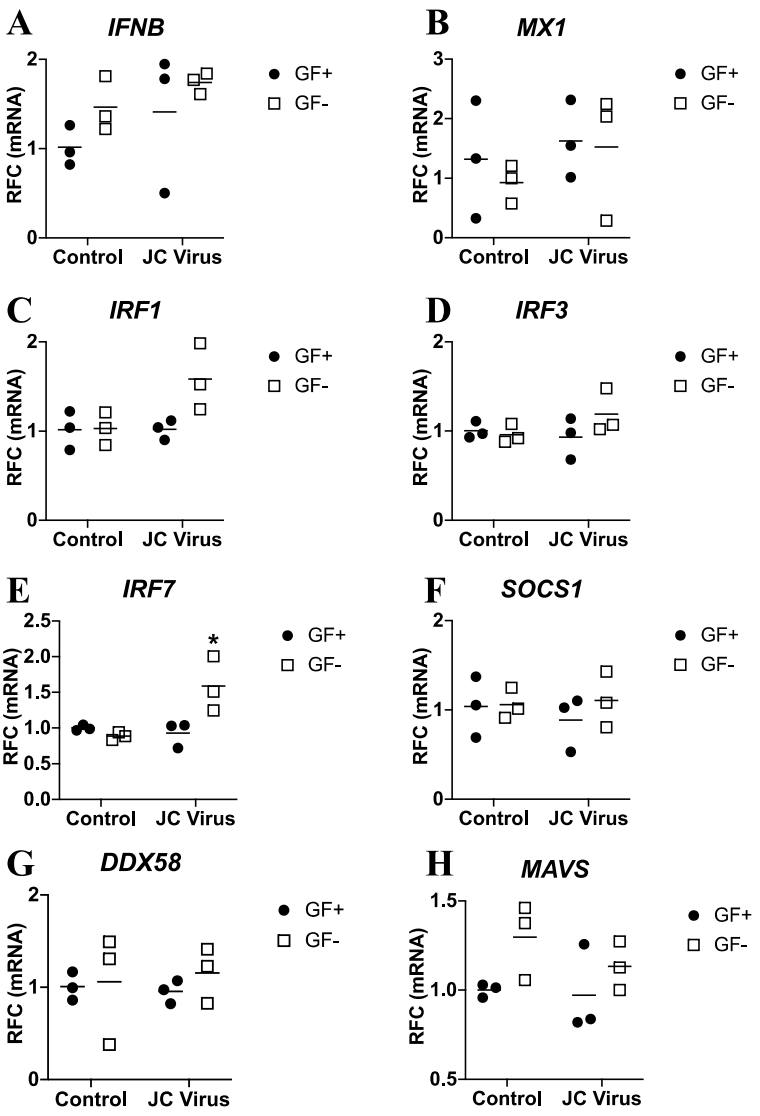

Figure 3.5 JC Virus infection causes restricted induction of antiviral genes in PDOs. qRT-PCR analysis of *IFNB* (A), *MX1* (B), *IRF1* (C), *IRF3* (D), *IRF7* (E), *SOCS1* (F), *DDX58* (G), and *MAVS* (H) were performed on GF+ (black circles) and GF- (white squares) PDOs infected with 1 MOI of Mad-4 strain of JC Virus for 3 days (n = 3). *IRF7* was only inducible in infected GF- PDOs. *p-value<0.05 by two-way ANOVA with Tukey's multiple comparison analysis. Asterisks indicate significant values when compared to corresponding controls.

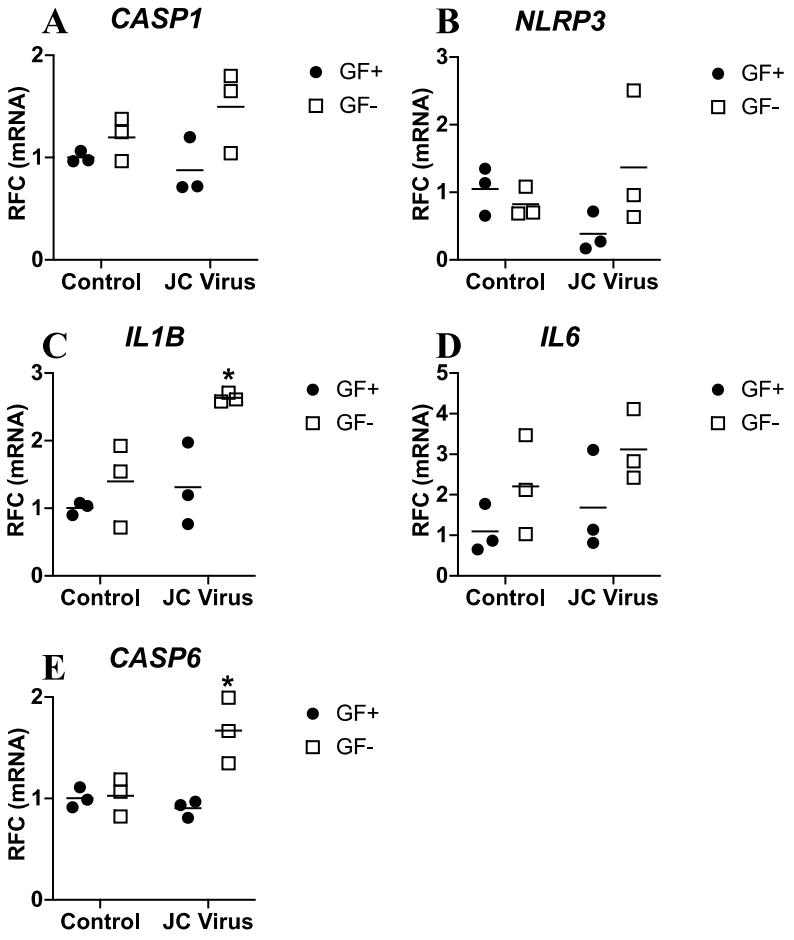

Figure 3.6 JC Virus infection induces limited transcriptional change in inflammasome-associated genes in PDOs. qRT-PCR analysis of *CASP1* (A), *NLR)P3* (B), *IL1B* (C), *IL6* (D), and *CASP6* (E) were performed on GF+ (black circles) and GF- (white squares) PDOs infected with 1 MOI of Mad-4 strain of JC Virus for 3 days ($n = 3$). *IL1B* and *CASP6* was inducible in GF- PDOs that were infected with JC virus. *p-value<0.05 by two-way ANOVA with Tukey's multiple comparison analysis. Asterisks indicate significant values when compared to corresponding controls.

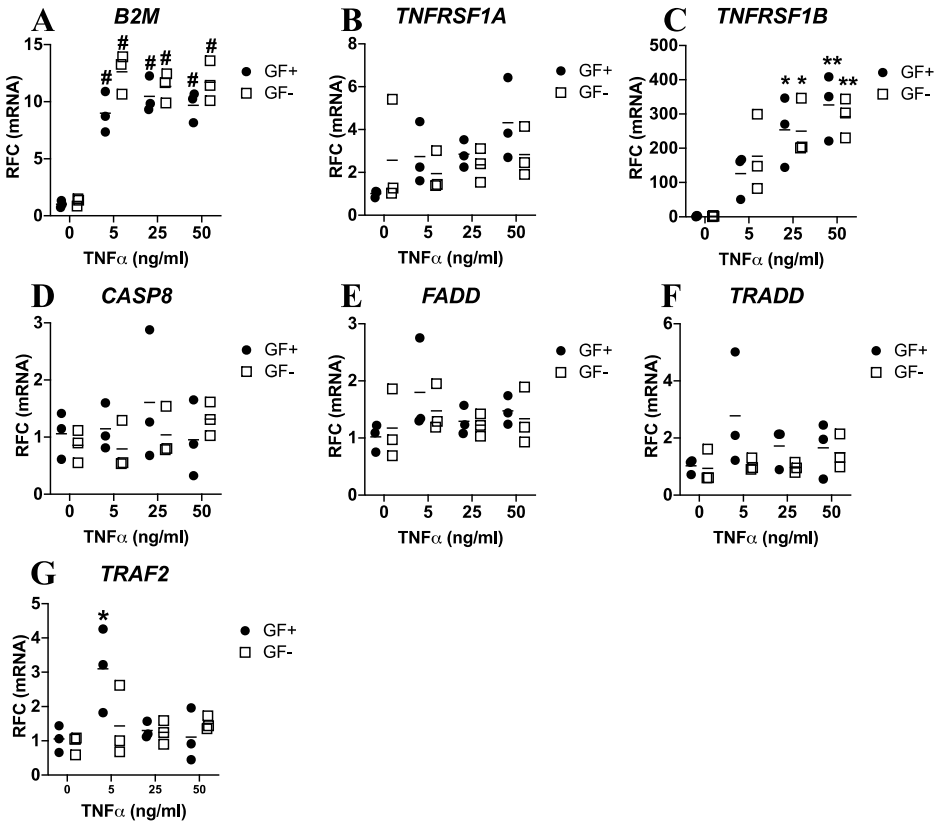

Figure 3.7 TNFα exposure leads to altered expression of inflammation- associated genes associated with inflammation in PDOs. qRT-PCR analysis of *B2M* (A), *TNFRSFA1* (B), and *IRF7* (C), *CASP8* (D), *FADD* (E), *TRADD* (F), and *TRAF2* (G) were performed on GF+ (black circles) and GF- (white squares) PDOs exposed to increasing concentrations of TNFα for 24 hours (n = 3). TNFα induced expression of *B2M* and *TNFRSF1B*, but not *TNFRSF1A* in GF+ and GF- PDOs. *TRAF2* expression was only induced in GF+ PDOs that were stimulated with low concentration of TNFα. *p-value<0.05, **p-value<0.01, #p-value<0.0001 by two-way ANOVA with Tukey's multiple comparison analysis. Asterisks indicate significant values when compared to corresponding controls.

3.4 TNFα exposure induces transcriptional changes of genes associated with inflammation.

Previous studies involving oligodendrocytes have described TNFα-associated apoptosis in oligodendrocytes[119, 120]. Nonetheless, there have been several different forms of

inflammatory cell death that have been characterised ever since the initial studies on oligodendrocytes were performed. As wide ranges of innate immune genes were found to be inducible in TNFα exposed PDOs (Fig. 3.3, 3.4), transcriptional changes in genes associated with inflammation and apoptosis were then assessed by qRT-PCR (Fig. 3.7). TNFα exposure highly induced *B2M* (Fig. 3.7A) and *TNFRSF1B* (Fig. 3.7C) transcripts in both GF+ and GF- PDOs, but not *TNFRSF1A* (Fig. 3.7C). The induction of *B2M* transcript, a gene that encodes β_2-microglobulin, was suggestive of the potential of these cells to express MHC-I molecules, which was recently demonstrated in murine oligodendrocytes in which the authors were able to show increased MHC-I and MHC-II expression in OPCs and oligodendrocytes[55]. The dichotomy between the TNFα receptor transcripts induced with TNFα exposure also suggested that PDOs might be undergoing an inflammatory phase, as TNF receptor superfamily member 1A (TNFRSF1A/TNFR1) is associated more with apoptosis[121], and TNFRSF1B (TNFR2) is more associated with inflammation[122]. This point is further underscored by the lack of apoptosis-related gene transcript induction in PDOs exposed to TNFα (Fig. 3.7D-G). In combination with the innate immune gene induction, these results suggest human oligodendrocytes might participate in inflammatory responses as well as undergo an inflammatory form of cell death instead of noninflammatory apoptosis.

3.5 Caspase-1 and gasdermin D proteins are detected in oligodendrocytes stimulated with TNFα.

Although transcript increase for multiple innate immune genes were observed in GF- PDOs, immunocytochemistry analysis was performed to confirm whether innate immune proteins were indeed produced in TNFα stimulated cells. Although many innate immune genes were found to be highly inducible with TNFα exposure, analyses was focused on caspase-1 and gasdermin D proteins because of its defined role in pyroptosis, an inflammatory form of programmed cell death that has been recently described[86]. Caspase-1 (Cy3) and gasdermin D (Cy5) immunoreactivity were detected in TNFα exposed GF- PDOs with minimal detection in control cells (Fig. 3.8). Caspase-1 and gasdermin D proteins were found along the cell membrane of immunopositive cells, an expected location in cells that are undergoing pyroptosis[123]. In addition, the cell bodies of GF- PDOs appeared to be smaller, with associated nuclear shrinkage compared to control cells. These results suggested that

oligodendrocytes are capable in generating proteins that are involved in inflammatory responses, raising the possibility that these cells were dying by a process other than apoptosis.

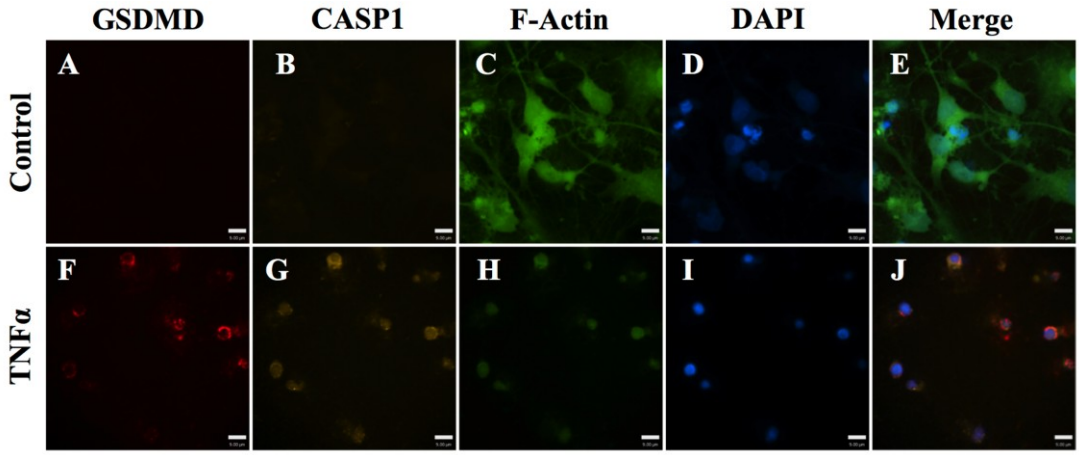

Figure 3.8 TNFα exposure induces pyroptosis-related protein expression in GF- PDOs. Immunofluorescence labeling of caspase-1 (CASP1, Cy3/amber), and gasdermin D (GSDMD, Cy5/red), and F-actin (FITC/green) and nuclear staining (DAPI/blue) were performed on GF- PDOs exposed to control (A-E) or 50ng/ml TNFα (F-G) for 24 hours. Caspase-1 and gasdermin D immunoreactivity were observed at the plasma membranes of subset of TNFα exposed cells, with associated nuclear shrinkage and reduced processes. Images were taken at 40X, size bars are 9 μm.

3.6 TNFα exposure does not promote inflammasome-associated cytokine release into cell supernatants by PDOs.

One of the described functions of caspase-1 is the ability to cleave pro-IL-1β and pro-IL-18 into their bioactive forms. As caspase-1 was detected in TNFα exposed GF- PDOs, supernatants from TNFα exposed GF+ and GF- PDOs were assessed for IL-1β and IL-18 release by ELISA (Fig. 3.9). Negligible IL-1β was detected in supernatants from GF+ and GF- PDOs (Fig. 3.9A and B). The levels of IL-18 detected in supernatants from TNFα exposed PDOs did not exceed the media only control (Fig. 3.9C and D), and thus any IL-18 detected in the TNFα exposed PDOs are also most likely contributed by culture media.

Overall, these results implied that IL-1β and IL-18 were not released into the supernatants by PDOs, despite the detection of caspase-1 in TNFα exposed GF- cells.

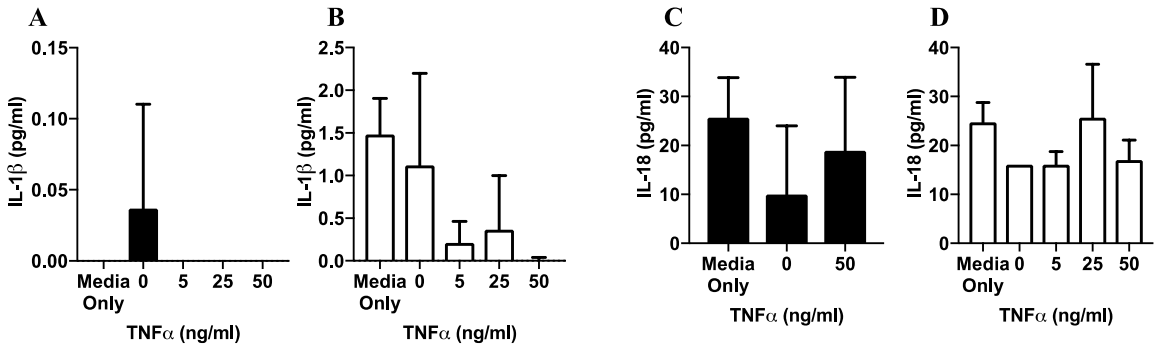

Figure 3.9 TNFα exposure does not cause the release of inflammasome- associated cytokines in PDOs. Supernatants from GF+ (white bars) and GF- (black bars) PDOs exposed to increasing concentrations of TNFα for 24 hours were analyzed for IL-1β (A and B) and IL-18 (C and D) release by ELISA (n = 3). IL-1β and IL-18 detected in supernatant samples did not exceed the media only conditions, suggesting negligible release of these cytokines after TNFα exposure.

Although IL-1β and IL-18 could not be detected in supernatants from PDOs, Type I IFN bioactivity was detected in supernatants when PDOs were exposed to TNFα, or infected with JC virus (Fig. A.3, page 134). Supernatants from TNFα exposed GF+ and GF- PDOs displayed a modest increase in Type I IFN activity at higher concentrations (Fig. A.3A, B). Type I IFN activity detected in supernatants from JC virus infected GF+ and GF- PDOs were much greater than in supernatants from TNFα exposed PDOs. For both stimuli, Type I IFN activity in these supernatants likely reflected IFNβ, as *IFNB* was the only Type I IFN transcript that was detected by qRT-PCR in these cells. Interestingly, although the induction of *IFNB* transcript was only detected in TNFα exposed cells, the JC virus infected cells had greater IFNβ in the supernatants, supporting the notion that gene transcription does not necessarily correlate with corresponding protein production.

3.7 TNFα stimulates the release of lactate dehydrogenase (LDH) into supernatants by PDOs.

Although release of IL-1β and IL-18 from PDOs could not be detected, the possibility of PDOs undergoing pyroptosis could not be eliminated as pyroptosis can take place in the absence of IL-1β release[90, 91]. The exposure of TNFα might not have been sufficient for IL-1β production and release by PDOs. Furthermore, since gasdermin D protein was detected in TNFα exposed GF- PDOs, the possibility of gasdermin D functioning as a pore-protein without release of IL-1β could not be dismissed. To assess whether TNFα exposure caused cell membrane damage due to activity of a pore-forming protein, such as gasdermin D, an LDH release assay was performed using supernatants from TNFα exposed PDOs (Fig. 3.10). Supernatants from TNFα exposed PDOs had increased LDH activity, with approximately 50% and 30% increase in LDH activity detected in TNFα stimulated GF+ (Fig. 3.10A) and GF- (Fig. 3.10B) PDOs, respectively. Based on these results, it was not possible to fully confirm gasdermin D function is the cause of the LDH release in TNFα stimulated PDOs. However, in combination with the immunocytochemistry data on caspase-1 and gasdermin D in GF- cells (Fig 3.8), the increased LDH activity in TNFα exposed cells suggested pyroptosis might be occurring in these cells.

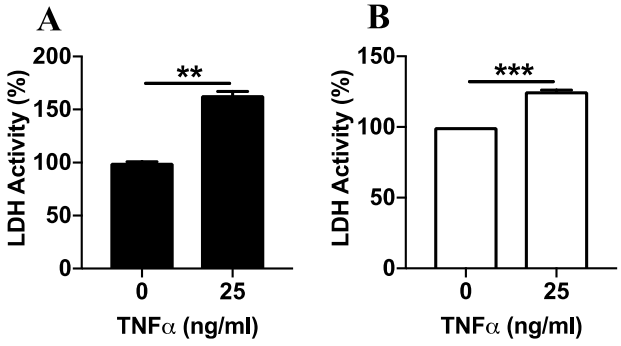

Figure 3.10 TNFα exposure induces lactate dehydrogenase (LDH) release by PDOs. Supernatants of GF+ (black bars, A) and GF- (white bars, B) PDOs exposed to 0 or 50ng/ml of TNFα for 24 hours were analyzed for LDH release (n = 3). LDH release was detected by GF+ and GF- PDOs. **p-value<0.01, ***p-value<0.001, by Student t-test.

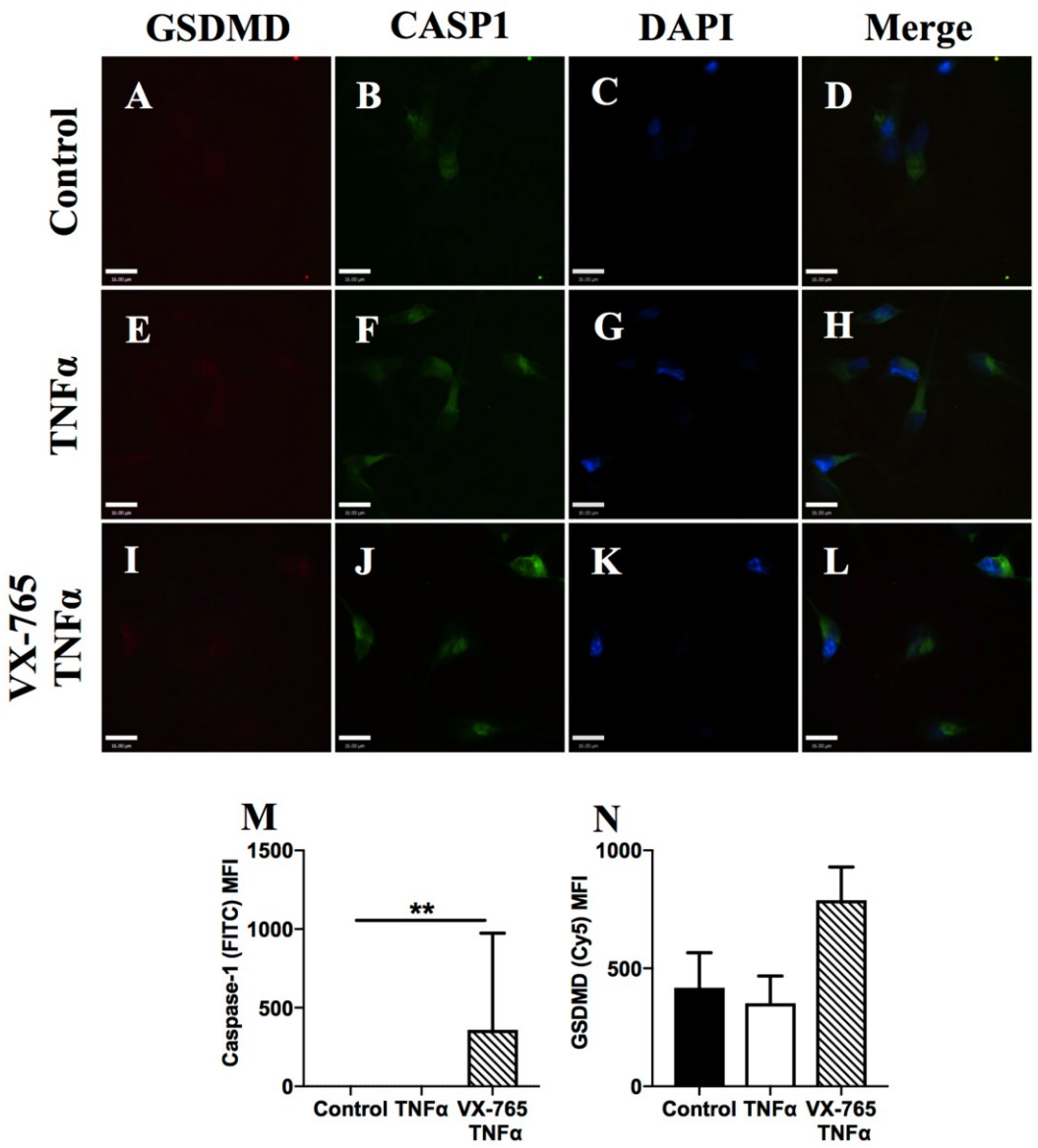

Figure 3.11 VX-765 pre-treatment has limited effect on pyroptosis-related protein expression in GF+ PDOs that were exposed to TNFα. Immunofluorescence staining of caspase-1 (CASP1, FITC/green), and gasdermin D (GSDMD, Cy5/red), with co-labelling of nuclei (DAPI/blue) were performed on GF+ PDOs exposed to control (A-D), 24 hour 50ng/ml TNFα (E-H), or 24 hour 50ng/ml TNFα with 4 hour 50μM VX-765 pre-treatment (I-L). Images were taken at 40X, size bars are 16 μm. Caspase-1 (FITC, M) and GSDMD (Cy5, N) immunofluorescence intensities relative to background was subsequently measured by selecting the cell bodies of PDOs. At least 100 cells from each condition were quantified. **p-value<0.01 by one-way ANOVA with Tukey's multiple comparison analysis.

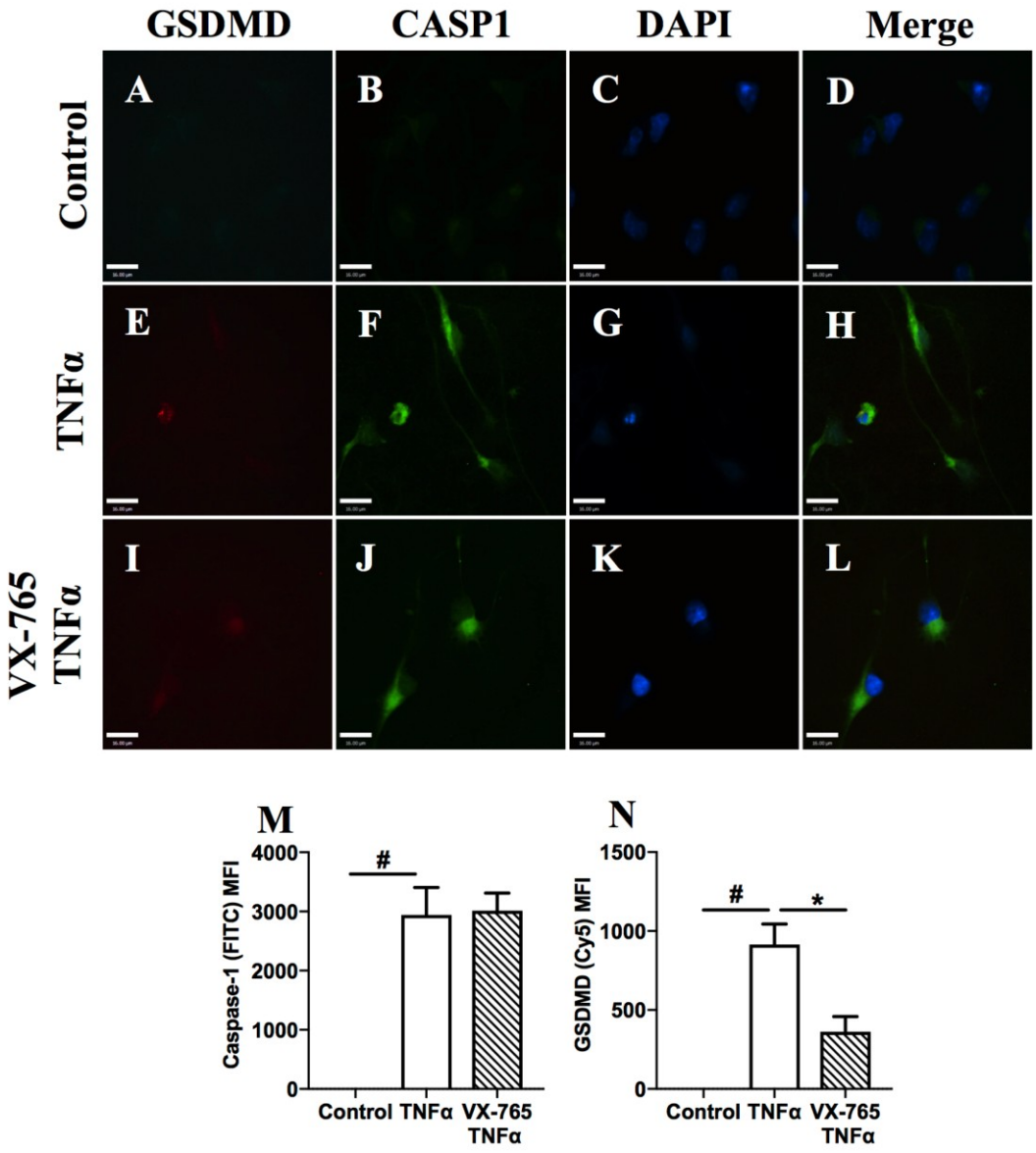

Figure 3.12 VX-765 pre-treatment reduces pyroptosis-related protein expression in GF-PDOs that were exposed to TNFα. Immunofluorescence labelling of caspase-1 (CASP1, FITC/green), and gasdermin D (GSDMD, Cy5/red), with co-labelling of nuclei (DAPI/blue), were performed on GF- PDOs exposed to control (A-D), 24 hour 50ng/ml TNFα (E-H), or 24 hour 50ng/ml TNFα with 4 hour 50μM VX-765 pre-treatment (I-L). Images were taken at 40X, size bars are 16μm. Caspase-1 (FITC, M) and GSDMD (Cy5, N) immunofluorescence intensities relative to background were subsequently measured by selecting the cell bodies of PDOs. At least 100 cells from each condition were quantified. *p-value<0.05, #p-value<0.0001 by one-way ANOVA with Tukey's multiple comparison analysis.

3.8 VX-765 treatment reduces TNFα induced caspase-1 and gasdermin D production in GF- PDOs.

To test whether caspase-1 is functional in TNFα exposed PDOs, cells were pre-treated with VX-765, a caspase-1 inhibitor[124], prior to TNFα exposure. VX-765 is a pro-drug that becomes active upon cleavage by host esterases. Once active, this drug acts as a high affinity active site inhibitor of caspase-1, and caspase-4 to a lesser extent. The effects on innate immune genes transcription, specifically *CASP1* and *GSDMD* was first assessed by qRT-PCR on VX-765 pre-treated, TNFα exposed PDOs (Fig. A.4, page 135). VX-765 pre-treatment had no effect on *CASP1* (Fig. A.4A) or *GSDMD* (Fig. A.4B) transcript levels induced by TNFα stimulation of GF- PDOs. These results were not unexpected, as caspase-1 is not known to act as a transcription factor.

To complement these studies, the effects of VX-765 on caspase-1 and gasdermin D by PDOs were assessed by immunocytochemistry. Although VX-765 did not influence transcriptional changes observed in TNFα exposed PDOs, it was more likely that the drug would have effects on protein production, specifically gasdermin D, since gasdermin D is an established substrate for caspase-1[86]. Sine caspase-1 and gasdermin D proteins were detected by immunofluorescence labelling (Fig. 3.8), a similar approach was taken to assess caspase-1 and gasdermin D protein expression on TNFα stimulated PDOs with VX-765 pre-treatment (Fig. 3.11 and 3.12). The fluorescence intensities of caspase-1 (FITC) and gasdermin D (Cy5) were quantified in cell bodies of GF+ (Fig. 3.11) and GF- (Fig. 3.12) PDOs by subtracting background levels from the raw values obtained in the analysis software, Volocity. Minimal caspase-1 (FITC) immunoreactivity was observed in control and TNFα exposed GF+ PDOs (Fig 3.11B, F and N), whereas a significant increase in caspase-1 immunoreactivity in VX-765 pre-treated TNFα exposed cells were detected (Fig. 3.11J and N). A similar trend was observed in gasdermin D, in which gasdermin D (Cy5) immunoreactivity for control (Fig. 3.11A and M) and TNFα (Fig. 3.11E and M) exposed cells were similar, and the fluorescence intensity was greater in cells with VX-765 pre-treatment (Fig. 3.11I and M). In contrast, caspase-1 (FITC) immunofluorescence was highly abundant in all TNFα exposed GF- cells (Fig. 3.12B, F, J and N). Gasdermin D (Cy5) was also observed in all TNFα exposed cells, with immunoreactivity being significantly lower in

cells that received VX-765 pre-treatment (Fig. 3.12A, E, I and M). Overall, TNFα exposure stimulated the production of caspase-1 and gasdermin D proteins by GF- PDOs, whereas no changes in protein expression was observed in GF+ cells. In GF- PDOs, VX-765 pre-treatment did not prevent caspase-1 protein induction, but it reduced the gasdermin D protein levels, whereas in GF+ PDOs, VX-765 pre-treatment appeared to only promote caspase-1 expression. As a caspase-1 inhibitor, VX-765 might have little effect on reducing caspase-1 protein expression. However, the reduction of gasdermin D protein expression by VX-765 suggested that there is active caspase-1 produced in GF- PDOs in response to TNFα exposure, as the presence of VX-765 in these cells are preventing the production of gasdermin D. In combination with earlier results, the presence of active caspase-1 and gasdermin D suggested that pyroptosis was occurring in GF- PDOs without IL-1β release. Collectively, these results show how the maturation state can influence the response generated from the same proinflammatory stimuli.

3.9 VX-765 treatment prevents morphological changes induced by TNFα exposure in GF- PDOs but not in GF+ PDOs.

In addition to quantifying caspase-1 and gasdermin D protein production by PDOs, the morphological alterations caused by TNFα exposure was also assessed in order to determine whether caspase-1 activity was also involved in morphological changes. To quantify these morphological alterations in PDOs, the F-actin of TNFα stimulated PDOs were fluorescently labelled with ActinGreen 488 ReadyProbe reagent (Life Technologies), and the number of processes, and the length of individual processes were measured using the Volocity software (Fig. 3.13). As observed in the fluorescence images, there appeared to be minimal differences in the appearances of GF+ PDOs across all groups (Fig. 3.13A-C). Other than a modest, albeit significant increase in process number in VX-765 and TNFα exposed cells, the number and length of processes was similar across all groups (Fig. 3.10D and E). Morphological changes were more evident in GF- PDOs, where TNFα stimulated PDOs appeared to have fewer and shorter processes (Fig. 3.13H), which was rescued with VX-765 pre-treatment (Fig. 3.13I). Indeed, TNFα stimulation led to fewer processes per cell (Fig. 3.13J), and shorter processes (Fig. 3.13K), both of which were recovered with VX-765 pre-treatment.

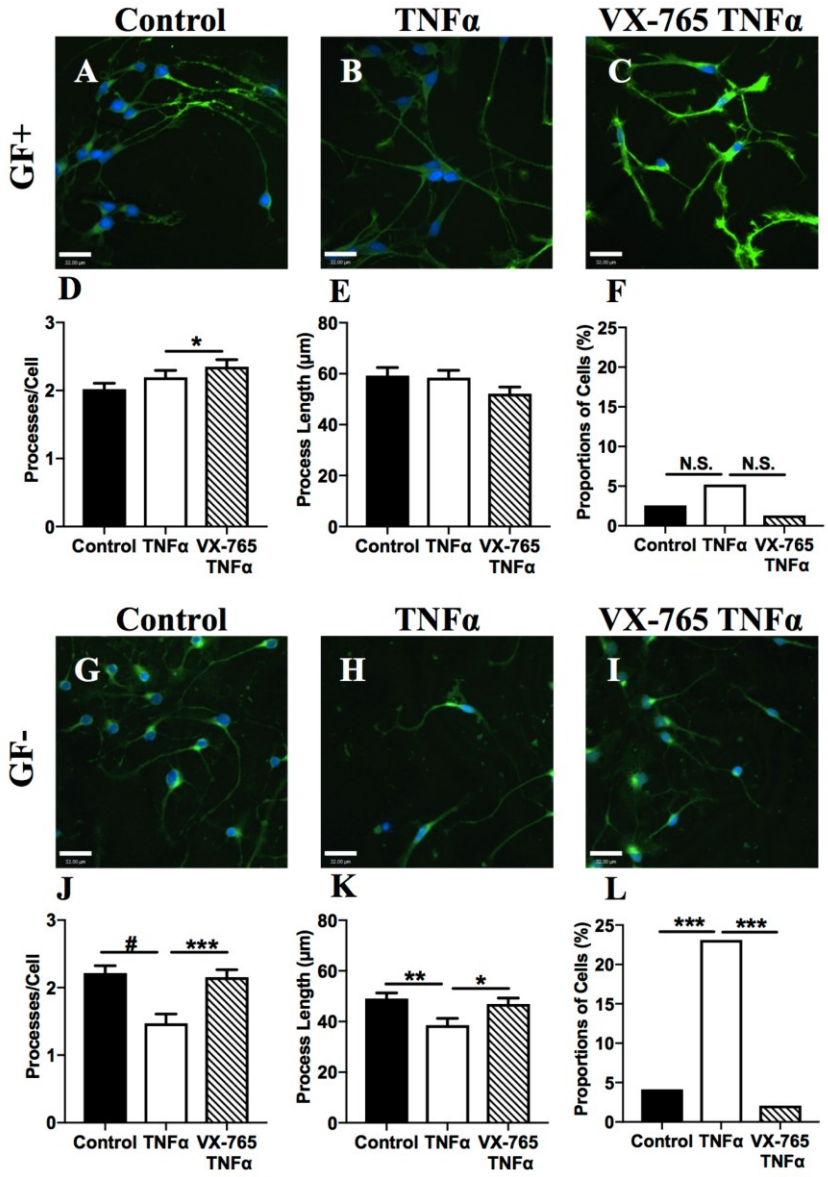

Figure 3.13 VX-765 pre-treatment prevents pyroptosis induced by TNFα in GF- PDOs, but not GF+ PDOs. F-actin (FITC/green) and nuclear staining (DAPI/blue) were performed on GF+ (A-C) and GF- (G-I) PDOs exposed to control, 24-hour 50ng/ml TNFα, or 24-hour 50ng/ml TNFα with 4-hour 50μM VX-765 pre- treatment. Images were taken at 20X, size bars are 32μm. PDO process length (D and J), number of processes from a single PDO (E and K), and number of pyroptotic cells (F and L) from each condition were quantified for GF+ (D-F) and GF- (J-L) PDOs. At least 100 cells were quantified for all measurements. *p-value<0.05, **p-value<0.01, ***p-value<0.001, #p-value<0.0001 by one-way ANOVA with Tukey's multiple comparison analysis (D, J, K), and ***p-value<0.001 by χ^2-test (L).

Dying cells were defined as cells with nuclear staining that lacked processes, which were counted in all experimental conditions. The number of dying cells was similar in GF+ PDOs across all conditions (Fig. 3.13F). In contrast, there was more than a 5-fold increase in the number of dying cells in GF- PDOs that were exposed to TNFα, compared to controls (Fig. 3.13L), with 23% of total cells having no processes in the TNFα group. This increase in dying cell counts was rescued by pre-treatment with VX-765. Since the reduction in the number of dying cells observed was with a caspase-1 inhibitor, these cells are unlikely to be undergoing apoptosis because caspase-1 is well documented to be not involved in apoptosis. Furthermore, these findings further support the notion these cells were undergoing pyroptosis, a caspase-1 and gasdermin D dependent form of cell death.

Chapter 4 – *In vivo* results: Developing the cuprizone model of demyelination

To investigate whether the innate immune molecules generated by PDOs *in vitro* can be observed *in vivo*, demyelinating brains from cuprizone-fed mice, were examined.
The cuprizone model of toxic demyelination was pursued instead of EAE because unlike EAE, cuprizone mediated demyelination is consistently observed on the same anatomic sites within the brain, such as the corpus callosum and hippocampus, making it easier to study oligodendrocytes in demyelinated areas[103]. In addition, the cuprizone model has the added benefit of also displaying local inflammation without infiltrating adaptive immune cells, such as autoreactive T-cells that are generated during EAE that can target oligodendrocytes directly[103, 104, 105]. This model thus permits examination of oligodendrocytes in the setting of localised, innate immune-mediated inflammation. To assess oligodendrocytes in cuprizone-fed mice brains, the cuprizone model was first optimised.

4.1 Demyelination is observed when mice are fed with 0.5% cuprizone diet, and not with 0.3% cuprizone diet.

To glean insights into the effects of cuprizone dose on ensuing demyelination, female C57BL/6J mice were fed with chow containing 0% (control), 0.3% or 0.5% cuprizone for 6 weeks. Weights for all mice were monitored weekly (Fig. A.5, page 136), as weight loss is a feature in this model. There were no differences observed in the weights between 0% and 0.3% cuprizone-fed groups, as both groups gained weight over the course of the experiment. Mice that were fed the 0.5% cuprizone diet steadily lost weight over the first three weeks of the experiment, and then started to gain weight back to baseline levels by the end of the experiment.

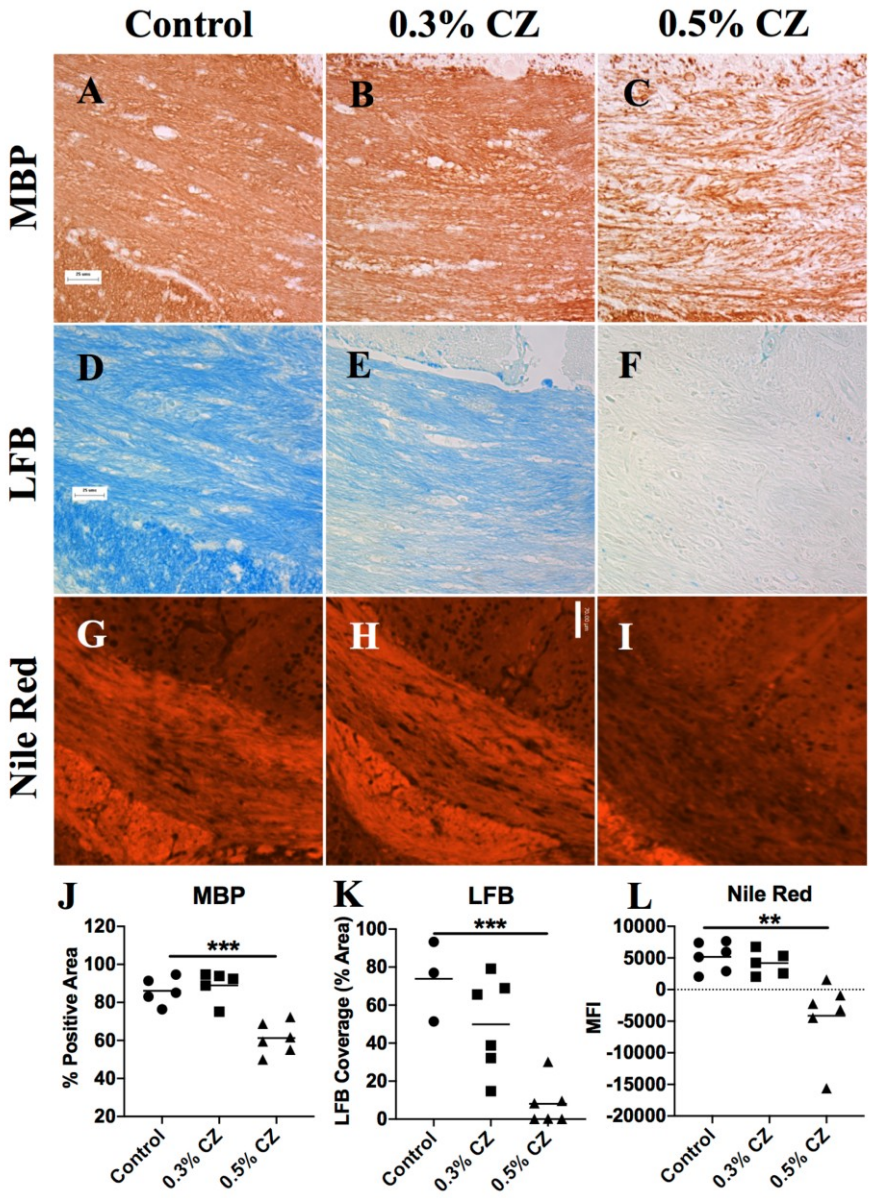

Figure 4.1 Demyelination is evident in mice receiving high dose cuprizone diet. Corpus callosum of female C57BL/6J mice fed with 0, 0.3 or 0.5% cuprizone (CZ) diet for 6-weeks were immunolabelled for MBP (A-C), stained with LFB (D-F), and with Nile Red (G-I). Quantification of MBP immunopositive area (J), LFB positive area (K) were performed using ImageJ software (n = 6). Quantification of Nile Red staining intensities (L) was performed using Volocity software (n = 6). Evident myelin loss is observed in mice fed with 0.5% cuprizone diet. MBP and LFB images are 40X, size bars are 25µm. Nile Red images are10X, size bars are 70µm. **p-value<0.01, ***p-value<0.001 by one-way ANOVA with Tukey's multiple comparison analysis.

Upon termination of the experiment, brains were harvested, PFA-fixed, paraffin-embedded from which brain sections were prepared and then were assessed for demyelination by performing MBP immunohistochemistry, and by LFB or Nile Red staining of myelin lipids (Fig. 4.1). Positive labelling of MBP and LFB, and Nile Red fluorescence intensity at the corpus callosum was quantified (Fig. 4.1J-L). MBP immunoreactivity (Fig. 4.1A-C, J), and Nile Red staining (Fig. 4.1G-I, L) of 0.3% cuprizone mice were similar to the 0% group. No difference in LFB staining (Fig. 4.1D-F, K) between 0% and 0.3% cuprizone groups was observed, but there was substantial variation in LFB positive area in 0.3% cuprizone group. In the 0.5% cuprizone group, not only was there a reduction in MBP immunopositive area (Fig. 4.1J), the myelin integrity appeared to be disrupted. LFB and Nile Red staining was absent in the corpus callosum of the 0.5% cuprizone group, and significant reductions in these stains were observed in this group (Fig. 4.1K and L). Overall, the analysis of the corpus callosum using these three methods highlighted demyelination in the 0.5% cuprizone group but not in 0.3% cuprizone group.

4.2 Cuprizone-induced glial cell activation

After assessing demyelination, changes in glial cell population in the corpus callosum were assessed by immunohistochemistry or by immunofluorescence analyses (Fig 4.2). In brain sections labelled with LFB and immunolabelled for Iba-1, a common marker for microglia and infiltrating macrophages, only the corpus callosum from 0.5% cuprizone group exhibited increased Iba-1 immunoreactivity, with accompanying loss of LFB staining compared to the 0% cuprizone group (Fig. 4.2A-C). Quantification of Iba-1 labelling revealed that the 0.5% cuprizone group showed an increase in Iba-1 immunopositive area, with more than a 10-fold increase in immunoreactivity (Fig. 4.2 G). The changes in astrocyte population were assessed by GFAP immunofluorescence analyses, with concurrent MBP immunolabelling. Similar to results observed on Fig. 4.1, the MBP (FITC) immunoreactivity was reduced in the 0.5% cuprizone group. GFAP (Cy3) immunoreactivity also appeared to be increased in the 0.5% cuprizone group (Fig. 4.2D-F). Approximately a 2-fold increase in Cy3 Mean Fluorescence Intensity (MFI) was observed in the 0.5% cuprizone group compared to the 0% cuprizone controls (Fig. 4.2H). These results highlighted that there was a significant increase in

microglial and astrocytic immunoreactivity in the corpus callosum of the 0.5% cuprizone group, whereas limited changes were observed in the 0.3% cuprizone group.

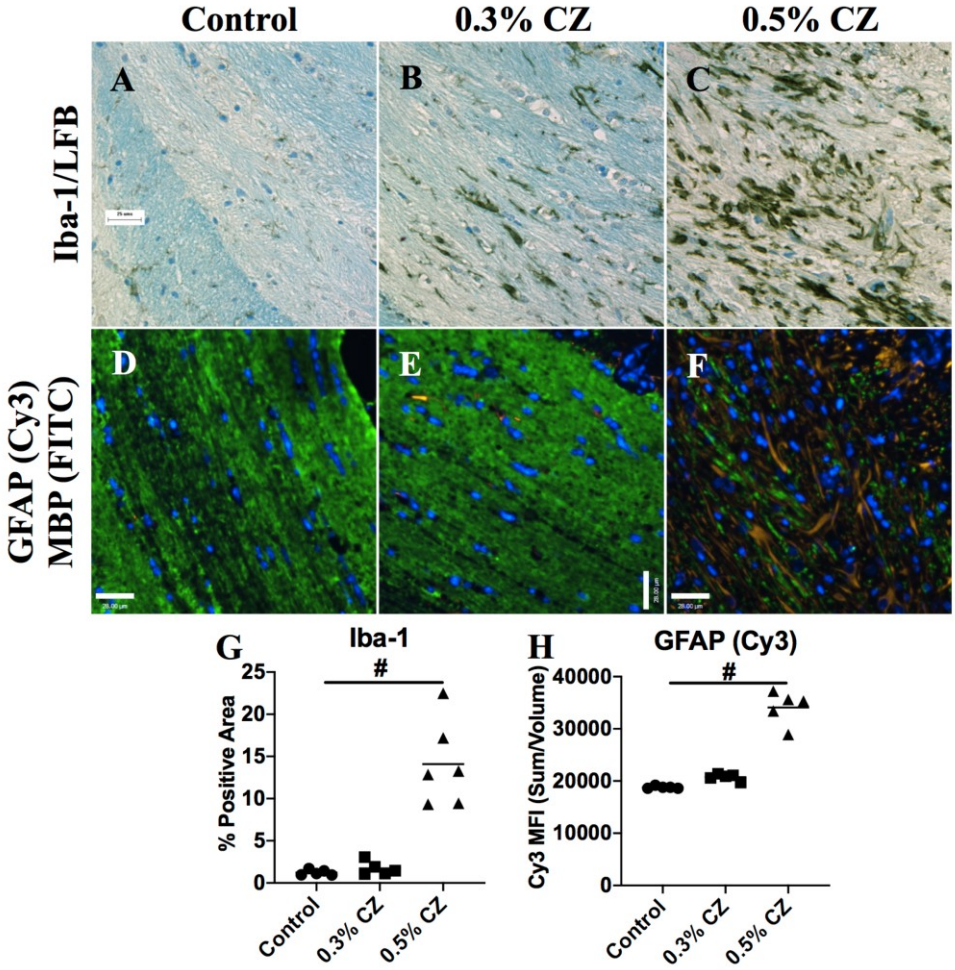

Figure 4.2 Glial cell activation is evident in mice receiving high dose cuprizone diet. Corpus callosum of female C57BL/6J mice fed with 0, 0.3 or 0.5% cuprizone (CZ) diet for 6-weeks were immunolabelled for Iba-1 (A-C), or sections were fluorescently immunolabelled with MBP (FITC/green), GFAP (Cy3/amber) and nuclei (DAPI/blue) (D-F). Quantification of Iba-1 immunopositive area was performed using ImageJ software (n = 6). Quantification of GFAP (Cy3) MFI was performed by dividing total sum of fluorescence by volume of tissue assessed using Volocity software (n = 6). DAB Images were taken at 40X, size bars are 25µm. Fluorescence images are 20X, size bars are 28µm. #p-value<0.0001 by one-way ANOVA with Tukey's multiple comparison analysis.

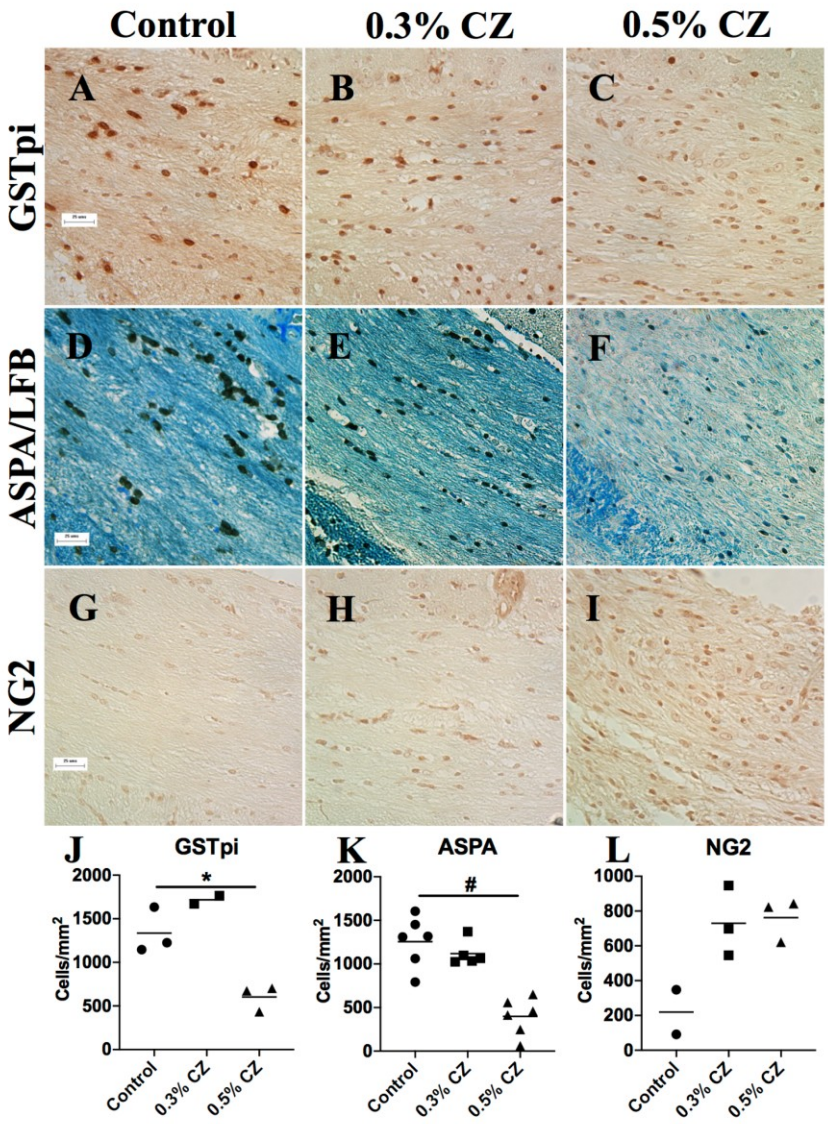

Figure 4.3 Oligodendrocyte loss is observed in the corpus callosum of mice receiving high dose cuprizone diet. Corpus callosum of female C57BL/6J mice fed with 0, 0.3% or 0.5% cuprizone (CZ) diet for 6-weeks were immunolabelled for GST-pi (A- C), ASPA (D-F), and NG2 (G-I). Quantification of GST-pi (J), ASPA (K), and NG2 (L) immunopositive cells were performed using ImageJ software (n = 3 for GST-pi and NG2, n = 6 for ASPA). Significant GST-pi and ASPA immunopositive cell loss with increase in NG2 immunopositive cells were observed only in mice fed with 0.5% cuprizone diet. Images were taken at 40X, size bars are 25µm. Statistics for NG2 could not be calculated due to missing controls. *p-value<0.05, #p-value<0.0001 by one-way ANOVA with Tukey's multiple comparison analysis.

4.3 Oligodendrocyte loss is observed with 0.5% cuprizone exposure.

In addition to assessing demyelination, the changes in mature oligodendrocyte and OPC populations were assessed by immunohistochemistry (Fig. 4.3). Oligodendrocytes were immunolabelled for GST-pi, a marker commonly used to label mature oligodendrocytes[125], and ASPA, an enzyme that is highly enriched in oligodendrocytes[33]. OPCs were immunolabelled against NG2, a protein that is enriched in OPCs[16]. Similar results were obtained with GST-pi (Fig. 4.3A-C, J) and ASPA (Fig. 4.3D-F, K) immunohistochemistry, where the immunopositive cells in the 0.3% cuprizone group were smaller than in the 0% cuprizone controls, although there were no differences in the number of immunopositive cells/mm^2. A significant reduction in GST-pi and ASPA immunopositive cells/mm^2 were observed in the 0.5% cuprizone group, and again the cell bodies appeared to be smaller than of controls. On the other hand, an apparent increase of NG2 positive cells/mm^2 was observed in the corpus callosum of cuprizone-fed mice, regardless of the concentration. OPCs are known to proliferate when there is loss of oligodendrocytes[16, 93]. The increase in NG2 immunopositive cells in the 0.5% cuprizone group were anticipated due to the loss of oligodendrocytes in this group. The increase in NG2 immunopositive cells in the 0.3% cuprizone group might have been due to the increase in injured oligodendrocytes, despite the lack of demyelination and loss of oligodendrocytes observed in these mice. In summary, the 0.5% cuprizone diet appeared to be required to induce demyelination, increase glial activation, and induce loss of oligodendrocytes. Thus, further analyses were focused on mice that were fed on the 0.5% cuprizone diet.

4.4 Sex does not appear to influence demyelination

The prevalence and severity of MS is known to be highly dependent on the sex of the individual. There are 2-3 times more females than males with relapsing-remitting MS[62, 65], whereas males with progressive MS have a more severe disease course than females[67, 69]. In the animal model, there have been some EAE models where sexual dimorphism in disease development was described[126]. In the cuprizone model, there has been mixed results with regards to the severity of demyelination based on the sex of the mouse[127, 128]. To assess whether a sex effect can be observed in the cuprizone model, experiments in male C57BL/6J

mice were conducted at the same time as the female cuprizone experiment outlined on Section 4.1. Weights were monitored on a weekly basis as well (Fig. A.5, page 136). Male mice that were fed with 0.3% cuprizone diet did not gain weight over the course of the experiment. Male mice that were fed with 0.5% cuprizone diet lost weight over the first 3 weeks of the experiment, but unlike female mice the weights of these mice did not recovered to baseline levels. At the end of the experiment, male mice brains were collected in the same manner as female mice brains.

Since demyelination was only observed in mice that were fed the 0.5% cuprizone diet, comparative analysis between female and male mice were also focused on 0.5% cuprizone-fed mice. The severity of demyelination was assessed by MBP immunohistochemistry analysis (Fig.4.4A-D, M), and by Nile Red stain analysis (Fig. 4.4E-H, N). The increase in glial proliferation was also assessed by Iba-1 immunohistochemistry analysis (Fig. 4.4I-L, O). Significant demyelination, assessed by reduction in MBP immunopositive area and loss of Nile Red staining of the corpus callosum, was observed in the male 0.5% cuprizone group. A significant increase in Iba-1 immunopositive area was also observed in cuprizone-fed male mice. However contrary to previous studies[127, 128], there were no differences between female and male cuprizone groups in terms of the severity of demyelination or Iba-1 immunopositivity in the corpus callosum. Because there were minimal differences between the two sexes at the corpus callosum of cuprizone-fed groups, female mice were selected for future analyses, as there are more female MS patients.

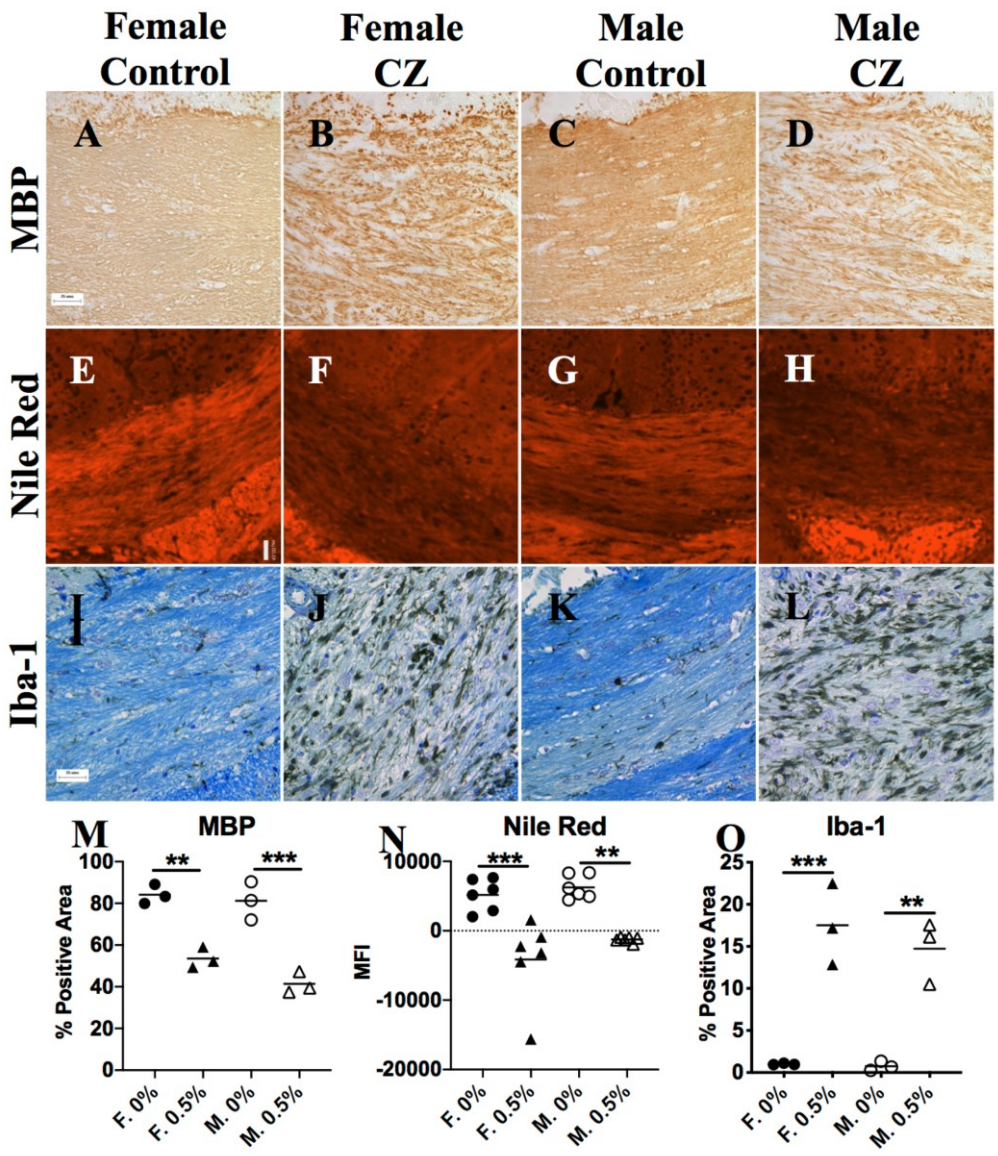

Figure 4.4 Cuprizone-induced demyelination is not influenced by sex. Corpus callosum of female and male C57BL/6J mice fed with 0 or 0.5% cuprizone (CZ) diet for 6-weeks were immunolabelled for MBP (A-D), stained with Nile Red (E-H), and immunolabelled for Iba-1 (I-L). Quantification of MBP (M), and Iba-1 (O) immunopositive area were performed using ImageJ software (n = 3). Quantification of Nile Red staining intensities (N) was performed using Volocity software (n = 6). No difference in the amount of demyelination, nor increase in Iba-1 immunopositive area was observed. MBP and Iba-1 images are 40X, size bars are 25µm. Nile Red images are10X, size bars are 70µm. **p-value<0.01, ***p-value<0.001 by one- way ANOVA with Tukey's multiple comparison analysis.

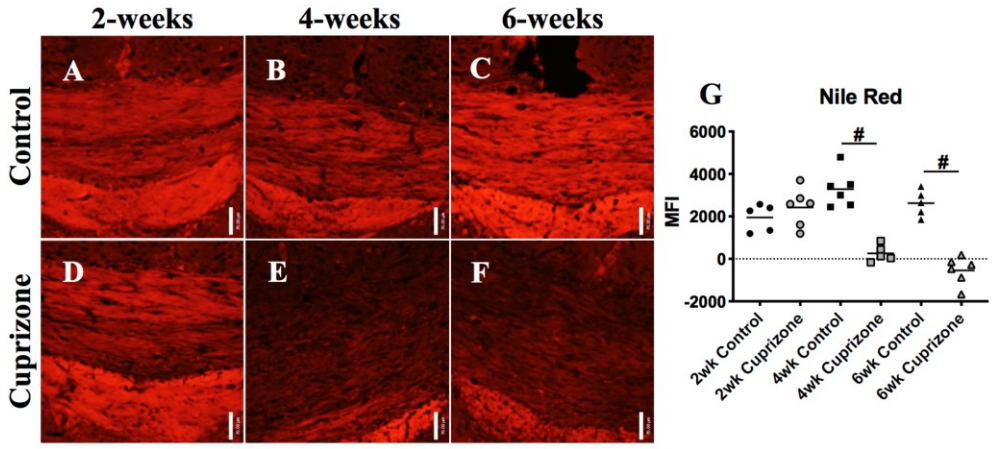

Figure 4.5 Cuprizone-induced demyelination is evident at 4 weeks. Corpus callosum of female C57BL/6J mice fed with 0 or 0.5% cuprizone (CZ) diet for 2 (A, D), 4 (B, E), or 6 (C, F) weeks were stained with Nile Red dye. Quantification of Nile Red staining intensities (G) was performed using Volocity software (n = 6). Evident myelin loss was observed after 4-weeks of feeding on cuprizone diet. The severity of demyelination at 6-weeks was like 4-weeks. Images are 10X, size bars are 70µm. #p-value<0.0001 by one-way ANOVA with Tukey's multiple comparison analysis.

4.5 Complete demyelination and oligodendrocyte loss is observed after 6 weeks of cuprizone feeding

As the optimal cuprizone dosing was determined to be 0.5%, the optimal duration of the cuprizone experiment was assessed next. Female C57BL/6J mice were fed with 0% (control) or 0.5% cuprizone diet for 2, 4, or 6 weeks. Weights for all mice were monitored on a weekly basis (Fig. A.6, page 137). Similar to previous cuprizone experiments, clear separations in weights between control-fed and cuprizone-fed mice were observed. At the end of 2, 4, or 6-weeks, mice were sacrificed, and brains were harvested. Nile Red stain analysis was performed to assess demyelination of the corpus callosum (Fig. 4.5). The appearance of Nile Red stained corpus callosum was similar in the controls (Fig. 4.5A-C), irrespective of the duration of the experiment. On the other hand, the corpus callosum of mice that were fed the 0.5% cuprizone diet for 2-weeks appeared similar to the 0% cuprizone control group (Fig. 4.5A, D). A notable loss of Nile Red staining was observed in the 0.5% cuprizone groups that

received cuprizone for 4 or 6-weeks (Fig. 4.5E, F). As expected, quantification of Texas Red fluorescence revealed significant loss of Nile Red staining of the corpus callosum in cuprizone mice that were fed for at least 4-weeks (Fig. 4.5G). In addition to the Nile Red stain analysis, corpus callosum was also assessed by GST-pi immunohistochemistry analysis (Fig. 4.6). Once again, all control mice appeared similar to one another (Fig. 4.6A-C). GST-pi immunopositive cells from 0.5% cuprizone groups appear smaller compared to the 0% cuprizone control group. Quantification of GST-pi immunopositive cells revealed no difference in the number of immunopositive cells in the corpus callosum between 0% and 0.5% cuprizone groups that were fed for 2-weeks (Fig. 4.6G). Only at 6-weeks was a significant reduction in GST-pi immunopositive cells observed despite the demyelination observed at 4-weeks of cuprizone feeding. Because oligodendrocyte loss in the corpus callosum was required for this model, 6-weeks of cuprizone feeding was determined to be necessary. Overall, the cuprizone model was optimised in female C57BL/6J mice, on the 0.5% cuprizone diet for 6 weeks.

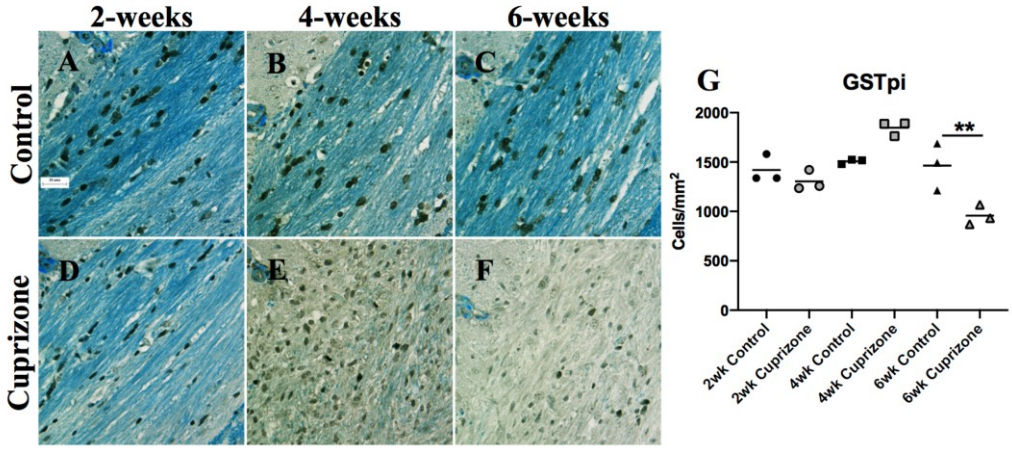

Figure 4.6 Cuprizone induces oligodendrocyte loss in the corpus callosum at 6 weeks. Corpus callosum of female C57BL/6J mice fed with 0, or 0.5% cuprizone (CZ) diet for 2 (A, D), 4 (B, E), or 6 (C, F) weeks were immunolabelled against GST-pi, with co-LFB staining. Quantification of GST-pi immunopositive cells (G) were performed using ImageJ software (n = 3). Loss of GST-pi immunopositive cells were only observed after feeding on cuprizone diet for6 weeks. Images are 40X, size bars are 25µm. **p-value<0.01 by one-way ANOVA with Tukey's multiple comparison analysis.

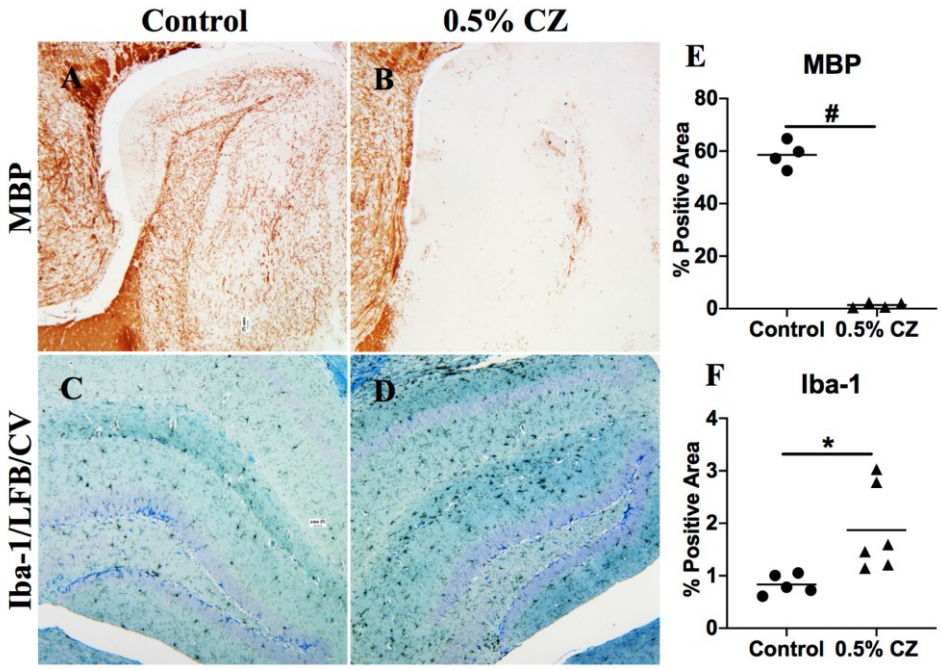

Figure 4.7 Hippocampal demyelination and glial activation of cuprizone-exposed mice. Hippocampus of female C57BL/6J mice fed with 0 or 0.5% cuprizone (CZ) diet for 6-weeks were immunolabelled for MBP (A and B), and Iba-1 (C and D). MBP (E), and Iba-1 (F) immunopositive areas were measured using ImageJ software (n = 6). Loss of MBP and increase in Iba-1 immunopositive area was observed in mice fed with 0.5% cuprizone diet. Images were taken at 10X, size bars are 25µm. *p-value<0.05, #p- value<0.0001 by one-way ANOVA with Tukey's multiple comparison analysis.

4.6 Cuprizone-induced demyelination and glial activation in the hippocampus

In addition to the corpus callosum, the hippocampus is another region of the brain that is known to be susceptible to demyelination[103]. To assess whether the hippocampus is affected in this cuprizone model, MBP (Fig. 4.7A, B) and Iba-1 (Fig. 4.7C, D) immunolabelled brain sections from female 0% and 0.5% cuprizone groups were analyzed, focusing on the Ammon's horn of the hippocampus. Immunopositive areas were also quantified (Fig. 4.7E, F). A striking reduction in MBP immunopositive area was observed in the 0.5% cuprizone group. This reduction in MBP labelling within the hippocampus was more severe than of the corpus callosum of the same group of mice (Fig. 4.1). For Iba-1 immunolabelling, like the corpus callosum, there was an increase in immunopositive area in the hippocampus of the

0.5% cuprizone group, indicating an increase in microglial activation in this group. However, unlike the corpus callosum (Fig. 4.2), the increase in Iba-1 immunopositive cells was less pronounced.

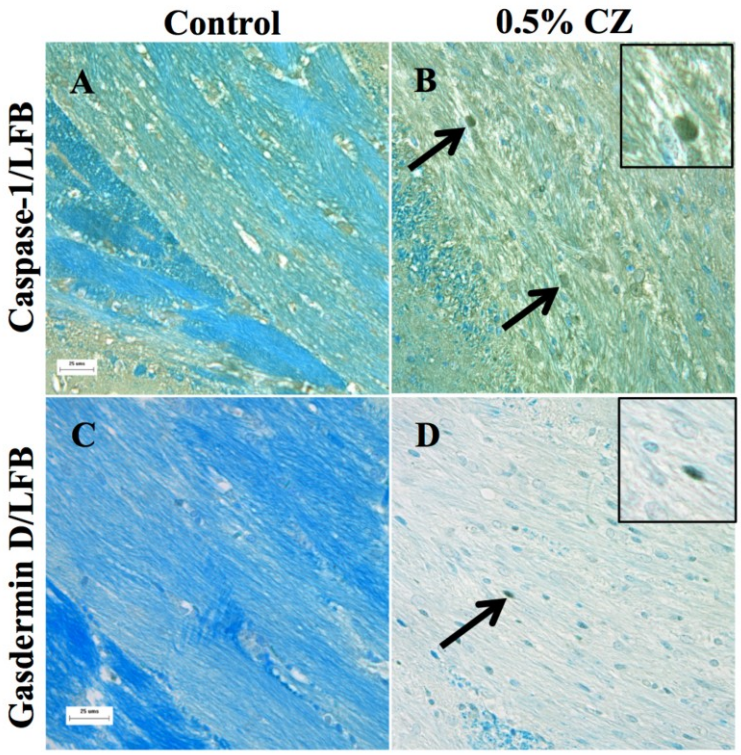

Figure 4.8 Cuprizone induces caspase-1 and gasdermin D expression in cells within the corpus callosum. Corpus callosum of female C57BL/6J mice fed with 0 or 0.5% cuprizone (CZ) diet for 6-weeks were immunolabelled for caspase-1 (A and B), and gasdermin D (C and D). Caspase-1 and gasdermin D immunopositive cells can be found in the corpus callosum of cuprizone-fed mice, indicated by black arrows. Insets are high magnification images of immunopositive cells. Images were taken at 40X, size bars are 25µm.

4.7 Caspase-1 and gasdermin D immunoreactivity in cuprizone brains

Before assessing whether oligodendrocytes from brains of cuprizone-fed mice can express innate immune molecules, the expression of innate immune molecules in the brain, specifically the corpus callosum, of mice fed on cuprizone diet was first assessed. The

analysis was focused on caspase-1 and gasdermin D protein expression, since these were induced by PDOs upon stimulation with TNFα as outlined on Chapter 3. The presence or absence of caspase-1 and gasdermin D proteins were assessed by immunohistochemistry of brain sections with concurrent LFB staining from the 0% and 0.5% cuprizone groups (Fig. 4.8). Caspase-1 (Fig. 4.8A and B) and gasdermin D (Fig. 4.8C and D) immunopositive cells were evident in the corpus callosum from the 0.5% cuprizone group, indicated by arrows in the figure, compared to the 0% cuprizone control group. These findings implied that there might be cells in the corpus callosum that are undergoing pyroptosis in the brains of cuprizone-fed mice. In addition to the caspase-1 and gasdermin D immunolabelling, other inflammasome-related proteins, IL-1β, IL-18, AIM2, and NLRX1 were analysed by immunohistochemistry (Fig. A.7, page 138). Unlike caspase-1 and gasdermin D (Fig. 4.8), positive immunolabelling of these other inflammasome-related proteins were not detected in the corpus callosum of 0.5% cuprizone group. It was plausible that in this model these proteins were not induced compared to proteins such as caspase-1 and gasdermin D. These results supported the notion of focusing analyses on these proteins.

4.8 Cuprizone-exposed mice do not display anxiety-like behaviour.

Neurocognitive impairments, leading to anxiety development are known to manifest in some MS patients[129]. Previous studies involving the cuprizone model have reported anxiety like behaviour in cuprizone-exposed mice. To assess if anxiety-like behaviour was also present in the current model, an Open Field test was performed on female and male mice exposed to 0%, 0.3%, or 0.5% cuprizone diet for 6-weeks (Fig. A.8, page 139). In the Open Field test, mice are considered to have anxiety-like behaviour if it spent less time in the centre of the open field bin compared to controls (Fig. A.8A). Additionally, the number of times the mice crossed each quadrant (Fig. A.8B), and the number of rearings were measured (Fig. A.8C). No cuprizone-induced effects could be observed in both female and male mice, suggesting these mice are not experiencing anxiety-like behaviour. Although there was a sex effect observed in the control and 0.5% cuprizone groups for the time spent in centre, and in 0.3% and 0.5% cuprizone groups for the number of crosses, these results show the differences between the sex at that particular group, but overall no cuprizone effect could be observed.

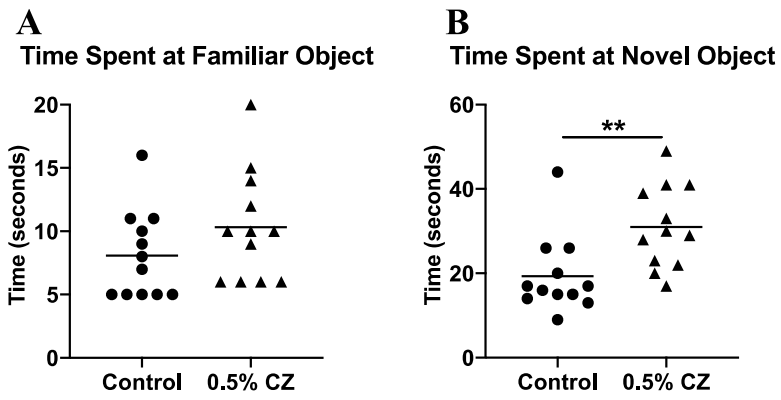

Figure 4.9 Cuprizone-exposed animals explore more than control mice in the Novel Object Recognition (NOR) test. Female C57BL/6J mice fed with 0 or 0.5% cuprizone (CZ) diet for 6-weeks were assessed by NOR test (n = 12) Mice were trained in an open field bin with two identical objects for 5 minutes. After 6 hours of rest, mice were tested in the same bin with one of the objects replaced with a novel object. The time spent exploring the familiar object (A) and novel object (B) were measured. Cuprizone-fed mice interacted with the novel object for a longer period compared to control mice. **p-value<0.01 by Student t-test.

4.9 Cuprizone-exposed mice exhibit enhanced exploratory behaviour in the Novel Object Recognition (NOR) test.

As previously described, the hippocampus is a region of the brain that is pivotal in memory-related behaviour function[130]. The hippocampus is another anatomic site of the brain that is affected in some MS patients, leading to development of cognitive impairments such as reduced short-term memory[73] Since a striking reduction in MBP immunopositive area was observed in the hippocampus of cuprizone-fed mice (Fig. 4.7), the memory function of 0% and 0.5% cuprizone groups were assessed by NOR test. In the NOR test, mice are first trained by placing in a bin with two identical objects for 5 minutes. Six hours later, mice are placed back in the same bin, with one familiar object (the same object used for training) and one novel object for 5 minutes; the duration of time that mice explores the two objects are recorded and compared. Due to the curious natures of mice, control mice or mice with intact memory will gravitate towards the novel object, and thus spend more time exploring the

novel object compared to the familiar object[131]. On the other hand, mice with memory impairments are more likely to consider the novel and the familiar objects as both being novel and are more likely to spend equal time exploring both objects. Female C57BL/6J mice that were fed on 0% or 0.5% cuprizone diet for 6 weeks were assessed by NOR test, and the time spent at the familiar object (Fig. 4.9A) and time spent on novel object (Fig. 4.9B) was recorded. No differences between groups were observed for the times spent exploring the familiar object. In contrast, the 0% cuprizone group spent more time exploring the novel object than the familiar object. The 0.5% cuprizone group spent significantly longer time exploring the novel object than the control mice. This prolonged exploration of the novel object suggests these mice may be experiencing attention or attraction impairment such as perseveration.

Chapter 5 – *In vivo* results: Intranasal delivery of the caspase-1 inhibitor VX-765 partially inhibits cuprizone-induced demyelination

5.1 VX-765 treatment partially inhibits myelin protein loss but does not affect myelin lipid composition in cuprizone-exposed mice.

In addition to the caspase-1 and gasdermin D immunoreactivity observed in female cuprizone mice (Fig. 4.8), previous studies have also detected inflammasome-related proteins in the corpus callosum of cuprizone-fed mice[132]. Because caspase-1 induction in cuprizone-fed mice was evident, the caspase-1 inhibitor, VX-765, could have potential beneficial effects by mitigating cuprizone-mediated demyelination. To explore this question, 0.5% cuprizone-fed mice were treated with daily intranasal VX-765 or vehicle (PBS:DMSO 1:1) starting 2 weeks after commencement of cuprizone diet. VX-765 treatment was initiated after 2 weeks of cuprizone feeding in order to assess VX-765 activity after early effects of cuprizone had already occurred, as observed in my previous findings on appearances of injured oligodendrocytes without full demyelination (Fig. 4.6). Weights for all mice were monitored on a weekly basis (Fig. A.9, page 140). Weight gain curve for this experiment was similar to previous experiments. Mice from the 0% cuprizone/vehicle group (control vehicle-treated group) gained weight steadily over the 6 weeks. The 0.5% cuprizone/vehicle group (cuprizone vehicle-treated group) lost weight over the first few weeks of the experiment, and steadily gained weight back to baseline levels. Unfortunately, no VX-765 effect was observed on the weights of the 0.5% cuprizone/VX-765 group (cuprizone VX-765-treated group) as the weight gain curve of these mice overlapped with the 0.5% cuprizone/vehicle group.

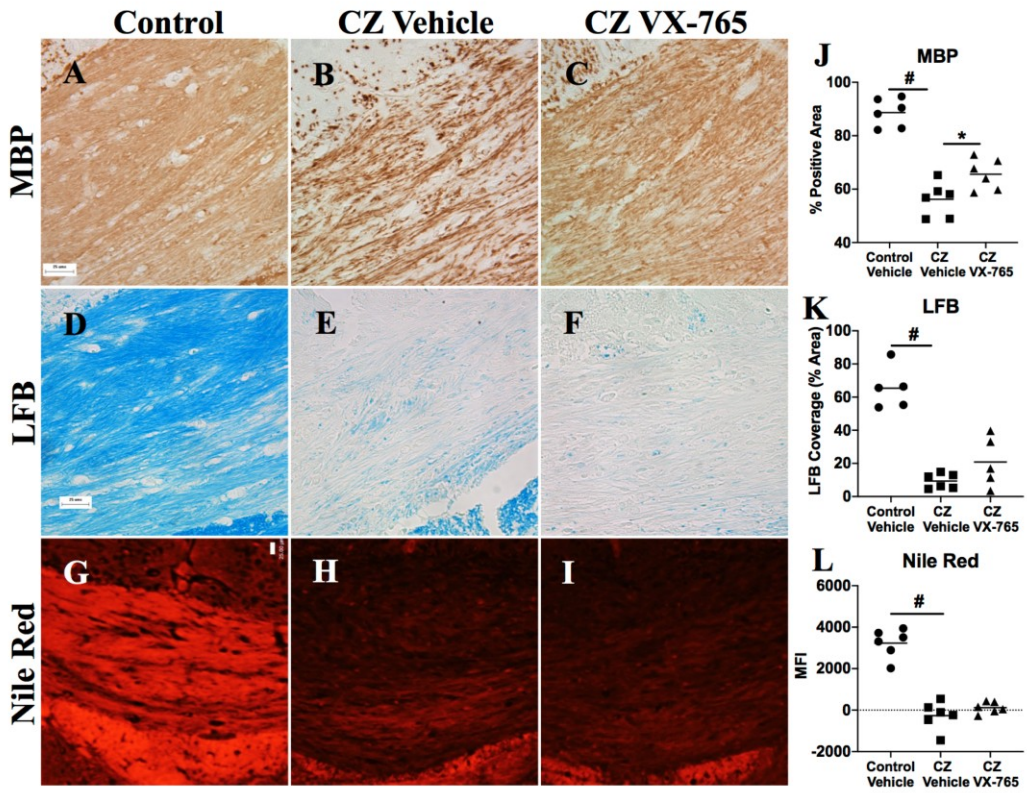

Figure 5.1 VX-765 treatment partially inhibits myelin protein loss in cuprizone-exposed mice. Female C57BL/6J mice were fed with 0 or 0.5% cuprizone (CZ) diet for 6-weeks, with 4 weeks of daily intranasal VX-765 or vehicle treatments. Corpus callosum were immunolabelled for MBP (A-C), stained with LFB (D-F), and with Nile Red (G-I). Quantification of MBP immunopositive area (J), and LFB positive area (K) were performed using ImageJ software (n = 6). Quantification of Nile Red staining intensities (L) was performed using Volocity software (n= 6). MBP preservation was observed in cuprizone-fed mouse that were treated with VX-765. MBP and LFB images are 40X, size bars are 25µm. Nile Red images are 10X, size bars are 25µm. *p-value<0.05, #p-value<0.0001 by one-way ANOVA with Tukey's multiple comparison analysis.

At the end of week 6 mice were sacrificed, and brains were collected. The severity of demyelination at the corpus callosum was assessed by MBP immunohistochemistry (Fig. 5.1A-C, J), LFB (Fig. 5.1D-F, K) and Nile Red (Fig. 5.1G-I, L) staining analysis. Approximately a 40 % reduction in MBP immunopositive area (Fig. 5.1J), with marked

reduction in LFB positive area (Fig. 5.1K), and Nile Red fluorescence intensity (Fig. 5.1L) were observed in the 0.5% cuprizone/vehicle group compared to 0% cuprizone/vehicle group. These results recapitulated the findings described earlier (Fig. 4.1) in the 0% and 0.5% cuprizone groups without vehicle treatments. Collectively, significant effects of the vehicle treatment were not observed in the vehicle-treated mice. On the other hand, the corpus callosum myelin integrity of the 0.5% cuprizone/VX-765 group was improved compared to the 0.5% cuprizone/vehicle group and resembled similar to the 0% cuprizone/vehicle group (Fig. 5.1A-C). Quantification of MBP immunopositive areas resulted in an approximately 16% increase in MBP immunopositive area in the corpus callosum (Fig. 5.1J) in the 0.5% cuprizone/VX-765 group compared to 0.5% cuprizone/vehicle group. However, VX-765 had no effect on LFB staining or Nile Red fluorescence intensity at the corpus callosum. These results suggested that VX-765 might be partially inhibiting myelin protein damage that was caused by cuprizone exposure.

5.2 VX-765 treatment reduces cuprizone induced glial activation and axonal injury.

As previously described in Fig. 4.2, in addition to demyelination, mice fed on 0.5% cuprizone diet also had increased Iba-1 and GFAP immunoreactivity, indicating activation of microglia and astrocytes respectively, in the corpus callosum. To test whether VX-765 treatment reduced Iba-1 and GFAP immunoreactivity that are increased in cuprizone-fed mice, brain sections from 0% cuprizone/vehicle, 0.5% cuprizone/vehicle, and 0.5% cuprizone/VX-765 groups were assessed by Iba-1 immunohistochemistry (Fig. 5.2A-C, J), and GFAP (Cy3) and MBP (FITC) immunofluorescence (Fig. 5.2D-F, K) analysis. Additionally, presence of axonal injuries was assessed by counting the number of amyloid precursor protein (APP) immunopositive blebs present per field of view (Fig. 5.2G-I, L). Similar to previous results, there was a significant increase in Iba-1 immunopositive area, and an increase in GFAP (Cy3) fluorescence intensity in the corpus callosum of 0.5% cuprizone/vehicle group compared to the 0% cuprizone/vehicle group. A significant increase in APP immunopositive axonal blebs was also present in the 0.5% cuprizone/vehicle group. These increases in glial cell immunoreactivity and axonal injury were significantly reduced with VX-765 treatment, but not to the extent of 0% cuprizone/vehicle group. Although the

VX-765 treatment effect was not fully protective, it nonetheless led to a reduction in glial activation, and axonal blebs that were induced by cuprizone feeding.

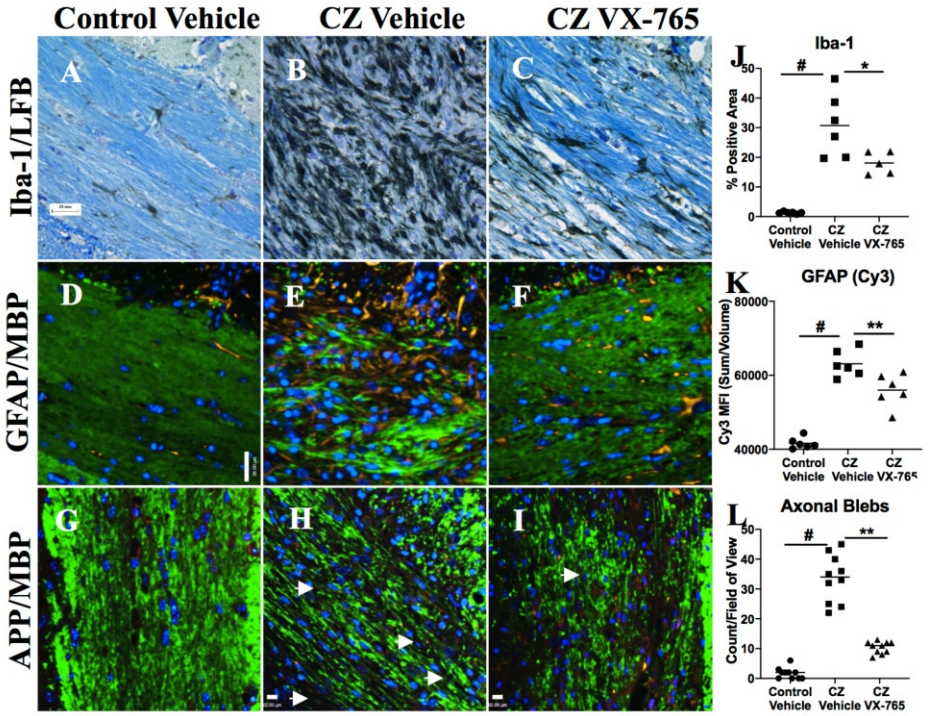

Figure 5.2 Cuprizone-induced glial cell activation is reduced with VX-765 treatment. Female C57BL/6J mice were fed with 0 or 0.5% cuprizone (CZ) diet for 6-weeks, with 4 weeks of daily intranasal VX-765 or vehicle treatments. Corpus callosum were immunolabelled for Iba-1 (A-C), or fluorescently immunolabelled with GFAP (Cy3/amber, D-F) or with APP (Cy3/amber, G-I), with co-labelling of MBP (FITC/green) and nuclei (DAPI/blue). White arrows indicate axonal blebs (H, I). Iba-1 immunopositive area was quantified using ImageJ software (n = 6). GFAP MFI was quantified by dividing total sum of fluorescence by volume of tissue assessed using Velocity software (n = 6). APP immunopositive axonal blebs were counted per field of view with a size threshold of 20µm^3 using Velocity software (n = 6). The increase in Iba-1, GFAP, and axonal injury detection observed in cuprizone brains were significantly reduced with VX-765 treatment. Iba-1 images are 40X, size bars are 25µm. Immunofluorescence images are 20X, size bars are 28µm. *p-value<0.05, **p-value<0.01, #p-value<0.0001 by one-way ANOVA with Tukey's multiple comparison analysis.

5.3 VX-765 treatment reduces cuprizone-induced OPC activation but does not protect oligodendrocytes.

As VX-765 was beneficial in reducing Iba-1 and GFAP immunoreactivity, it was then assessed whether VX-765 was also beneficial in protecting oligodendrocytes that are lost with cuprizone exposure. GST-pi (Fig. 5.3A-C), ASPA (Fig 5.3D-F), and NG2 (Fig. 5.3G-I) immunohistochemistry analyses were performed on brain sections from 0% cuprizone/vehicle, 0.5% cuprizone/vehicle, and 0.5% cuprizone/VX-765 groups, followed by quantification of immunopositive cells in the corpus callosum (Fig. 5.3J-L). A reduction of GST-pi and ASPA immunopositive cells were observed in 0.5% cuprizone/vehicle group, representing a loss of oligodendrocytes in the corpus callosum compared to 0% cuprizone/vehicle group. Similar to the LFB and Nile Red staining results (Fig. 5.1), VX-765 treatment did not increase the number of GST-pi and ASPA immunopositive cells compared to 0.5% cuprizone/vehicle group, indicating that VX-765 did not prevent the cuprizone-induced loss of oligodendrocytes. The observed increase in NG2 immunopositive cells in 0.5% cuprizone/vehicle group compared to 0% cuprizone/vehicle group was similar to the increase in NG2 immunopositive cells observed in cuprizone-fed mice without treatment (Fig. 4.3G-I, L), again confirming the minimal effects of the vehicle treatment. Unlike the markers for mature oligodendrocytes, VX-765 treatment was effective in reducing the number of NG2 immunopositive cells in the corpus callosum. The reduction in NG2 immunopositive cells observed with VX-765 treatment was similar to the reduction of Iba-1 immunopositive area and GFAP (Cy3) fluorescence intensity observed (Fig. 5.2), in which it was a partial recovery. It was not possible to determine based on these results whether the reduction in NG2 immunopositive cells was due to VX-765 treatment inhibiting OPC proliferation, or if VX-765 is inhibiting the activation of OPCs that would lead to proliferation. Collectively, VX-765 treatment in cuprizone-fed mice reduced the activation of microglia, astrocytes, and OPCs, accompanied by an increase in MBP immunoreactivity in the corpus callosum, despite the lack of recovery of mature oligodendrocytes.

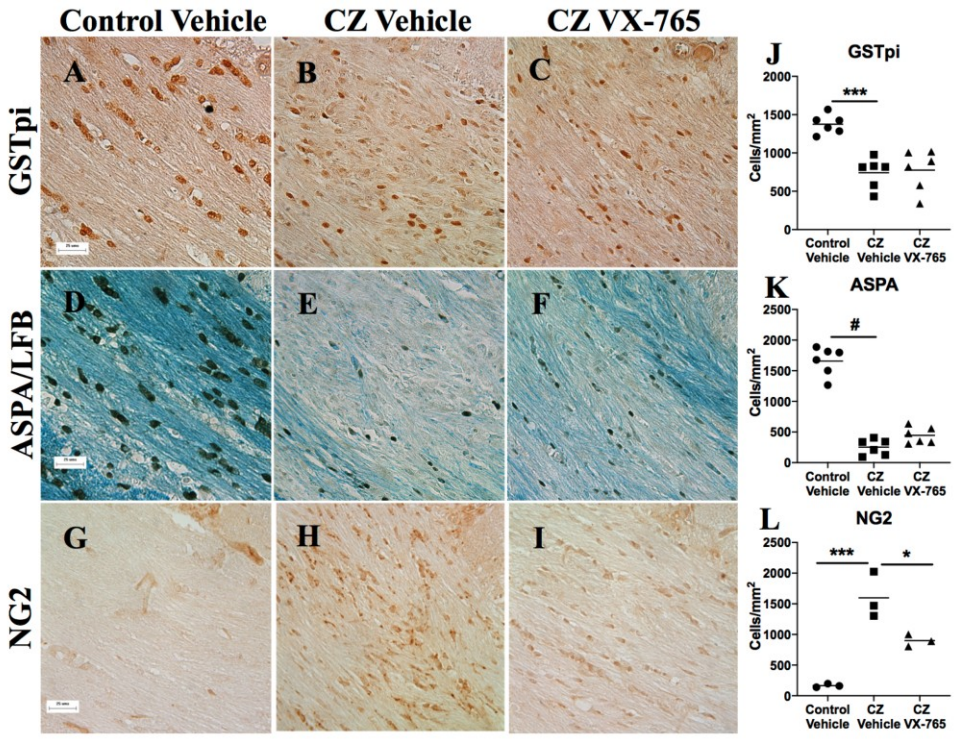

Figure 5.3 VX-765 treatment prevents OPC activation in cuprizone-exposed animals. Female C57BL/6J mice were fed with 0 or 0.5% cuprizone (CZ) diet for 6-weeks, with 4 weeks of daily intranasal VX-765 or vehicle treatments. Corpus callosum were immunolabelled for GST-pi (A-C), ASPA (D-F), or with NG2 (G-I). Quantification of GST-pi (J), ASPA (K), and NG2 (L) immunopositive cells were performed using ImageJ software (n = 6 for GST-pi and ASPA, n = 3 for NG2). The loss of GST-pi and ASPA immunopositive cells in cuprizone mice were not rescued with VX-765 treatment. Images are 40X, size bars are 25µm. *p-value<0.05, ***p-value<0.001, #p-value<0.0001 by one-way ANOVA with Tukey's multiple comparison analysis.

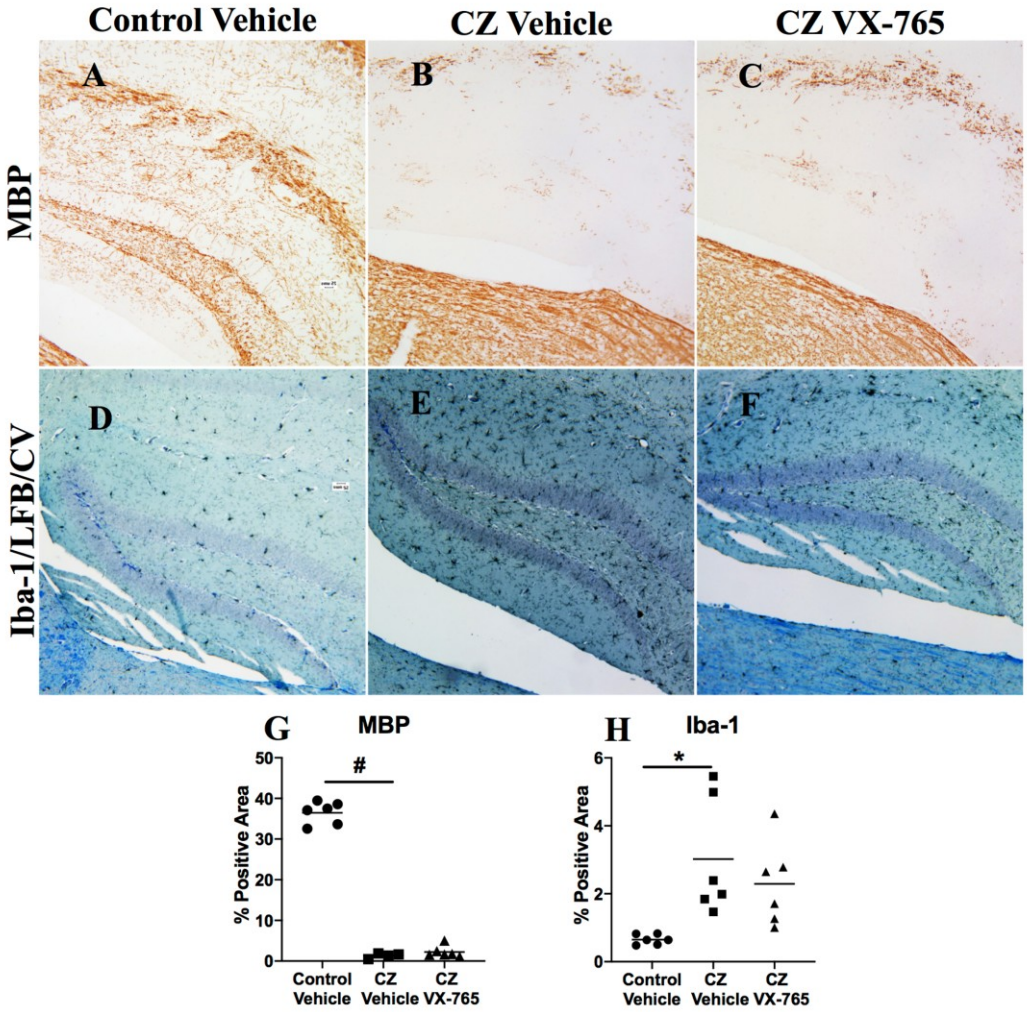

Figure 5.4 Cuprizone-induced demyelination and glial activation in the hippocampus is unaffected by VX-765 treatment. Female C57BL/6J mice were fed with 0, or 0.5% cuprizone (CZ) diet for 6-weeks, with 4 weeks of daily intranasal VX-765 or vehicle treatment. Hippocampus were immunolabelled for MBP (A-C), and Iba-1 (D-F). Quantification of immunopositive area were performed using ImageJ software (n = 6). The loss of MBP and increase of Iba-1 immunopositive area observed in cuprizone mice were not reversed with VX-765 treatment. Images are 10X, size bars are 25µm. *p-value<0.05, #p-value<0.0001 by one-way ANOVA with Tukey's multiple comparison analysis.

5.4 VX-765 treatment does not inhibit cuprizone-mediated alterations in the hippocampus.

As reported previously, the hippocampus was also susceptible to the effects of cuprizone, in which MBP immunopositive area was markedly reduced with a significant increase in Iba-1 immunopositive area in the 0.5% cuprizone group (Fig. 4.4). To assess whether VX-765 treatment also inhibited myelin loss and glial activation in the hippocampus, MBP (Fig. 5.4 A-C, G) and Iba-1 (Fig. 5.4 D-F, H) immunolabelled brain sections from 0% cuprizone/vehicle, 0.5% cuprizone/vehicle, and 0.5% cuprizone/VX-765 groups were assessed. Loss of MBP immunopositive area and an increase in Iba-1 immunopositive area in Ammon's horn of the hippocampus was observed in 0.5% cuprizone/vehicle group compared to 0% cuprizone/vehicle group. VX-765 treatment had no effect on altering MBP and Iba-1 immunopositive area in the 0.5% cuprizone/VX-765 group. In combination with the results of the corpus callosum, these results show the effects of VX-765 treatment are dependent on brain anatomic site.

5.5 VX-765 does not suppress cuprizone-induced gasdermin D in oligodendrocytes.

The *in vitro* analyses of PDOs, caspase-1 and gasdermin D protein expression were induced by TNFα exposure. Caspase-1 and gasdermin D expressing cells were also found in the corpus callosum of 0.5% cuprizone-fed mice (Fig. 4.8). To assess whether corpus callosal oligodendrocytes from cuprizone-fed mice expressed caspase-1 and gasdermin D, immunofluorescence analyses of both proteins along with an oligodendrocyte marker were performed. However, due to challenges from primary and secondary antibody combinations, only the analysis of gasdermin D was pursued. Brain sections from 0% cuprizone/vehicle, 0.5% cuprizone/vehicle, and 0.5% cuprizone/VX-765 groups were immunolabelled for GST-pi (Cy5), gasdermin D (Cy3), and ASPA (FITC), together with DAPI nuclear staining (Fig. 5.5).

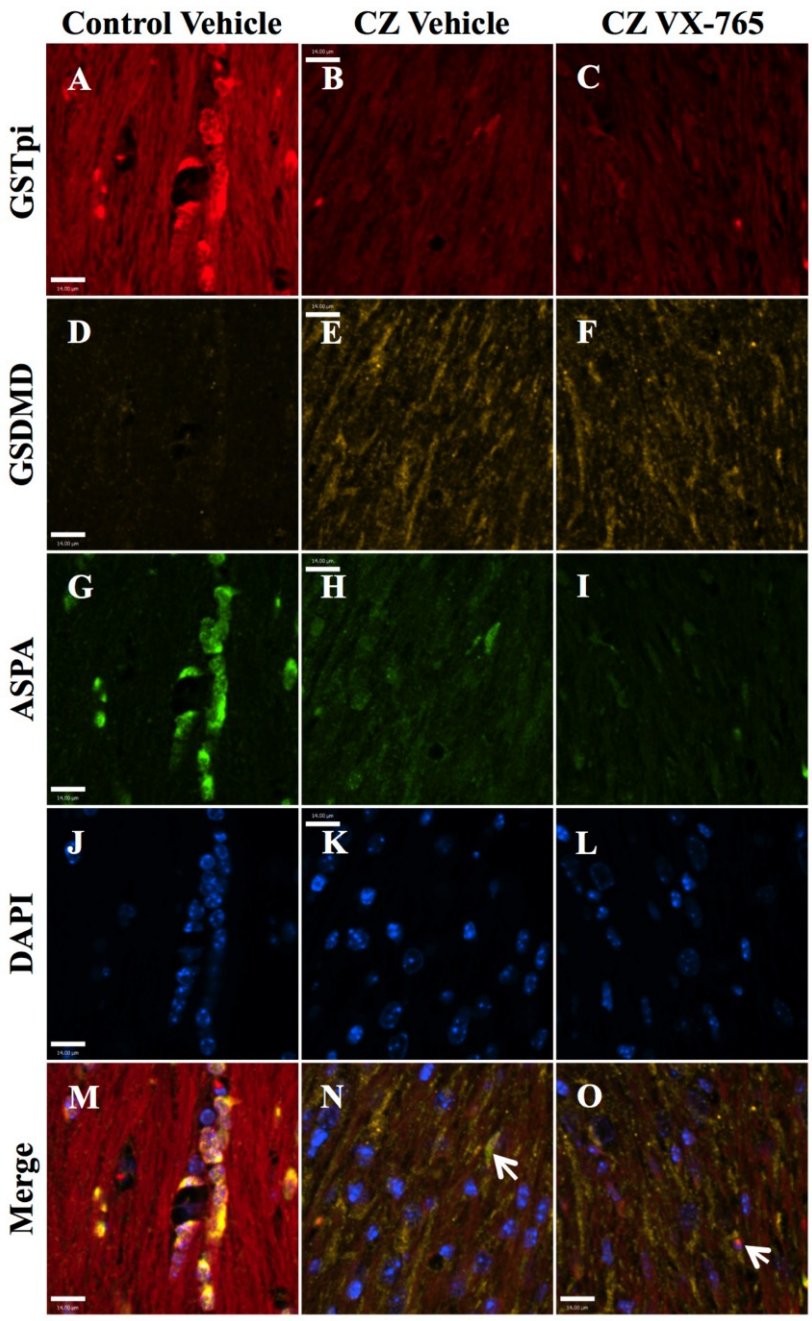

Figure 5.5 Oligodendrocytes express gasdermin D in cuprizone-fed mice brains. Female C57BL/6J mice were fed with 0, or 0.5% cuprizone (CZ) diet for 6-weeks, with 4 weeks of daily intranasal VX-765 or vehicle treatment. Corpus callosum were immunolabelled with GST-pi -(Cy5/red, A-C), GSDMD (Cy3/amber, D-F), ASPA (FITC/green, G-I), and with nuclei (DAPI/blue, J-L). Merged images M-O. GSDMD, ASPA, and GST-pi immunopositive cells are present in cuprizone-fed mice brains. Arrows indicate GST-pi+ ASPA+ GSDMD+ cell. Images are 40X, size bars are 14μm.

The loss of GST-pi (Fig. 5.5A-C) and ASPA (Fig. 5.5G-I) immunopositive cells observed in the 0.5% cuprizone/vehicle group was not inhibited with VX-765 treatment, as expected from previous findings (Fig. 5.3). Minimal gasdermin D immunoreactivity was observed in the corpus callosum of 0% cuprizone/vehicle group (Fig. 5.5 D), whereas intense gasdermin D immunopositive areas were observed in 0.5% cuprizone/vehicle group (Fig. 5.5E). Gasdermin D immunoreactivity was observed in intact cells indicated by DAPI co-labelling, including ASPA and GST-pi immunopositive cells (Fig. 5.5N, white arrow). Interestingly, some gasdermin D immunoreactivity appeared as linear structures (Fig. 5.5E) suggestive of gasdermin D expression in axons. VX-765 treatment did not reduce gasdermin D immunoreactivity in the corpus callosum (Fig. 5.5F), as images from 0.5% cuprizone/VX-765 group appeared very similar to images from 0.5% cuprizone/vehicle group. Additionally, apparent increase in full-length gasdermin D protein was detected by Western blot analysis of corpus callosum lysates, with associated MBP loss in the 0.5% cuprizone/vehicle group (Fig. 5.6A). Although the quantified protein expression levels were not significant across all groups (Fig. 5.6B, C), this may be attributed to the poor quality of the immunoblot.

Although VX-765 treatment did not affect gasdermin D expression in the corpus callosum, gasdermin D immunopositive cells were quantified (Fig. 5.7), specifically to determine if there was a reduction in gasdermin D immunopositive oligodendrocytes with VX-765 treatment. Cells were considered to be gasdermin D immunopositive if Cy3 fluorescence signal was observed on the perimeter of cells, or within cell bodies with intact DAPI co-labelling. As all tissue immunofluorescence slides were imaged as z-stacks, every cell was assessed at several different stacks to confirm that gasdermin D immunoreactivity was associated with a given cell, and not with cells located above and below the cell of interest. For this quantification, cells were categorised either as ASPA- gasdermin D-, ASPA- gasdermin D+, ASPA+ gasdermin D-, or ASPA+ gasdermin D+. Since there is overlap between GST-pi and ASPA immunoreactivity on oligodendrocyte cell bodies, only ASPA immunoreactivity was analysed as ASPA immunolabelling resulted in less myelin reactivity compared to GST-pi. All cells from several different fields of view within the central corpus callosum were assessed. More than 100 cells were quantified per mouse brain sample. The total number of cells in each category was determined, and calculated as number of cells per

mm^3, for each mouse brain sample. This was repeated for all mice brain samples, and the number of ASPA- gasdermin D- (Fig. 5.7A), ASPA- gasdermin D+ (Fig. 5.7B), ASPA+ gasdermin D- (Fig. 5.7C), or ASPA+ gasdermin D+ (Fig. 5.7D) cells per mm^3 for each mice brain samples were graphed.

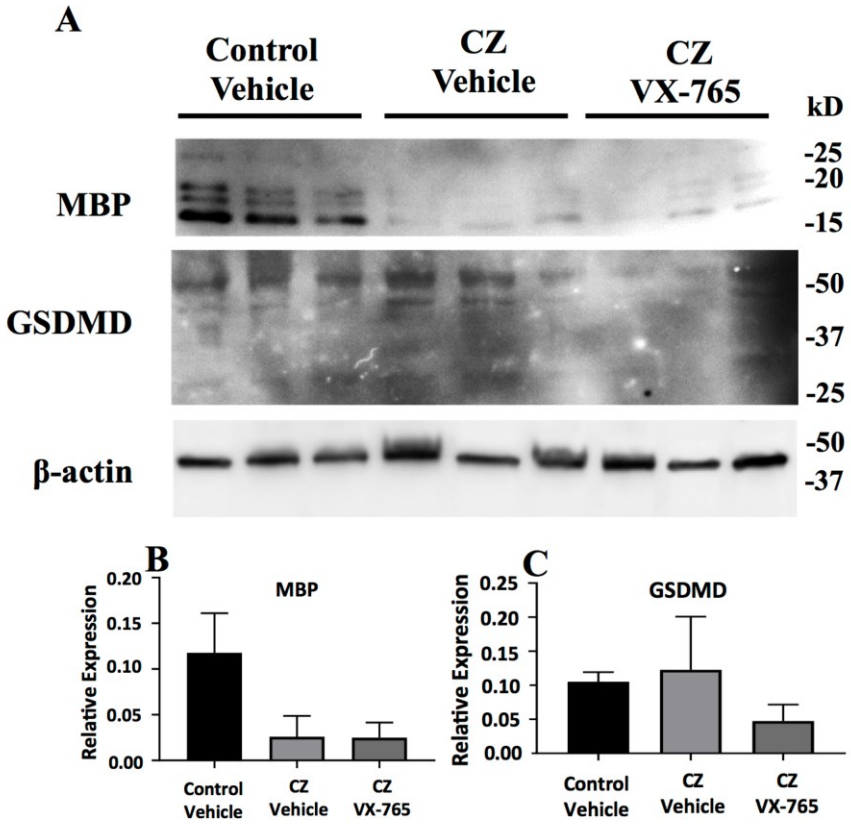

Figure 5.6 Cuprizone-feeding appears to reduce MBP expression and increase in gasdermin D (GSDMD) protein expression. Female C57BL/6J mice were fed with 0, or 0.5% cuprizone (CZ) diet for 6-weeks, with 4 weeks of daily intranasal VX-765 or vehicle treatment. Protein samples from corpus callosum lysates were immunoblotted for MBP, gasdermin D and β-actin (A). The relative expression of MBP (B) and gasdermin D (C) normalized to β-actin levels were quantified (n = 3). An apparent reduction of MBP (21kDa) and increase in full-length gasdermin D (53kDa) were observed with cuprizone exposure.

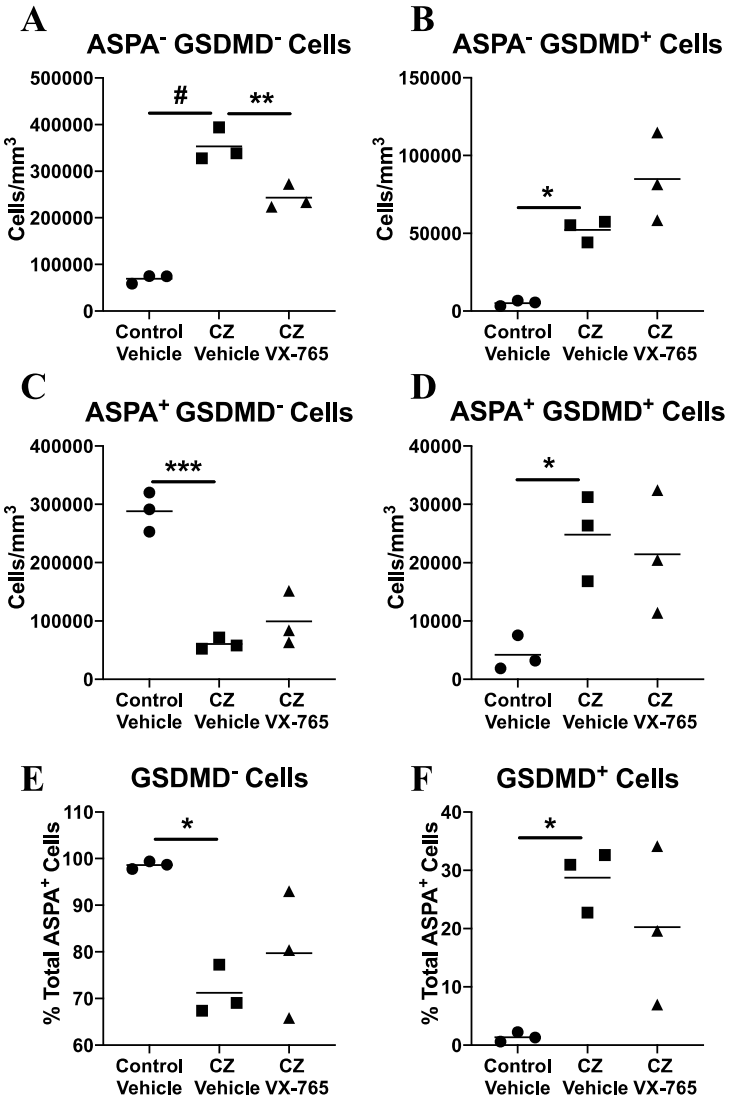

Figure 5.7 Gasdermin D immunopositive cells are increased in cuprizone mice brains but are unaffected by VX-765 treatment. Corpus callosum immunofluorescence images of control vehicle, cuprizone (CZ) vehicle, or CZ VX-765 mice from Fig. 5.5 immunolabelled with gasdermin D (GSDMD), ASPA, and DAPI were quantified using Volocity software (*n* = 3). The ASPA- GSDMD- cells (A), ASPA- GSDMD+ cells (B), ASPA+ GSDMD- (C), and ASPA+ GSDMD+ cells (D) were measured per volume (mm^3). The GSDMD- cells (E) and GSDMD+ cells (F) were also measured as a proportion of total ASPA+ cells identified over several fields of view. The increase in GSDMD+ cells observed in cuprizone-fed mice are not reduced with VX-765 treatment. *p-value<0.05, **p-value<0.01, ***p-value<0.001 #p-value<0.0001 by one-way ANOVA with Tukey's multiple comparison analysis.

As expected, most cells in the corpus callosum of 0% cuprizone/vehicle group were ASPA+ gasdermin D- cells. Almost a 5-fold reduction in ASPA+ gasdermin D- cells was observed in 0.5% cuprizone/vehicle group (Fig. 5.7C). VX-765 treatment had no effect on the ASPA+ gasdermin D- cells that were reduced by cuprizone feeding. For ASPA- gasdermin D- cells, there were fewer cells observed in the 0% cuprizone/vehicle group (Fig. 5.7A) compared to ASPA+ gasdermin D- cells (Fig. 5.7C). Approximately a 5-fold increase in ASPA- gasdermin D- cells was observed in the 0.5% cuprizone/vehicle group, and VX-765 treatment was able to partially reduce this increase. These results on ASPA+ gasdermin D- cells and ASPA- gasdermin D- cells are in agreement of immunohistochemistry results presented earlier (Fig. 5.2, 5.3). ASPA and GST-pi immunopositive cells were reduced in 0.5% cuprizone/vehicle group, and recovery of these cells was not observed with VX-765 treatment (Fig. 5.3). The ASPA- gasdermin D- cells observed are likely a mixture of cells, including microglia, astrocytes, and OPCs, since all three cell types were found to be increased in 0.5% cuprizone/vehicle group, and all three cell types were reduced in the 0.5% cuprizone/VX-765 group.

As expected from Fig. 5.5, the 0% cuprizone/vehicle group had very few cells that expressed gasdermin D (Fig. 5.7B, D), with the total gasdermin D expressing cells being approximately 2% of total cells observed in the corpus callosum. The number of gasdermin D+ cells was increased in 0.5% cuprizone/vehicle group, with an approximately a 7-fold increase in ASPA+ gasdermin D+ cells, and approximately a 10-fold increase in ASPA- gasdermin D+ cells. Although a significant increase in gasdermin D+ cells in the 0.5% cuprizone/vehicle group was observed, the number of gasdermin D- cells was far greater than gasdermin D+ cells. Focusing on ASPA+ cells, approximately 70% of all ASPA+ cells in 0.5% cuprizone/vehicle group were gasdermin D- (Fig. 5.7E), and 30% of ASPA+ cells were gasdermin D+ (Fig. 5.7F). Although VX-765 treatment was effective in reducing activation of ASPA- non-oligodendrocyte cells in the corpus callosum of cuprizone-fed mice, it did not appear to have an effect on the number of gasdermin D+ cells. For ASPA+ cells, VX-765 treatment also had no effect on altering the proportion of ASPA+ cells that were also gasdermin D+ (Fig. 5.7F). The results obtained from the quantification suggests that VX-765 is effective in reducing cuprizone induced non-oligodendrocyte glia cell activation as long as

the cells are not expressing gasdermin D. These results suggest that VX-765 treatment might only be beneficial if the cells are not expressing gasdermin D. Cells might already be destined to gasdermin D expression within the first 2 weeks of cuprizone feeding, and once this fate has been determined, VX-765 might not be effective in these cells, thus no alterations were observed in 0.5% cuprizone/VX-765 group with regards to gasdermin D immunopositive cells.

5.6 Surviving oligodendrocytes in cuprizone-fed mice are injured despite VX-765 treatment.

Although the number of gasdermin D immunopositive cells did not decrease with VX-765 treatment, oligodendrocytes in the corpus callosum from 0% cuprizone/vehicle, 0.5% cuprizone/vehicle, and 0.5% cuprizone/VX-765 groups were assessed for cell injury (Fig. 5.8), since VX-765 pre-treatment was beneficial in reversing the TNFα-induced morphological alterations in GF- PDOs (Fig. 3.13). In the PDO studies described in Chapter 3, PDO morphology (process numbers and length) was assessed to determine cell injury. However, since ASPA immunolabelling is only observed in the cell bodies of oligodendrocytes, unlike *in vitro* immunofluorescence analyses, only the cell bodies of ASPA immunopositive cells were assessed. For this analysis, the volume of DAPI positive, ASPA immunopositive cell bodies were assessed (Fig. 5.8A). In addition, the ASPA (FITC) MFI of the same cells were assessed (Fig. 5.8B). The volume of ASPA immunopositive cells in the 0.5% cuprizone/vehicle group were determined to be 1.5 times smaller than ASPA immunopositive cells in the 0% cuprizone/vehicle group. VX-765 treatment did not alter the volume of ASPA immunopositive cells in the corpus callosum. The ASPA (FITC) MFI in 0.5% cuprizone/vehicle group was also reduced by approximately 1.4-fold, with no VX-765 treatment effect observed. These results implied that although there are few surviving oligodendrocytes in the corpus callosum of cuprizone-fed mice, these cells are most likely injured, as observed by the reduced cell body volume and reduced ASPA immunoreactivity. Thus, the fate of oligodendrocytes might be determined during the first two weeks of cuprizone feeding, before VX-765 treatment was initiated.

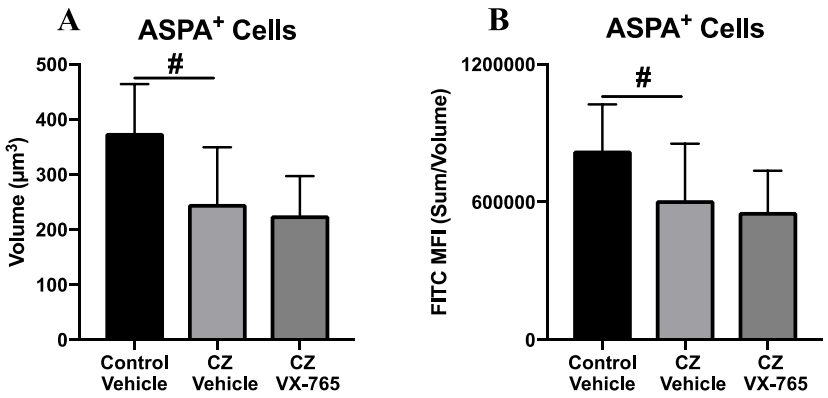

Figure 5.8 Cuprizone-induced oligodendrocyte atrophy is unaffected by VX-765 treatment. Corpus callosum immunofluorescence images of control vehicle, cuprizone (CZ) vehicle, or CZ VX-765 mice brains from Fig. 5.5 immunolabelled with ASPA, and DAPI were quantified using Volocity software. The volume of ASPA immunopositive cell bodies (A), and ASPA (FITC) fluorescence intensities (B) were measured (n = 3). All ASPA immunopositive cells in multiple fields of view within the corpus callosum were assessed. ASPA immunopositive cells from CZ vehicle mice have reduced cell volume, as well as reduced ASPA (FITC) fluorescence intensity that was not prevented by VX-765 treatment. #p-value<0.0001 by one-way ANOVA with Tukey's multiple comparison analysis.

5.7 Intranasal VX-765 treatment does not influence cuprizone-induced neurobehavioural deficits.

Previously it was observed that 0.5% cuprizone-fed mice displayed increased attraction towards the novel object in the NOR test (Fig. 4.9). To assess whether this altered behaviour observed in the 0.5% cuprizone group was prevented by VX-765 treatment, the NOR test was conducted on 0% cuprizone/vehicle, 0.5% cuprizone/vehicle, and 0.5% cuprizone/VX-765 groups (Fig. 5.9). The same experimental design as the previous NOR test was used, and the times spent at the familiar object (Fig. 5.9A) and novel object (Fig. 5.9B) were recorded. Similar to results illustrated on Fig. 4.6, all mice explored the familiar object for a similar amount of time (Fig. 5.9A), and the 0.5% cuprizone/vehicle group explored the novel object longer than the 0% cuprizone/vehicle group. Intranasal VX-765 treatment did not influence

the time spent at the novel object in the 0.5% cuprizone-exposed mice. These results are in agreement with the immunohistochemistry results from Fig. 5.4, since VX-765 treatment did not influence hippocampal demyelination and microglial activation. The enhanced novel object exploration observed in the NOR test might reflect the lack of VX-765 protection observed in cuprizone-induced hippocampal demyelination.

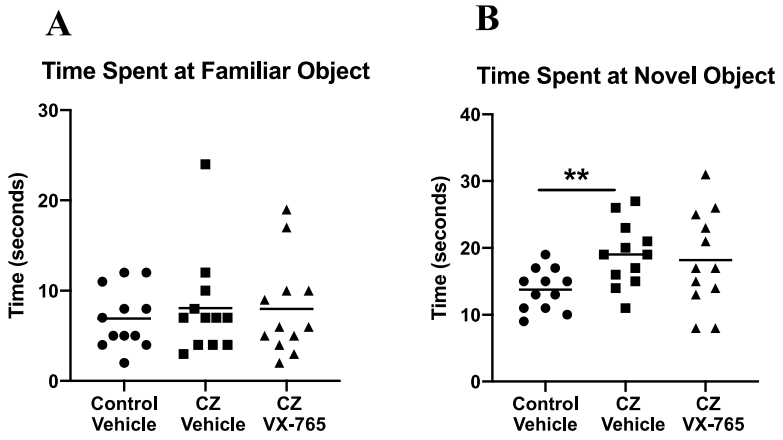

Figure 5.9 Increased novel object exploration in cuprizone-exposed animals was unaffected by VX-765 treatment. Female C57BL/6J mice were fed with 0 or 0.5% cuprizone (CZ) diet for 6-weeks accompanied by 4 weeks of daily intranasal VX-765 or vehicle treatment and were assessed by Novel Object Recognition test at 6 weeks (n = 12). Mice were trained in an open field bin with two identical objects for 5 minutes. After 6 hours of rest, mice were tested in the same bin with one of the objects replaced with a novel object. The time spent exploring the familiar object (A) and novel object (B) were measured. VX-765 treatment did not alter the enhanced exploration of the novel object in cuprizone-exposed mice. **p-value<0.01 by Student t-test.

Chapter 6 – Discussion

6.1 Novel findings within the thesis and how these support the working hypotheses

Among the most exciting findings within this thesis were my observations that supported the notion that human oligodendrocytes are capable of participating in inflammatory processes. Studies involving innate immune responses in oligodendrocytes have been limited[51,52,54], and many studies were performed using rodent cells. In my *in vitro* studies, several inflammasome-associated and Type I IFN-related immune gene transcripts were found to be induced in TNFα exposed GF- PDOs. Additionally, TNFα exposure induced release of Type I IFNs into the supernatants of PDOs. The expression of caspase-1 and gasdermin D proteins were also confirmed in TNFα exposed GF- PDOs. Collectively, these results suggested human oligodendrocytes are not immunologically inert, and are capable of responding upon exposure to a proinflammatory environment by generating an innate immune response.

In addition to the induction of innate immune responses, my *in vitro* studies revealed oligodendrocytes underwent pyroptosis, an inflammatory programmed cell death, upon exposure to TNFα, but without IL-1β or IL-18 release. Previous studies utilising mouse brain sections detected NLRP3 and caspase-1 expression in oligodendrocytes[52]. However, the detection of gasdermin D, a key executioner in pyroptosis, in TNFα exposed PDOs makes this study the first to assess gasdermin D expression and pyroptosis in oligodendrocytes. The TNFα-induced gasdermin D expression in GF- PDOs was reduced when cells were pre-treated with the caspase-1 inhibitor VX-765, pointing to caspase-1 dependent cleavage of gasdermin D expression. The lytic nature of pyroptosis was also confirmed by the increased LDH released into the supernatants of TNFα exposed PDOs, indicating increased cell membrane permeability in these cells, which was verified by the evidence of cell loss through reduced DAPI staining. In summary, these *in vitro* findings fully support my first hypothesis of human oligodendrocytes expressing innate immune proteins. Pyroptotic oligodendrocytes also have the potential to contribute to CNS inflammation because the lytic nature of pyroptosis leads to the release of cellular contents including DAMPs that accentuate inflammation[133].

Another novel finding reported in this thesis was the involvement of caspase-1 in the CNS of cuprizone-fed mice. The non-oligodendrocyte glial (microglia and astrocytes) activation observed in demyelinated regions, especially in the corpus callosum, in cuprizone-fed mice was significantly reduced with VX-765 treatment, suggesting the glial activation is in part due to caspase-1 activity. Gasdermin D expression by oligodendrocytes was also observed in cuprizone-fed mice, suggesting oligodendrocytes might also undergo pyroptosis *in vivo*. Caspase-1 expression in the corpus callosum of cuprizone-exposed mice has been previously reported[132] but this is the first study that assessed gasdermin D expression in the cuprizone model. Thus, these results represent the first description of pyroptosis as one of the potential cell death mechanisms affecting oligodendrocytes in the cuprizone model of demyelination. However, unlike my *in vitro* results, VX-765 treatment was not beneficial in reducing the number of gasdermin D immunopositive oligodendrocytes as determined by immunofluorescence analysis, although the drug protected myelin in the present studies. The limited therapeutic effect observed with VX-765 might reflect the antibody used to detect gasdermin D as it binds both cleaved (active) and full-length (inactive) protein. Since VX-765 exerted effects on other glial cells, it is improbable that there was reduced VX-765 uptake by oligodendrocytes. Nonetheless, VX-765 might be preventing cleavage of gasdermin D by inhibiting caspase-1 activity. Since VX-765 treatment did not commence until two weeks after cuprizone initiation, this delay might have been sufficient to induce oligodendrocyte injury and damage, leading to the transcription and translation of gasdermin D. Overall, these results partially support my second hypothesis, as the lack of full protection of oligodendrocytes and myelin, leaves some uncertainty about the extent of inflammasome activation in oligodendrocytes of cuprizone-fed mice.

6.2 Discussion of *in vitro* findings

Since studies involving investigation of innate immune responses in human oligodendrocytes are limited, one of the fist steps taken to assess the capacity of human oligodendrocytes to participate in innate immune responses was by stimulating PDOs with several different MS-relevant stimuli, and assessing the expression of a variety of innate immune genes by qRT-PCR. This approach was made because it was uncertain if PDOs would display immune

responses to any of the stimuli used. Both TNFα and IL-1β are cytokines that are induced in MS brains[5], and earlier studies have demonstrated human oligodendrocytes to express TNF receptors[49, 134], while the IL-1 receptor has been detected on rodent oligodendrocytes[53]. JC virus can naturally infect oligodendrocytes[117], and is known to cause opportunistic infection in some natalizumab treated MS patients[57]. It was necessary to test stimuli that could be detected by oligodendrocytes and were immunologically relevant to MS, in order to minimise the possibility of unresponsiveness by PDOs due to the lack of appropriate receptors needed to detect the stimuli used. One of the most striking observations made with the qRT-PCR analyses was the vastly different transcriptional responses observed by GF-PDOs depending on the stimulus used for these exposure experiments. The largest transcriptional changes were observed when PDOs were stimulated with TNFα (Fig. 3.3, 3.4), in which a significant induction of several innate immune-related gene transcript was observed, including *CASP1*, where there was more than a 100-fold increase in transcript levels. This transcriptional activation was most likely mediated through NFκB, as TNFα has been shown to induce NFκB signalling[81], and NFκB is well documented to induce transcription for variety of immune genes[135]. On the other hand, JC virus infection only induced a modest transcriptional induction in a few innate-immune genes (Fig. 3.5, 3.6), while no transcriptional changes were observed when PDOs were stimulated with IL-1β (Fig. A.2). The transcriptional responses induced by JC virus infection of PDOs were assessed at 3 days post-infection was to ensure adequate time for infection of these cells due to the low infectivity of the virus[118], although this may have ultimately suppressed the transcriptional response. Additionally, the limited immune gene transcriptional responses could be attributed to immune dysregulation by the JC virus, but this is unlikely due the detection of Type I IFN activity in the supernatants of infected cells. The lack of immunologic response observed by IL-1β exposed cells might be due to several reasons. It is possible that there is a threshold effect, and that the concentrations used in this study was not high enough to stimulate a response by PDOs, although this cannot be confirmed since only one concentration of IL-1β was tested. It is also possible that IL-1β induced non-inflammatory cell death (apoptosis), however this also cannot be confirmed as only a limited number of transcriptional analysis was performed on these samples. And finally, it is plausible that PDOs do not express the IL-1 receptor, despite expression on rodent oligodendrocytes[53], making them resistant to this

stimulus. Nonetheless, because TNFα exposure led to the most diverse innate immune-related transcriptional changes, and TNFα is highly germane to neuroinflammation in many diseases[136], further analyses were focused on TNFα exposed cells.

TNFα has been reported previously to induce oligodendrocyte cell death[119] and thus it was not surprising to observe reduction in oligodendrocyte specific gene transcripts. Cytokine-induced cell injury has also been previously demonstrated to cause reduction in myelin proteins[137], which is what is most likely occurring in TNFα exposed PDOs. What was unexpected was the induction of *B2M* and *TNFRSF1B* transcripts in both GF+ and GF- PDOs, while minimal changes were observed in apoptosis-related genes (Fig. 3.7). The induction of *B2M* transcripts is suggestive of MHC-I induction, as β_2-microglobulin is necessary for MHC-I surface expression[138]. *TNFRSF1B* encodes TNFRSF1B, also known as TNFR2 that is known to participate in downstream NFκB signalling[122] The induction of both of these genes was suggestive of PDOs having an immune phenotype, as induction of MHC molecules and cytokine receptors are common phenotypes observed in cells that are responding to local inflammation[139, 140]. These results are in agreement with recent findings showing induction of MHC-I and MHC-II molecules expression in murine OPCs and oligodendrocytes from EAE mice, as well as oligodendrocytes from post-mortem brain samples from MS patients[55]. The combination of my results, as well as the work form Falcao *et al.*[55] supports the concept that mature oligodendrocytes, represented by GF- PDOs, are capable of responding to proinflammatory stimuli, and also capable in exerting a limited immune response. Although few innate immune-related and oligodendrocyte cell marker-related gene transcriptional changes were observed in TNFα exposed GF+ PDOs, the induction of *B2M* and *TNFRSF1B* transcripts also suggested that immature oligodendrocytes, represented by GF+ PDOs, were also capable of responding, but in a different manner to mature oligodendrocytes.

One of the most exciting results in this thesis was the detection of caspase-1 and gasdermin D proteins in GF- PDOs after exposure to TNFα (Fig. 3.8, 3.12), along with evidence of PDOs undergoing pyroptosis. Although TNFα induced expression of a variety of innate immune genes by GF- PDOs, my analysis was focused on caspase-1 and gasdermin D since the transcripts for these two proteins were highly inducible in GF- PDOs, and because of the

reported involvement of both proteins in pyroptosis[141]. The detection of caspase-1 and gasdermin D in GF- PDOs raised the possibility of oligodendrocytes undergoing an inflammatory form of programmed cell death upon TNFα exposure in addition to apoptosis that has been reported previously[119, 120]. Since gasdermin D is an established substrate for caspase-1[82], the reduction in gasdermin D detection in immunocytochemistry analysis when GF- PDOs were pre- treated with VX-765 prior to TNFα exposure was indicative of caspase-1 activation in these cells. It was not surprising to see no changes in caspase-1 detection by immunocytochemistry, as VX-765 is an active site inhibitor of caspase-1[124], and it is unlikely to influence the transcription nor translation of casapse-1 protein. Additionally, VX-765 pre-treatment was beneficial in preventing the TNFα-induced morphological alterations observed in GF- PDOs (Fig. 3.13). Previous studies have also demonstrated morphological changes, as determined by loss of cell processes, in TNFα-induced cell death in adult human oligodendrocytes[119]. The complete rescue of processes, and prevention of cell death by VX-765 treatment in GF- PDOs were an indicator of caspase-1 and gasdermin D involvement in GF- PDO cell injury and pointing towards pyroptotic cell death.

Another indicator of pyroptosis observed in this study was the increase in LDH released into the supernatants of TNFα stimulated GF- PDOs. Unlike chromium-51 release assay, the LDH assay is a non-radioactive assay for measuring cell membrane integrity[142]. LDH is an enzyme that is found in the cell cytoplasm, and it is unable to cross the plasma membrane when intact[143, 144]. Because LDH is only permeable when the plasma membrane integrity is compromised, the detection of LDH in the supernatants indicated loss of plasma membrane integrity[144], a feature that is present in non-apoptotic cell death[145, 146]. In this study, LDH release in supernatants were detected when GF+ and GF- PDOs were stimulated with TNFα. The combined results of LDH release, immunocytochemistry analysis, and the VX-765 prevention experiments strongly indicated that pyroptosis is likely occurring in TNFα stimulated GF- PDOs. Unlike GF- PDOs, the GF+ PDOs are unlikely to be undergoing pyroptosis. Although TNFα stimulation of GF+ PDOs led to LDH detection in supernatants, I did not observe morphological changes, that are suggestive of cell death, nor was there detection of caspase-1 and gasdermin D by immunocytochemistry analyses. The increase in LDH detection in supernatants of GF+ PDOs suggested loss of cell membrane integrity in

some GF+ PDOs. Although quantification of dying cells did not reveal any statistically significant change in TNFα stimulated GF+ PDOs, it is still possible that the GF+ PDOs were undergoing cell injury without displaying morphological or transcriptional changes that were observed in GF- PDOs. Overall, immature oligodendrocytes might have been more resistant to the effects of TNFα.

The presence of pyroptosis in GF- PDOs was exciting but it was not surprising based on evidence from previous studies involving oligodendrocytes that displayed results implying cells might be undergoing an inflammatory form of cell death, although it was assumed to be apoptosis at the time[108, 147]. Previous studies involving oligodendrocytes from rodent brains showed apoptosis in cells after TNFα[147] or nerve growth factor (NGF)[108] exposure with caspase-1 induction. In both studies, cell death, as determined by TUNEL labelling, was prevented by treating the cells with the caspase-1 inhibitor acetyl-tyrosyl-valyl-analyl-aspart-1-aldehyde (YVAD-CHO)[108, 147]. Because cell death was prevented with a caspase-1 inhibitor, it raises the possibility of oligodendrocytes undergoing pyroptosis instead of apoptosis. Additionally, previous studies have also demonstrated TNFα induced TNFRSF1B signalling to be protective and promoted proliferation in mice OPCs[148]. As TNFRSF1B signalling has been demonstrated in oligodendrocyte lineage cells, and with the detection of gasdermin D on PDOs, oligodendrocytes might undergo pyroptosis when exposed to inflammatory conditions. One important point to keep in mind is that the results of this project demonstrate how oligodendrocytes are also capable in undergoing an inflammatory form of cell death in addition to apoptosis. Past works by Pouly *et al.*[149] and D'Souza *et al.*[119, 120] report a lack of LDH release by human adult oligodendrocytes after TNFα stimulation. In addition, TNFα stimulation of TNFRSF1A was demonstrated to induce apoptosis[121]. Overall, the mechanism of oligodendrocyte death induced by TNFα is likely to be influenced by the specific TNF receptor that it activates, but more research needs to be performed to confirm this idea.

With the detection of gasdermin D and evidence of pyroptosis in GF- PDOs, the lack of IL-1β and IL-18 release in the supernatants of TNFα exposed GF- PDOs was unexpected. The cleavage of pro-IL-1β and pro-IL-18 into their active forms by caspase-1 is a hallmark of

canonical inflammasome activation[82], and because of the initial detection of caspase-1 and gasdermin D, it was also thought that cytokine release would also be observed. It is plausible to attribute the lack of IL-1β and IL-18 detection in TNFα exposed PDO supernatants due to the lack of transcriptional induction. Although TNFα has been demonstrated to induce pro-IL-1β and pro-IL-18 in other cell types[79], oligodendrocytes might be resistant to transcription and translation of these two proinflammatory genes. Alternatively, oligodendrocytes might require exposure to an additional or a different stimulus to induce pro-IL-1β and pro-IL-18. Additionally, there are studies that suggest gasdermin D cleavage can be mediated by pro-caspase-1[86, 90], although mature caspase-1 is required for the cleavages of pro-IL-1β and pro-IL-18[86]. The antibody detecting caspase-1 used in this study can detect full length as well as cleaved caspase-1. It is possible that it was pro-caspase-1 that mediated gasdermin D cleavage in GF- PDOs as transcript of other inflammasome-related genes, *NLRP3*, *ASC*, and *IL1B* were not induced with TNFα exposure. Based on the present data obtained, I cannot conclude whether gasdermin D activation is mediated by pro-caspase-1 or by cleaved caspase-1, but the combination of these results suggest pyroptosis, mediated by gasdermin D activation occurs in TNFα-exposed cells, without the release of IL-1β and IL-18.

Although TNFα did not induce IL-1β and IL-18 release by PDOs, modest bioactive Type I IFN activity was detected in supernatants from TNFα exposed GF+ and GF- PDOs. Since *IFNB* (and not *IFNA* or *IFNL1/2/3*) transcript was detected in PDOs, the Type I IFN activity detected in the supernatants from PDOs was likely to be IFNβ. The Type I IFN activity detected in the supernatants support previous findings of limited Type I IFN production by oligodendrocytes[51]. Despite the minimal IFNβ released by PDOs, this appears to be sufficient in inducing ISGs, in GF- PDOs (Fig. 3.4). It is possible that the ISGs that are upregulated in TNFα exposed GF- PDOs is due to downstream IFNβ signalling[150], although more studies will be necessary to confirm this. Interestingly, unlike TNFα exposure, JC virus infection induced higher Type I IFN activity in the supernatants from PDOs, yet the antiviral-related genes were not induced to the level of TNFα-stimulated cells. This is most likely due to a feature of JC virus infection as previous infection studies using primary human foetal glial cells (PHFG) also described minimal ISG transcription induction at 3 days post infection[151], although the proportion of oligodendrocytes to astrocytes in the PHFG culture used in this

study is not certain. In summary, my results suggested oligodendrocytes are likely to have intact IFN signalling system that can be activated by TNFα exposure, recapitulating events that are present in proinflammatory environments, such as brains from MS patients.

Finally, another important finding made in my study was the differentiation-state dependent responses observed in most experiments conducted on PDOs. For most of my analyses, the GF- PDOs were more reactive to TNFα exposure than the GF+ PDOs, with greater transcript induction, with the detection of caspase-1 and gasdermin D, and with regards to morphological changes. Based on these results mature oligodendrocytes, represented by GF- PDOs, were more sensitive to the effects of TNFα exposure. The GF+ PDOs are by no means unresponsive, based on the observation of *B2M* and *TNFRSF1B* transcript induction, LDH release, and Type I IFN activity detected in supernatants, but GF+ PDOs showed higher survival after TNFα exposure than GF- PDOs. Immature oligodendrocytes (represented by GF+ PDOs) might be more resistant to proinflammatory environments, perhaps because these cells have the potential to be involved in remyelination within the CNS[93]. As mentioned previously, since TNFRSF1B signalling has protective effects on OPCs[148], it is also possible that TNFRSF1B signalling might also promote cell survival in immature oligodendrocytes. On the other hand, mature oligodendrocytes are terminally differentiated cells, which are not implicated in remyelination[93]. Because of this, it is possible that mature oligodendrocytes participate in local inflammation by inducing innate immune activation that could lead to inflammatory cell death. Although the involvement of oligodendrocytes in CNS inflammation is counter intuitive, it is possible that what is observed in conditions such as MS is the aberrant immune activation of oligodendrocytes, contributing to MS pathogenesis.

6.3 Discussion of *in vivo* findings

In order to assess the effects of local CNS inflammation on oligodendrocytes *in vivo*, the cuprizone model had to be first optimised. Several factors including dosing of the cuprizone, duration of the experiment, anatomic sites of analysis, and the sex of the mice used were assessed. A typical cuprizone experiment described in literature uses between 0.2-0.3% of cuprizone into the mouse diet (w/w) [152]. For this thesis, diets containing 0.3% and 0.5% (after adjusting for the volume of water added, the true dose is 0.13% and 0.22% respectively)

cuprizone were implemented to determine if a dose-dependent effect of cuprizone was observed on demyelination. As outlined on Fig. 4.1, 4.2 and 4.3, only mice that received the 0.5% cuprizone diet displayed consistent demyelination with significant glial activation and loss of oligodendrocytes. Although the number of oligodendrocytes did not decrease in mice that were fed with 0.3% cuprizone diet, the cell bodies of oligodendrocytes appeared to be smaller than in mice that were fed the control 0% cuprizone diet. It is possible that oligodendrocytes may be injured even when exposed to low doses of cuprizone, however further assessments were not made since I was interested in the oligodendrocyte response to local inflammation and demyelination that was not apparent at the lower cuprizone dose. In the 0.5% cuprizone group, the demyelination and glial activation observed at the central corpus callosum (directly below the sagittal sinus) after 6-weeks of feeding was comparable to previous reports[153, 154]. Based on these results, the correct dosing of cuprizone necessary to induce demyelination had been obtained. Cuprizone models from other groups have demonstrated presence of demyelination between 4-6 weeks of cuprizone feeding[101, 154]. Although robust demyelination was observed after 4-weeks of 0.5% cuprizone diet feeding, the reduction in mature oligodendrocytes in the corpus callosum was not observed until 6 weeks of 0.5% cuprizone diet feeding. Although loss of mature oligodendrocytes was demonstrated by 4 weeks in previous studies[154], the number of surviving mature oligodendrocytes after 6 weeks of 0.5% cuprizone diet feeding was comparable to previous studies[153]. One possible reason for the delayed loss of mature oligodendrocyte in my model may be due to the cuprizone diet that was used. The NeutraGel diet that is used in this thesis was found to contain more copper than the standard chow issued by HSLAS. Since cuprizone is a copper chelator, the higher copper concentration in the diet may interact with the cuprizone, inducing a delay in loss of mature oligodendrocytes. Nonetheless, the demyelination and glial activation observed in the corpus callosum was comparable to previous studies by 6 weeks[153].

One area with several discrepancies reported in the cuprizone model of toxic demyelination is the sex effect on demyelination. There are studies that have demonstrated that male mice exhibit worse disease than females[127], whereas other studies have observed no sex effect with regards to cuprizone-induced demyelination[128]. In my studies, the sex of the mice did not

appear to influence the severity of myelin loss, nor did it affect the proportion of activated microglia/macrophages (Fig. 4.4), however male mice experienced greater weight loss. Since no major differences between female and male mice were observed in demyelination and glial activation within the corpus callosum, all subsequent experiments were conducted on female mice. This is comparable with clinical circumstances where there are more female MS patients than male patients[62, 65], and because male mice experienced greater comorbidity (weight loss) than female mice for a similar experimental outcome.

In addition to demyelination and glial activation, previous studies using the cuprizone model have described increased anxiety in mice that were exposed to cuprizone[132]. Anxiety behaviours in mice can be assessed by performing an Open Field Test, where less time spent in the centre of an open field corresponds to increased anxiety behaviour in mice[155]. My Open Field Test results reflected no obvious anxiety behaviour in mice that were exposed to the cuprizone diet (Fig. A.8). The reported differences in behaviour observed may be due to differences in the experimental design. Studies that demonstrated increased anxiety in cuprizone exposed mice have utilised a larger Open Field apparatus than what I used in this thesis[132].

One of the most striking observations made while optimising the cuprizone model was the effect it had on the hippocampus (Fig. 4.7). Hippocampus loss of myelin proteins and glial activation has also been reported previously[156, 157]. Since the hippocampus has pivotal role in memory function[130], there has been several groups that have assessed memory in cuprizone-exposed mice with varying results[158, 159]. The differences in the type of results obtained are most likely reflected by the different experimental design used by each groups. For this thesis, to assess memory impairments, the NOR test was conducted on mice that were fed with 0% and 0.5% cuprizone diet (Fig. 4.9). Surprisingly, the 0.5% cuprizone group spent more time exploring the novel object than the 0% cuprizone group. These results suggest that mice from the 0.5% cuprizone group had an increased attraction towards the novel object. The altered exploration behaviour observed by the 0.5% cuprizone group may be attributed to perseveration, an abnormal behaviour involving repetition of a behaviour[160], although it has been previously associated with increased time spent at the familiar object in rodents[161].

Perseveration is observed among patients with neurocognitive impairments[162]. Although the 0.5% cuprizone group spent more time at the novel object, this enhanced exploration may be attributed to the demyelination effect observed in the hippocampus, causing functional impairment.

In the present thesis, cells expressing caspase-1 and gasdermin D were detected by immunohistochemistry in the corpus callosum of 0.5% cuprizone group (Fig. 4.8). Additionally, previous studies have also demonstrated expression of caspase-1 and other inflammasome-related proteins in the corpus callosum from cuprizone-exposed mice[132]. Since caspase-1 induction appeared to be involved in cuprizone-induced demyelination, 0.5% cuprizone diet-fed mice were treated with intranasal VX-765 to determine if demyelination could be prevented. VX-765 was delivered intranasally, which is a preferred drug delivery mode for patients compared to intravenous or oral delivery mode. The majority of MS DMTs available are injectable drugs, which is taxing for patients[163, 164]. The VX-765 treatment proved to be beneficial in partially maintaining myelin integrity in mice that were fed with 0.5% cuprizone diet, with preservation of MBP immunoreactivity but not in LFB or Nile Red staining (Fig. 5.1). One important point that distinguishes myelin quantification by staining with dyes (LFB and Nile Red) versus MBP immunolabelling is that the dyes label lipids that are present within myelin[165]. LFB predominantly stains phospholipids[166], while Nile Red labels polar lipids (including phospholipids)[167]. As approximately 40% of intact myelin is comprised by phospholipids[168], the absence of LFB or Nile Red labeling of myelin in 0.5% cuprizone/vehicle group could be due to the loss of specific lipids and might not mean all lipids within myelin are lost due to cuprizone-mediated demyelination. This point is emphasised by the fact that MBP immunolabelling is not completely lost in the 0.5% cuprizone/vehicle group, thus there may be altered myelin lipid composition while still expressing myelin proteins. However, it is important to note that the MBP being detected in cuprizone-exposed mice may be degraded MBP and not intact MBP, as MBP degradation has been demonstrated in the cuprizone model[169]. Although VX-765 treatment was beneficial in retaining some MBP, the MBP might be degraded, and it did not improve the altered myelin lipid composition that may be associated with cuprizone-mediated demyelination. The myelin might still be injured despite treatment, and thus VX-765 treatment may just be

reducing the magnitude of myelin protein damage and demyelination in cuprizone-exposed mice. Alternatively, if the MBP detected in VX-765 treated mice are not degraded it is possible that VX-765 treatment may be preventing demyelination, although further studies will be necessary to determine this. Overall, these results revealed that VX-765 was able to reduce the extent of demyelination, as observed by increased MBP immunolabelling.

Similar to the effects observed with myelin, VX-765 treatment was only beneficial in protecting some glial cells (Fig. 5.2, 5.3). VX-765 was highly beneficial in reducing the activation of microglia, astrocytes and OPCs in the 0.5% cuprizone/vehicle group, whereas VX-765 did not have any therapeutic effects on preserving the number of mature oligodendrocytes in the corpus callosum. Since VX-765 treatment diminished activation of microglia, astrocyte, and OPCs in the corpus callosum, these results implied that caspase-1 activation participated in the activation of these cells after cuprizone exposure, as well as demyelination. Since microglia and astrocyte activity has been reported to be necessary for demyelination in the cuprizone model[103, 104, 105], caspase-1 activation in one or both of these cells types, or another cell type might be inducing the enhanced glial activation observed in cuprizone-fed mice. However further analyses are necessary to determine which cell types are expressing active caspase-1. Overall, based on my immunohistochemistry data obtained, it is reasonable to conclude that cuprizone exposure may be stimulating the activation of caspase-1 in microglia, astrocytes, and/or OPCs, and which may lead to the activation of these cells such by producing proinflammatory mediators.

In addition to the reduced detection of microglia and astrocytes, VX-765 treatment was also effective in reducing OPC detection in the 0.5% cuprizone/VX-765 group. The reduction in the number of NG2 immunopositive OPCs in the VX-765 treated mice is most likely not because of the increased differentiation of OPCs into mature oligodendrocytes, as VX-765 treatment did not increase the number of surviving mature oligodendrocytes in the corpus callosum. As OPC differentiation into mature oligodendrocytes can contribute to remyelination in mice[93], increase in mature oligodendrocytes is observed during remyelination[128]. Since there were no differences in the number of surviving oligodendrocytes between 0.5% cuprizone/vehicle and 0.5% cuprizone/VX-765 groups, the

increased MBP immunolabelling observed in 0.5% cuprizone/VX-765 group may be due to prevention of demyelination, and not remyelination through increased OPC differentiation into oligodendrocytes. It is important to keep in mind that based on the results obtained it is not fully possible to determine whether if the surviving oligodendrocytes at time of experiment termination were differentiated before or after cuprizone exposure. If the surviving oligodendrocytes were developed prior to cuprizone exposure, the improvement of MBP immunolabelling in VX-765 treated mice may indicate prevention of demyelination or reduced demyelination, as previously stated. In contrast, if the surviving oligodendrocytes were differentiated after cuprizone exposure, alluding to the loss of previously existing oligodendrocytes, it is possible that the increase in MBP immunolabelling in VX-765 treated mice may indicate new myelin synthesis or remyelination that may not be possible without VX-765 treatment because of the enhanced glial activation. However, further experiments involving fate mapping of oligodendrocyte lineage cells, or assessing the presence of myelinating oligodendrocytes will be required to confirm this conclusion.

In the *in vitro* portion of this thesis, I demonstrated that oligodendrocytes could express caspase-1 and gasdermin D in response to proinflammatory stimuli. To examine if this can be reproduced *in vivo*, gasdermin D expression in corpus callosal oligodendrocytes were also assessed from 0% cuprizone/vehicle, 0.5% cuprizone/vehicle, and 0.5% cuprizone/VX-765 mice by immunofluorescence analysis (Fig. 5.5, 5.6). Gasdermin D immunofluorescence analysis without concurrent caspase-1 immunodetection was performed due to incompatibility between antibodies. Based on immunofluorescence analysis, there was an increase in gasdermin D immunolabelling in the 0.5% cuprizone/vehicle group, although there was no VX-765 effect. In both groups, some surviving oligodendrocytes were gasdermin D immunopositive, but the majority of the gasdermin D immunopositive cells were non-oligodendrocyte cells, most likely other glial cells. Among the gasdermin D immunonegative cells, VX-765 treatment reduced the number of non-oligodendrocyte glia but had no effect on oligodendrocytes in 0.5% cuprizone/VX- 765 group in comparison to 0.5% cuprizone/vehicle group. Thus, the key observation from this analysis was that VX-765 treatment seemed to reduce the number of non-oligodendrocyte glia that did not express gasdermin D, while having no effects on the number of gasdermin D expressing non-

oligodendrocyte glia. Since the immunohistochemistry results (Fig. 5.2, 5.3) demonstrated that there was a VX-765 effect in reducing glial cell (microglia, astrocyte, OPC) detection, the lack of a VX-765 effect on gasdermin D expressing cells, observed by immunofluorescence analysis, may have been due to limitations with the reagents used for this immunofluorescence analysis. The antibody used to label gasdermin D detects full-length (inactive) and cleaved (active) gasdermin D. Thus, VX-765 could be inhibiting the caspase-1 in the gasdermin D immunopositive cells by not cleaving full-length gasdermin D and other caspase-1 substrates. However, with the ongoing cuprizone exposure, it is possible for these cells to have an accumulation of full-length gasdermin D over the course of the experiment. Another interesting observation was that the number of gasdermin D immunonegative non- oligodendrocytes in 0% cuprizone/vehicle group is similar to the number of gasdermin D immunopositive 0.5% cuprizone/vehicle and 0.5% cuprizone/VX-765 group. This raises the possibility of the cells that were present within the corpus callosum prior to cuprizone exposure may be the cells that are undergoing caspase-1 activation. One of the downstream effects of activated caspase-1 is the cleavage of pro- IL-1β into IL-1β[79]. Previous studies have detected active IL-1β from the corpus callosum of mice that were exposed to cuprizone[132]. IL-1β has been demonstrated to have trophic effects and can induce proliferation in microglia[170]. Although IL-1β release is now known to be mediated by gasdermin D[86], prior to the discovery of gasdermin D IL-1β maturation had been observed without pyroptosis[171], raising the possibility of IL-1β mediated proliferation of non-oligodendrocyte glial cells may be taking place in cuprizone-exposed mice. Thus, the reduction in glial cell detection by immunohistochemistry in 0.5% cuprizone/VX-765 group may be contributed by the reduction of IL-1β release due to caspase-1 inhibition by VX-765. Additionally, caspase-1 activity has been demonstrated to influence phagosome development[172], and thus might influence the phagocytic capacity of microglia. Phagocytosis of myelin and myelin debris by microglia has been demonstrated to be involved with demyelination in the cuprizone model[173], therefore VX-765 treatment may also be reducing the phagocytic capacity of microglia, leading to increase in MBP immunodetection by immunohistochemistry analysis.

Figure 6.1 is a simple illustration of a possible model for the VX-765 effect on the cuprizone model, based on the results obtained in this thesis. Cuprizone exposure may trigger the initial injury in oligodendrocytes, apparent as smaller oligodendrocytes observed within 2-weeks of cuprizone exposure. This may lead to inflammasome activation in some oligodendrocytes resulting in the production of active gasdermin D, and eventual death by pyroptosis, while a subset of oligodendrocytes may die in other ways not discussed in this thesis. The oligodendrocytes undergoing pyroptosis, as determined by gasdermin D expression[141], might mediate release of DAMPs, which may promote activation of non-oligodendrocyte glia, such as microglia and astrocytes. These glial cells may also undergo inflammasome activation, leading to gasdermin D expression, and potentially mediate release of active IL-1β, which can promote proliferation and activation of other glial cells. Since cuprizone-exposure may not be a robust inflammatory stimulus for non-oligodendrocyte glia[174], pyroptosis is unlikely in these cells. The increased activated glial cells can then induce demyelination, potentially by release of proinflammatory mediators, and by myelin phagocytosis by microglia. The action of activated glial cells may possibly further contribute to oligodendrocyte injury. VX-765 treatment, initiated after 2-weeks of cuprizone exposure, could inhibit caspase-1 activity after this point compared to untreated cuprizone-exposed mice, potentially leading to reduced IL-1β release, thus preventing enhanced glial activation and proliferation. However since there is a 2-week window of no treatment, it is plausible that cells activated during this period might still contribute to demyelination even after initiation of VX-765 treatment, since oligodendrocytes would still be injured from the cuprizone exposure, evident by the smaller cell bodies with less ASPA immunoreactivity (Fig. 5.7). With VX-765 treatment, oligodendrocytes might not undergo pyroptosis because of VX-765 inhibition of caspase-1 activity, which is required for cleaving gasdermin D into its active form that is required for pyroptosis[141]. VX-765 treatment may prolong the survival of oligodendrocytes that otherwise would have been destined to die by pyroptosis, leading to preservation of some myelin. Alternatively, retention of myelin with VX-765 treatment may be attributed to the reduced phagocytic activity by microglia due to caspase-1 inhibition. Overall, based on the data obtained, Hypothesis 2 could not be completely validated, although caspse-1 does have a role in cuprizone-mediated demyelination, and gasdermin D expressing cells including oligodendrocytes are present in the corpus callosum of cuprizone-exposed mice.

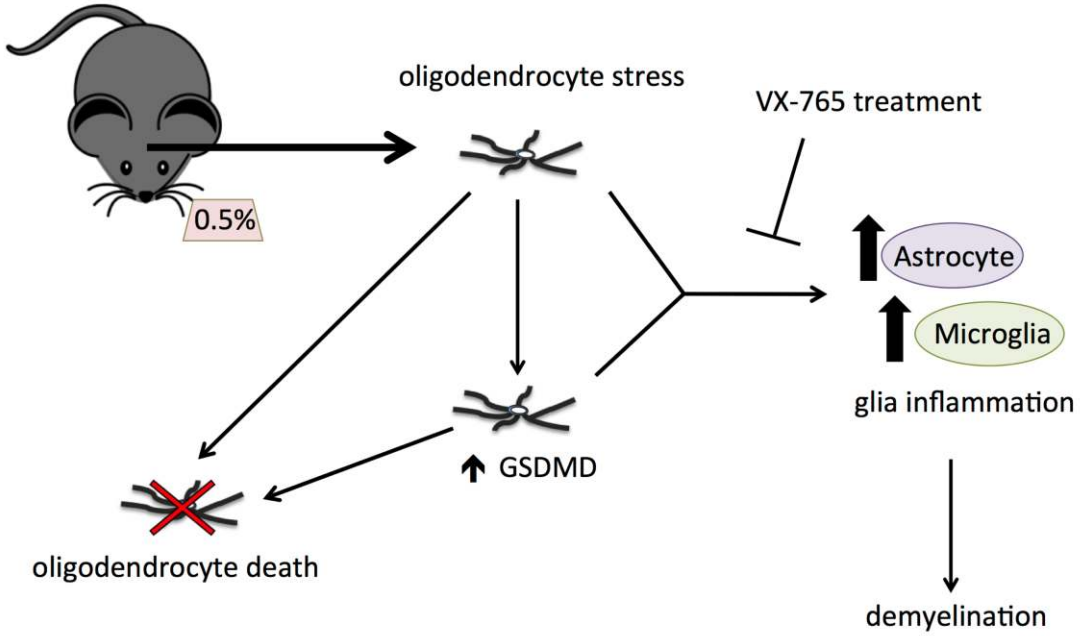

Figure 6.1 A model of the disease mechanisms underlying the cuprizone model of demyelination and its response to VX-765. Cuprizone exposure may induce oligodendrocyte stress and injury, leading to either cell death or inflammasome activation and subsequent gasdermin D expression. The injured oligodendrocytes may initiate microglia and astrocyte activation, which exacerbates demyelination and perhaps axonal damage. VX-765 treatment is likely limiting the extent of microglia and astrocyte activation, without protecting injured oligodendrocytes.

VX-765 treatment partially inhibited cuprizone-induced demyelination in the corpus callosum. Given that MBP loss, and microglial activation were observed in the hippocampus of the 0.5% cuprizone-exposed mice, I also examined the effects of VX-765 on the hippocampus (Fig. 5.4). Unlike the corpus callosum where there was reduced demyelination by MBP immunohistochemistry, and reduced microglial activation by Iba-1 immunohistochemistry, VX-765-mediated effects were not evident in the hippocampus. The anatomic site dependent cuprizone-mediated injury may have a role in the limited VX-765 effect in the hippocampus. Unlike in the corpus callosum, MBP immunoreactivity loss in the Ammon's horn was striking, while the Iba-1 immunoreactivity was approximately 10-fold

smaller in the 0.5% cuprizone/vehicle group. Thus, the hippocampus might be more vulnerable to cuprizone-mediated injury than the corpus callosum, and the extent of injury induced by cuprizone in the first 2-weeks of feeding may have precluded effects from VX-765 treatment. Because of the limited effect VX-765 had on hippocampus pathology, it was not surprising that VX-765 treatment also had no effect on the altered behaviour as assessed by the NOR test (Fig. 5.8). The enhanced exploration of the novel object observed in mice fed on 0.5% cuprizone diet in Fig. 4.9 was also apparent in the 0.5% cuprizone/vehicle group. In combination with the lack of MBP preservation with VX- 765 treatment at the hippocampus, the exploration time at the novel object was not influenced by VX-765 treatment. Again, the cuprizone-induced behaviour impairment observed might have been prevented if VX-765 treatment were to have started at the beginning of cuprizone feeding.

6.4 Limitations to the thesis

One of the key features of this project is the use of PDOs, a primary albeit differentiated human cell oligodendrocyte. Using PDOs has advantages over rodent cells as these cells are more likely to respond similarly to cells in the human CNS, thus it is possible to glean insights into how oligodendrocytes in the human brain might interact in a proinflammatory environment. Rodents and rodent-derived cells are frequently used to model human diseases such as MS, but there are notable differences between rodents and mice. Major differences in fundamental biology between humans and rodents are evident by the numerous failed MS therapies that were successful in the EAE model[97]. Although PDOs have strengths over rodent cells, there are also limitations. The PDOs used are of foetal origin, and thus may not fully recapitulate the mature oligodendrocytes that are found in adult brains. Furthermore, although GF- PDOs generate myelin proteins, these cells are grown solitarily in culture and thus do not form myelin. It is possible to artificially induce myelination *in vitro* by culturing oligodendrocytes with nanofibres[175], however this was not performed with the GF- PDOs due to challenges experienced with culturing the cells, now was it certain if this method would be feasible in the PDO culture. Had I been able to induce GF- PDOs to myelinate, it would be possible that these cells might have generated different responses to TNFα stimulation with the added metabolic stress caused by maintaining myelin.

Handling of PDOs was another challenging aspect of this thesis. All culturing experiments using PDOs were performed at the NIH due to unsuccessful attempts to culture PDOs at the Power lab. This may have been due to implementing optimal medium regents for growing PDOs, as some media reagents that are used for culturing PDOs at the NIH were only available within the United States. Additionally, culturing PDOs to high numbers were challenging due to the natural morphology of the cell. PDOs are cells with small cell bodies that have several long processes that limit the number of cells that can be cultured within a single flask. Because of this, I was unable to generate enough protein that would be necessary for Western blot analysis, thus all caspase-1 and gasdermin D immunodetection studies were performed solely by immunofluorescence analysis.

One of the chief limitations in any *in vivo* studies are the variations that can be observed using animals. In my cuprizone experiments, variation in results obtained by immunohistochemistry and immunofluorescence analyses were observed. Unlike EAE, where a set amount of myelin protein and adjuvant is injected in every mice[98], the administration of cuprizone is done by diet alone[98]. Since there can be variation in the amount of food that is consumed by individual mice within a cage, it is possible that this might have contributed to the variation observed in some immunohistochemistry and immunofluorescence results obtained. Another limitation was that randomisation of drug treatment could not be performed since intranasal delivery of VX-765 was performed. In injection-based treatments, it is possible to randomly assign mice within the same cage to different treatments. However, in intranasal delivery of drugs, since the administered drug can be released back into the cage if the mice were to sneeze, mice with the same treatment group must be housed in the same cage to avoid cross-contamination of treatments. Because of this, a cage effect may potentially influence the results obtained.

I also experienced challenges with the immunofluorescence analyses of PDO samples as well as mice brain samples, particularly with limited antibody availability for immunolabelling studies. For example, the caspase-1 and gasdermin D antibodies used in this thesis both detected full length as well as cleaved proteins, making it challenging for data analysis and interpretation. The immunofluorescence analysis of mice brains samples also had the added

limitation on the availability of the fluorescence lasers available. I have found that myelin can be visualised using the Cy5 channel without incubating the brain tissue slides with Cy5-conjugated secondary antibody, unless the Cy5 laser intensity is set very low. This meant that only very abundant proteins, such as cell-surface markers (e.g. GST-pi on oligodendrocytes) could be examined using the Cy5 channel.

6.5 Future lines of research

In this thesis, I discovered that GF- PDOs have robust transcriptional activation in terms of Type I IFN related genes, along with production of some Type I IFN in the cell supernatants. It would be interesting to see if any of the ISGs induced transcriptionally by TNFα are translated in PDOs and see how this may contribute to inflammation. Based on the results obtained from this thesis, oligodendrocytes appear to have capacity of generating a robust Type I IFN response, and this may have an impact on local inflammation. It would also be exciting to determine if these responses are also observed during JC virus infection of PDOs. In this study, only non-myelinating PDOs were used; as normal adult brain oligodendrocytes make myelin, especially in the white matter. It would be important to take this issue into consideration for future experiments, as myelinated oligodendrocytes would best represent the cells that will be found in the CNS. It is possible that the innate immune responses generated by myelinating oligodendrocytes in response to cytokine exposure such as TNFα may be different compared to unmyelinated PDOs.

Based on the results obtained in this thesis, oligodendrocytes appear to be able to undergo pyroptosis when stimulated with TNFα. It would be interesting to confirm if cell death observed caused by exposure to other cytokines can also induce pyroptosis. Additionally, TNFα has also been documented to cause apoptosis in oligodendrocytes[119, 120]. It is important to define the proportion of cells that might undergo apoptosis instead of pyroptosis and determining what specific factors influence the death program fate upon exposure to TNFα. Since in this thesis it was found that oligodendrocytes could also undergo pyroptosis when exposed to proinflammatory stimuli, it would be interesting to see if oligodendrocytes with intact myelin contribute to demyelination.

Based on the *in vivo* section of this thesis, it was determined that the effects of cuprizone-mediated injury can be reduced by VX-765 treatment. In this thesis, it could not be determined in which non-oligodendrocyte cell caspase-1 was activated, but it would be interesting to assess if caspase-1 activation was present in microglia or other glia types, and the specific role caspase-1 might be having in these cells. Furthermore, it would be interesting to assess the difference in cell function between glial cells that were gasdermin D immunopositive and gasdermin D immunonegative in the corpus callosum. Additionally, it will also be beneficial to assess whether the surviving oligodendrocytes at the end of the 6-week experiments are surviving oligodendrocytes, or newly differentiated oligodendrocytes. Since this study focused analysis at the pathological changes observed at the corpus callosum, it would be interesting to look into the hippocampal changes as well. Further analysis of the hippocampal changes may yield insights into the NOR results.

References

1. Tuladhar, A., Mitrousis, N., Führmann, T., Shoichet, M.S. Chapter 30 - Central Nervous System In: Atala, A., and Allickson, J.G. (ed). *Translational Regenerative Medicine*. Academic Press: The Boulevard, Langford Lane, Kidlington, Oxford OX5 1GB, UK, 2015, pp 415-435.

2. Klein, R.S. & Hunter, C.A. Protective and Pathological Immunity during Central Nervous System Infections. *Immunity* **46**, 891-909 (2017).

3. Saab, A.S. & Nave, K.A. Myelin dynamics: protecting and shaping neuronal functions. *Curr Opin Neurobiol* **47**, 104-112 (2017).

4. Allen, N.J. & Lyons, D.A. Glia as architects of central nervous system formation and function. *Science* **362**, 181-185 (2018).

5. Filippi, M. *et al.* Multiple sclerosis. *Nat Rev Dis Primers* **4**, 43 (2018).

6. DiSabato, D.J., Quan, N. & Godbout, J.P. Neuroinflammation: the devil is in the details. *J Neurochem* **139 Suppl 2**, 136-153 (2016).

7. von Bartheld, C.S., Bahney, J. & Herculano-Houzel, S. The search for true numbers of neurons and glial cells in the human brain: A review of 150 years of cell counting. *J Comp Neurol* **524**, 3865-3895 (2016).

8. Nicolas-Avila, J.A., Hidalgo, A. & Ballesteros, I. Specialized functions of resident macrophages in brain and heart. *J Leukoc Biol* **104**, 743-756 (2018).

9. Hartline, D.K. The evolutionary origins of glia. *Glia* **59**, 1215-1236 (2011).

10. Hoeffel, G. *et al.* C-Myb(+) erythro-myeloid progenitor-derived fetal monocytes give rise to adult tissue-resident macrophages. *Immunity* **42**, 665-678 (2015).

11. von Bernhardi, R., Heredia, F., Salgado, N. & Munoz, P. Microglia Function in the Normal Brain. *Adv Exp Med Biol* **949**, 67-92 (2016).

12. Magaki, S.D., Williams, C.K. & Vinters, H.V. Glial function (and dysfunction) in the normal & ischemic brain. *Neuropharmacology* **134**, 218-225 (2018).

13. Daneman, R. & Prat, A. The blood-brain barrier. *Cold Spring Harb Perspect Biol* **7**, a020412 (2015).

14. Miller, D.S. Regulation of ABC transporters at the blood-brain barrier. *Clin Pharmacol Ther* **97**, 395-403 (2015).

15. Mederos, S., Gonzalez-Arias, C. & Perea, G. Astrocyte-Neuron Networks: A Multilane Highway of Signaling for Homeostatic Brain Function. *Front Synaptic Neurosci* **10**, 45 (2018).

16. Pepper, R.E., Pitman, K.A., Cullen, C.L. & Young, K.M. How Do Cells of the Oligodendrocyte Lineage Affect Neuronal Circuits to Influence Motor Function, Memory and Mood? *Front Cell Neurosci* **12**, 399 (2018).

17. Dimou, L. & Gallo, V. NG2-glia and their functions in the central nervous system. *Glia* **63**, 1429-1451 (2015).

18. Eugenin-von Bernhardi, J. & Dimou, L. NG2-glia, More Than Progenitor Cells. *Adv Exp Med Biol* **949**, 27-45 (2016).

19. Zhu, X. *et al.* Age-dependent fate and lineage restriction of single NG2 cells. *Development* **138**, 745-753 (2011).

20. Baumann, N. & Pham-Dinh, D. Biology of oligodendrocyte and myelin in the mammalian central nervous system. *Physiol Rev* **81**, 871-927 (2001).

21. Santos, A.K. *et al.* Decoding cell signalling and regulation of oligodendrocyte differentiation. *Semin Cell Dev Biol* (2018).

22. Traiffort, E., Zakaria, M., Laouarem, Y. & Ferent, J. Hedgehog: A Key Signaling in the Development of the Oligodendrocyte Lineage. *J Dev Biol* **4** (2016).

23. Miller, R.H. Regulation of oligodendrocyte development in the vertebrate CNS. *Prog Neurobiol* **67**, 451-467 (2002).

24. Leferink, P.S. & Heine, V.M. The Healthy and Diseased Microenvironments Regulate Oligodendrocyte Properties: Implications for Regenerative Medicine. *Am J Pathol* **188**, 39-52 (2018).

25. Goldman, S.A. & Kuypers, N.J. How to make an oligodendrocyte. *Development* **142**, 3983-3995 (2015).

26. Monaco, M.C. *et al.* Progenitor-derived oligodendrocyte culture system from human fetal brain. *J Vis Exp* (2012).

27. Elbaz, B. & Popko, B. Molecular Control of Oligodendrocyte Development. *Trends Neurosci* **42**, 263-277 (2019).

28. Roth, A.D. & Nunez, M.T. Oligodendrocytes: Functioning in a Delicate Balance Between High Metabolic Requirements and Oxidative Damage. *Adv Exp Med Biol* **949**, 167-181 (2016).

29. Shi, Y., Cai, M., Zhou, L. & Wang, H. The structure and function of cell membranes studied by atomic force microscopy. *Semin Cell Dev Biol* **73**, 31-44 (2018).

30. Min, Y. *et al.* Interaction forces and adhesion of supported myelin lipid bilayers modulated by myelin basic protein. *Proc Natl Acad Sci U S A* **106**, 3154-3159 (2009).

31. Baron, W. & Hoekstra, D. On the biogenesis of myelin membranes: sorting, trafficking and cell polarity. *FEBS Lett* **584**, 1760-1770 (2010).

32. Philips, T. & Rothstein, J.D. Oligodendroglia: metabolic supporters of neurons. *J Clin Invest* **127**, 3271-3280 (2017).

33. Roscoe, R.B., Elliott, C., Zarros, A. & Baillie, G.S. Non-genetic therapeutic approaches to Canavan disease. *J Neurol Sci* **366**, 116-124 (2016).

34. Moffett, J.R., Ross, B., Arun, P., Madhavarao, C.N. & Namboodiri, A.M. N-Acetylaspartate in the CNS: from neurodiagnostics to neurobiology. *Prog Neurobiol* **81**, 89-131 (2007).

35. Engelhardt, B., Vajkoczy, P. & Weller, R.O. The movers and shapers in immune privilege of the CNS. *Nat Immunol* **18**, 123-131 (2017).

36. Lampron, A., Elali, A. & Rivest, S. Innate immunity in the CNS: redefining the relationship between the CNS and Its environment. *Neuron* **78**, 214-232 (2013).

37. Negi, N. & Das, B.K. CNS: Not an immunoprivilaged site anymore but a virtual secondary lymphoid organ. *Int Rev Immunol* **37**, 57-68 (2018).

38. Stephenson, J., Nutma, E., van der Valk, P. & Amor, S. Inflammation in CNS neurodegenerative diseases. *Immunology* **154**, 204-219 (2018).

39. Klein, R.S., Garber, C. & Howard, N. Infectious immunity in the central nervous system and brain function. *Nat Immunol* **18**, 132-141 (2017).

40. Forrester, J.V., McMenamin, P.G. & Dando, S.J. CNS infection and immune privilege. *Nat Rev Neurosci* **19**, 655-671 (2018).

41. Shechter, R., London, A. & Schwartz, M. Orchestrated leukocyte recruitment to immune-privileged sites: absolute barriers versus educational gates. *Nat Rev Immunol* **13**, 206-218 (2013).

42. Rua, R. & McGavern, D.B. Advances in Meningeal Immunity. *Trends Mol Med* **24**, 542-559 (2018).

43. Ransohoff, R.M. & Engelhardt, B. The anatomical and cellular basis of immune surveillance in the central nervous system. *Nat Rev Immunol* **12**, 623-635 (2012).

44. Patel, M.M. & Patel, B.M. Crossing the Blood-Brain Barrier: Recent Advances in Drug Delivery to the Brain. *CNS Drugs* **31**, 109-133 (2017).

45. Kigerl, K.A., de Rivero Vaccari, J.P., Dietrich, W.D., Popovich, P.G. & Keane, R.W. Pattern recognition receptors and central nervous system repair. *Exp Neurol* **258**, 5-16 (2014).

46. Stephan, A.H., Barres, B.A. & Stevens, B. The complement system: an unexpected role in synaptic pruning during development and disease. *Annu Rev Neurosci* **35**, 369-389 (2012).

47. Liddelow, S.A. & Barres, B.A. Reactive Astrocytes: Production, Function, and Therapeutic Potential. *Immunity* **46**, 957-967 (2017).

48. Bsibsi, M., Nomden, A., van Noort, J.M. & Baron, W. Toll-like receptors 2 and 3 agonists differentially affect oligodendrocyte survival, differentiation, and myelin membrane formation. *J Neurosci Res* **90**, 388-398 (2012).

49. Aguirre, A., Maturana, C.J., Harcha, P.A. & Saez, J.C. Possible involvement of TLRs and hemichannels in stress-induced CNS dysfunction via mastocytes, and glia activation. *Mediators Inflamm* **2013**, 893521 (2013).

50. Choi, J.Y. *et al.* Role of toll-like receptor 2 in ischemic demyelination and oligodendrocyte death. *Neurobiol Aging* **35**, 1643-1653 (2014).

51. Kapil, P., Butchi, N.B., Stohlman, S.A. & Bergmann, C.C. Oligodendroglia are limited in type I interferon induction and responsiveness in vivo. *Glia* **60**, 1555-1566 (2012).

52. Maturana, C.J., Aguirre, A. & Saez, J.C. High glucocorticoid levels during gestation activate the inflammasome in hippocampal oligodendrocytes of the offspring. *Dev Neurobiol* (2016).

53. Wang, X.F. *et al.* Upregulation of type I interleukin-1 receptor after traumatic spinal cord injury in adult rats. *Acta Neuropathol* **111**, 220-228 (2006).

54. Peferoen, L., Kipp, M., van der Valk, P., van Noort, J.M. & Amor, S. Oligodendrocyte-microglia cross-talk in the central nervous system. *Immunology* **141**, 302-313 (2014).

55. Falcao, A.M. *et al.* Disease-specific oligodendrocyte lineage cells arise in multiple sclerosis. *Nat Med* **24**, 1837-1844 (2018).

56. Bohra, C., Sokol, L. & Dalia, S. Progressive Multifocal Leukoencephalopathy and Monoclonal Antibodies: A Review. *Cancer Control* **24**, 1073274817729901 (2017).

57. Brandstadter, R. & Katz Sand, I. The use of natalizumab for multiple sclerosis. *Neuropsychiatr Dis Treat* **13**, 1691-1702 (2017).

58. Gerber, B. *et al.* The impact of treatment adherence on clinical and economic outcomes in multiple sclerosis: Real world evidence from Alberta, Canada. *Mult Scler Relat Disord* **18**, 218-224 (2017).

59. Dargahi, N. *et al.* Multiple Sclerosis: Immunopathology and Treatment Update. *Brain Sci* **7** (2017).

60. Disease-modifying therapies. [Website] 2019 2019 [cited 2019 April 30 2019]Available from: https://mssociety.ca/managing-ms/treatments/medications/disease-modifying-therapies-dmts

61. Ascherio, A. & Munger, K.L. Epidemiology of Multiple Sclerosis: From Risk Factors to Prevention-An Update. *Semin Neurol* **36**, 103-114 (2016).

62. Dobson, R. & Giovannoni, G. Multiple sclerosis - a review. *Eur J Neurol* **26**, 27-40 (2019).

63. Omerhoca, S., Akkas, S.Y. & Icen, N.K. Multiple Sclerosis: Diagnosis and Differential Diagnosis. *Noro Psikiyatr Ars* **55**, S1-S9 (2018).

64. Barclay, W. & Shinohara, M.L. Inflammasome activation in multiple sclerosis and experimental autoimmune encephalomyelitis (EAE). *Brain Pathol* **27**, 213-219 (2017).

65. Doshi, A. & Chataway, J. Multiple sclerosis, a treatable disease. *Clin Med (Lond)* **17**, 530-536 (2017).

66. Rubtsova, K., Marrack, P. & Rubtsov, A.V. Sexual dimorphism in autoimmunity. *J Clin Invest* **125**, 2187-2193 (2015).

67. Ramien, C. *et al.* Sex effects on inflammatory and neurodegenerative processes in multiple sclerosis. *Neurosci Biobehav Rev* **67**, 137-146 (2016).

68. Dendrou, C.A., Fugger, L. & Friese, M.A. Immunopathology of multiple sclerosis. *Nat Rev Immunol* **15**, 545-558 (2015).

69. Correale, J., Gaitan, M.I., Ysrraelit, M.C. & Fiol, M.P. Progressive multiple sclerosis: from pathogenic mechanisms to treatment. *Brain* **140**, 527-546 (2017).

70. Gelfand, J.M. Multiple sclerosis: diagnosis, differential diagnosis, and clinical presentation. *Handb Clin Neurol* **122**, 269-290 (2014).

71. Schiess, N. & Calabresi, P.A. Multiple Sclerosis. *Semin Neurol* **36**, 350-356 (2016).

72. Willis, M.A. & Fox, R.J. Progressive Multiple Sclerosis. *Continuum (Minneap Minn)* **22**, 785-798 (2016).

73. Macias Islas, M.A. & Ciampi, E. Assessment and Impact of Cognitive Impairment in Multiple Sclerosis: An Overview. *Biomedicines* **7** (2019).

74. Files, D.K., Jausurawong, T., Katrajian, R. & Danoff, R. Multiple sclerosis. *Prim Care* **42**, 159-175 (2015).

75. Dulamea, A.O. Role of Oligodendrocyte Dysfunction in Demyelination, Remyelination and Neurodegeneration in Multiple Sclerosis. *Adv Exp Med Biol* **958**, 91-127 (2017).

76. Konnecke, H. & Bechmann, I. The role of microglia and matrix metalloproteinases involvement in neuroinflammation and gliomas. *Clin Dev Immunol* **2013**, 914104 (2013).

77. Mallucci, G., Peruzzotti-Jametti, L., Bernstock, J.D. & Pluchino, S. The role of immune cells, glia and neurons in white and gray matter pathology in multiple sclerosis. *Prog Neurobiol* **127-128**, 1-22 (2015).

78. Platnich, J.M. & Muruve, D.A. NOD-like receptors and inflammasomes: A review of their canonical and non-canonical signaling pathways. *Arch Biochem Biophys* (2019).

79. Mamik, M.K. & Power, C. Inflammasomes in neurological diseases: emerging pathogenic and therapeutic concepts. *Brain* **140**, 2273-2285 (2017).

80. Gharagozloo, M. *et al.* NLR-Dependent Regulation of Inflammation in Multiple Sclerosis. *Front Immunol* **8**, 2012 (2017).

81. Lawrence, T. The nuclear factor NF-kappaB pathway in inflammation. *Cold Spring Harb Perspect Biol* **1**, a001651 (2009).

82. Swanson, K.V., Deng, M. & Ting, J.P. The NLRP3 inflammasome: molecular activation and regulation to therapeutics. *Nat Rev Immunol* (2019).

83. Voet, S., Srinivasan, S., Lamkanfi, M. & van Loo, G. Inflammasomes in neuroinflammatory and neurodegenerative diseases. *EMBO Mol Med* (2019).

84. Shi, J., Gao, W. & Shao, F. Pyroptosis: Gasdermin-Mediated Programmed Necrotic Cell Death. *Trends Biochem Sci* **42**, 245-254 (2017).

85. Kovacs, S.B. & Miao, E.A. Gasdermins: Effectors of Pyroptosis. *Trends Cell Biol* **27**, 673-684 (2017).

86. He, W.T. *et al.* Gasdermin D is an executor of pyroptosis and required for interleukin-1beta secretion. *Cell Res* **25**, 1285-1298 (2015).

87. Shi, J. *et al.* Cleavage of GSDMD by inflammatory caspases determines pyroptotic cell death. *Nature* **526**, 660-665 (2015).

88. Van Opdenbosch, N. & Lamkanfi, M. Caspases in Cell Death, Inflammation, and Disease. *Immunity* **50**, 1352-1364 (2019).

89. Pellegrini, C., Antonioli, L., Lopez-Castejon, G., Blandizzi, C. & Fornai, M. Canonical and Non-Canonical Activation of NLRP3 Inflammasome at the Crossroad between Immune Tolerance and Intestinal Inflammation. *Front Immunol* **8**, 36 (2017).

90. Okondo, M.C. *et al.* DPP8 and DPP9 inhibition induces pro-caspase-1-dependent monocyte and macrophage pyroptosis. *Nat Chem Biol* **13**, 46-53 (2017).

91. Miao, E.A. *et al.* Caspase-1-induced pyroptosis is an innate immune effector mechanism against intracellular bacteria. *Nat Immunol* **11**, 1136-1142 (2010).

92. Plemel, J.R., Liu, W.Q. & Yong, V.W. Remyelination therapies: a new direction and challenge in multiple sclerosis. *Nat Rev Drug Discov* **16**, 617-634 (2017).

93. Franklin, R.J.M. & Ffrench-Constant, C. Regenerating CNS myelin - from mechanisms to experimental medicines. *Nat Rev Neurosci* **18**, 753-769 (2017).

94. Kutzelnigg, A. & Lassmann, H. Pathology of multiple sclerosis and related inflammatory demyelinating diseases. *Handb Clin Neurol* **122**, 15-58 (2014).

95. Ljubisavljevic, S. Oxidative Stress and Neurobiology of Demyelination. *Mol Neurobiol* **53**, 744-758 (2016).

96. Duncan, I.D. *et al.* The adult oligodendrocyte can participate in remyelination. *Proc Natl Acad Sci U S A* **115**, E11807-E11816 (2018).

97. Mix, E., Meyer-Rienecker, H., Hartung, H.P. & Zettl, U.K. Animal models of multiple sclerosis--potentials and limitations. *Prog Neurobiol* **92**, 386-404 (2010).

98. Procaccini, C., De Rosa, V., Pucino, V., Formisano, L. & Matarese, G. Animal models of Multiple Sclerosis. *Eur J Pharmacol* **759**, 182-191 (2015).

99. Lassmann, H. & Bradl, M. Multiple sclerosis: experimental models and reality. *Acta Neuropathol* **133**, 223-244 (2017).

100. Palumbo, S. & Pellegrini, S. Experimental In Vivo Models of Multiple Sclerosis: State of the Art. In: Zagon, I.S. & McLaughlin, P.J. (eds). *Multiple Sclerosis: Perspectives in Treatment and Pathogenesis*: Brisbane (AU), 2017.

101. Kipp, M. *et al.* Experimental in vivo and in vitro models of multiple sclerosis: EAE and beyond. *Mult Scler Relat Disord* **1**, 15-28 (2012).

102. Sharma, R. *et al.* Inflammation induced by innate immunity in the central nervous system leads to primary astrocyte dysfunction followed by demyelination. *Acta Neuropathol* **120**, 223-236 (2010).

103. McMurran, C.E., Zhao, C. & Franklin, R.J.M. Toxin-Based Models to Investigate Demyelination and Remyelination. *Methods Mol Biol* **1936**, 377-396 (2019).

104. Praet, J., Guglielmetti, C., Berneman, Z., Van der Linden, A. & Ponsaerts, P. Cellular and molecular neuropathology of the cuprizone mouse model: clinical relevance for multiple sclerosis. *Neurosci Biobehav Rev* **47**, 485-505 (2014).

105. Liu, L. *et al.* CXCR2-positive neutrophils are essential for cuprizone-induced demyelination: relevance to multiple sclerosis. *Nat Neurosci* **13**, 319-326 (2010).

106. Pasquini, L.A. *et al.* The neurotoxic effect of cuprizone on oligodendrocytes depends on the presence of pro-inflammatory cytokines secreted by microglia. *Neurochem Res* **32**, 279-292 (2007).

107. Hovelmeyer, N. *et al.* Apoptosis of oligodendrocytes via Fas and TNF-R1 is a key event in the induction of experimental autoimmune encephalomyelitis. *J Immunol* **175**, 5875-5884 (2005).

108. Gu, C., Casaccia-Bonnefil, P., Srinivasan, A. & Chao, M.V. Oligodendrocyte apoptosis mediated by caspase activation. *J Neurosci* **19**, 3043-3049 (1999).

109. Cannella, B., Gaupp, S., Omari, K.M. & Raine, C.S. Multiple sclerosis: death receptor expression and oligodendrocyte apoptosis in established lesions. *J Neuroimmunol* **188**, 128-137 (2007).

110. Linkermann, A. *et al.* Regulated cell death in AKI. *J Am Soc Nephrol* **25**, 2689-2701 (2014).

111. Seth, P., Diaz, F., Tao-Cheng, J.H. & Major, E.O. JC virus induces nonapoptotic cell death of human central nervous system progenitor cell-derived astrocytes. *J Virol* **78**, 4884-4891 (2004).

112. Ferenczy, M.W. *et al.* Clonal immortalized human glial cell lines support varying levels of JC virus infection due to differences in cellular gene expression. *J Neuroimmune Pharmacol* **8**, 1303-1319 (2013).

113. Boghozian, R. *et al.* Suppressed oligodendrocyte steroidogenesis in multiple sclerosis: Implications for regulation of neuroinflammation. *Glia* **65**, 1590-1606 (2017).

114. Walsh, J.G. *et al.* Rapid inflammasome activation in microglia contributes to brain disease in HIV/AIDS. *Retrovirology* **11**, 35 (2014).

115. Bego, M.G., Mercier, J. & Cohen, E.A. Virus-activated interferon regulatory factor 7 upregulates expression of the interferon-regulated BST2 gene independently of interferon signaling. *J Virol* **86**, 3513-3527 (2012).

116. McKenzie, B.A. *et al.* Caspase-1 inhibition prevents glial inflammasome activation and pyroptosis in models of multiple sclerosis. *Proc Natl Acad Sci U S A* **115**, E6065-E6074 (2018).

117. Monaco, M.C. & Major, E.O. Immune System Involvement in the Pathogenesis of JC Virus Induced PML: What is Learned from Studies of Patients with Underlying Diseases and Therapies as Risk Factors. *Front Immunol* **6**, 159 (2015).

118. Major, E.O. *et al.* Establishment of a line of human fetal glial cells that supports JC virus multiplication. *Proc Natl Acad Sci U S A* **82**, 1257-1261 (1985).

119. D'Souza, S., Alinauskas, K., McCrea, E., Goodyer, C. & Antel, J.P. Differential susceptibility of human CNS-derived cell populations to TNF-dependent and independent immune-mediated injury. *J Neurosci* **15**, 7293-7300 (1995).

120. D'Souza, S.D., Alinauskas, K.A. & Antel, J.P. Ciliary neurotrophic factor selectively protects human oligodendrocytes from tumor necrosis factor-mediated injury. *J Neurosci Res* **43**, 289-298 (1996).

121. Elmore, S. Apoptosis: a review of programmed cell death. *Toxicol Pathol* **35**, 495-516 (2007).

122. Kast, R.E. Evidence of a mechanism by which etanercept increased TNF-alpha in multiple myeloma: new insights into the biology of TNF-alpha giving new treatment opportunities--the role of bupropion. *Leuk Res* **29**, 1459-1463 (2005).

123. Gaidt, M.M. & Hornung, V. Pore formation by GSDMD is the effector mechanism of pyroptosis. *EMBO J* **35**, 2167-2169 (2016).

124. Boxer, M.B., Shen, M., Auld, D.S., Wells, J.A. & Thomas, C.J. A small molecule inhibitor of Caspase 1. *Probe Reports from the NIH Molecular Libraries Program*: Bethesda (MD), 2010.

125. Tamura, Y. *et al.* Intracellular translocation of glutathione S-transferase pi during oligodendrocyte differentiation in adult rat cerebral cortex in vivo. *Neuroscience* **148**, 535-540 (2007).

126. Russi, A.E., Ebel, M.E., Yang, Y. & Brown, M.A. Male-specific IL-33 expression regulates sex-dimorphic EAE susceptibility. *Proc Natl Acad Sci U S A* **115**, E1520-E1529 (2018).

127. Moore, S., Patel, R., Hannsun, G., Yang, J. & Tiwari-Woodruff, S.K. Sex chromosome complement influences functional callosal myelination. *Neuroscience* **245**, 166-178 (2013).

128. Taylor, L.C., Gilmore, W., Ting, J.P. & Matsushima, G.K. Cuprizone induces similar demyelination in male and female C57BL/6 mice and results in disruption of the estrous cycle. *J Neurosci Res* **88**, 391-402 (2010).

129. Boeschoten, R.E. *et al.* Prevalence of depression and anxiety in Multiple Sclerosis: A systematic review and meta-analysis. *J Neurol Sci* **372**, 331-341 (2017).

130. Opitz, B. Memory function and the hippocampus. *Front Neurol Neurosci* **34**, 51-59 (2014).

131. Leger, M. *et al.* Object recognition test in mice. *Nat Protoc* **8**, 2531-2537 (2013).

132. Yu, H. *et al.* Prednisone alleviates demyelination through regulation of the NLRP3 inflammasome in a C57BL/6 mouse model of cuprizone-induced demyelination. *Brain Res* **1678**, 75-84 (2018).

133. Man, S.M., Karki, R. & Kanneganti, T.D. Molecular mechanisms and functions of pyroptosis, inflammatory caspases and inflammasomes in infectious diseases. *Immunol Rev* **277**, 61-75 (2017).

134. Zeis, T., Enz, L. & Schaeren-Wiemers, N. The immunomodulatory oligodendrocyte. *Brain Res* **1641**, 139-148 (2016).

135. Mc Guire, C., Prinz, M., Beyaert, R. & van Loo, G. Nuclear factor kappa B (NF-kappaB) in multiple sclerosis pathology. *Trends Mol Med* **19**, 604-613 (2013).

136. Kempuraj, D. *et al.* Neuroinflammation Induces Neurodegeneration. *J Neurol Neurosurg Spine* **1** (2016).

137. Jana, M. & Pahan, K. Redox regulation of cytokine-mediated inhibition of myelin gene expression in human primary oligodendrocytes. *Free Radic Biol Med* **39**, 823-831 (2005).

138. Pamer, E. & Cresswell, P. Mechanisms of MHC class I--restricted antigen processing. *Annu Rev Immunol* **16**, 323-358 (1998).

139. Lucas, S.M., Rothwell, N.J. & Gibson, R.M. The role of inflammation in CNS injury and disease. *Br J Pharmacol* **147 Suppl 1**, S232-240 (2006).

140. Taubitz, A., Schwarz, M., Eltrich, N., Lindenmeyer, M.T. & Vielhauer, V. Distinct contributions of TNF receptor 1 and 2 to TNF-induced glomerular inflammation in mice. *PLoS One* **8**, e68167 (2013).

141. Malik, A. & Kanneganti, T.D. Inflammasome activation and assembly at a glance. *J Cell Sci* **130**, 3955-3963 (2017).

142. Ito, M., Watanabe, M., Kamiya, H. & Sakurai, M. Non-radioactive assay of natural killer cell-mediated cytotoxicity against cytomegalovirus-infected fibroblasts by DNA fragmentation ELISA. *J Virol Methods* **56**, 77-84 (1996).

143. Kumar, P., Nagarajan, A. & Uchil, P.D. Analysis of Cell Viability by the Lactate Dehydrogenase Assay. *Cold Spring Harb Protoc* **2018**, pdb prot095497 (2018).

144. Kabakov, A.E. & Gabai, V.L. Cell Death and Survival Assays. *Methods Mol Biol* **1709**, 107-127 (2018).

145. Zhang, Y., Chen, X., Gueydan, C. & Han, J. Plasma membrane changes during programmed cell deaths. *Cell Res* **28**, 9-21 (2018).

146. Cummings, B.S. & Schnellmann, R.G. Measurement of cell death in mammalian cells. *Curr Protoc Pharmacol* **Chapter 12**, Unit 12 18 (2004).

147. Hisahara, S., Shoji, S., Okano, H. & Miura, M. ICE/CED-3 family executes oligodendrocyte apoptosis by tumor necrosis factor. *J Neurochem* **69**, 10-20 (1997).

148. Maier, O., Fischer, R., Agresti, C. & Pfizenmaier, K. TNF receptor 2 protects oligodendrocyte progenitor cells against oxidative stress. *Biochem Biophys Res Commun* **440**, 336-341 (2013).

149. Pouly, S., Becher, B., Blain, M. & Antel, J.P. Interferon-gamma modulates human oligodendrocyte susceptibility to Fas-mediated apoptosis. *J Neuropathol Exp Neurol* **59**, 280-286 (2000).

150. Savan, R. Post-transcriptional regulation of interferons and their signaling pathways. *J Interferon Cytokine Res* **34**, 318-329 (2014).

151. Verma, S. *et al.* JC virus induces altered patterns of cellular gene expression: interferon-inducible genes as major transcriptional targets. *Virology* **345**, 457-467 (2006).

152. Torkildsen, O., Brunborg, L.A., Myhr, K.M. & Bo, L. The cuprizone model for demyelination. *Acta Neurol Scand Suppl* **188**, 72-76 (2008).

153. Teo, R.T.Y. *et al.* Impaired Remyelination in a Mouse Model of Huntington Disease. *Mol Neurobiol* (2019).

154. Yu, Q. *et al.* Strain differences in cuprizone induced demyelination. *Cell Biosci* **7**, 59 (2017).

155. Ennaceur, A. Tests of unconditioned anxiety - pitfalls and disappointments. *Physiol Behav* **135**, 55-71 (2014).

156. Ohgomori, T. & Jinno, S. Cuprizone-induced demyelination in the mouse hippocampus is alleviated by phytoestrogen genistein. *Toxicol Appl Pharmacol* **363**, 98-110 (2019).

157. Kipp, M. *et al.* The hippocampal fimbria of cuprizone-treated animals as a structure for studying neuroprotection in multiple sclerosis. *Inflamm Res* **60**, 723-726 (2011).

158. Chang, H. *et al.* Increased central dopaminergic activity might be involved in the behavioral abnormality of cuprizone exposure mice. *Behav Brain Res* **331**, 143-150 (2017).

159. Shao, Y., Peng, H., Huang, Q., Kong, J. & Xu, H. Quetiapine mitigates the neuroinflammation and oligodendrocyte loss in the brain of C57BL/6 mouse following cuprizone exposure for one week. *Eur J Pharmacol* **765**, 249-257 (2015).

160. Christman, S.S., Boutsen, F.R. & Buckingham, H.W. Perseveration and other repetitive verbal behaviors: functional dissociations. *Semin Speech Lang* **25**, 295-307 (2004).

161. Hoeffer, C.A. *et al.* Removal of FKBP12 enhances mTOR-Raptor interactions, LTP, memory, and perseverative/repetitive behavior. *Neuron* **60**, 832-845 (2008).

162. Santiago, O., Guardia, J., Casado, V., Carmona, O. & Arbizu, T. Specificity of frontal dysfunctions in relapsing-remitting multiple sclerosis. *Arch Clin Neuropsychol* **22**, 623-629 (2007).

163. Wingerchuk, D.M. & Weinshenker, B.G. Disease modifying therapies for relapsing multiple sclerosis. *BMJ* **354**, i3518 (2016).

164. Higuera, L., Carlin, C.S. & Anderson, S. Adherence to Disease-Modifying Therapies for Multiple Sclerosis. *J Manag Care Spec Pharm* **22**, 1394-1401 (2016).

165. Poon, K.W.C. *et al.* Lipid biochemical changes detected in normal appearing white matter of chronic multiple sclerosis by spectral coherent Raman imaging. *Chem Sci* **9**, 1586-1595 (2018).

166. Lycette, R.M., Danforth, W.F., Koppel, J.L. & Olwin, J.H. The binding of luxol fast blue ARN by various biological lipids. *Stain Technol* **45**, 155-160 (1970).

167. Halder, A. *et al.* Lipid chain saturation and the cholesterol in the phospholipid membrane affect the spectroscopic properties of lipophilic dye nile red. *Spectrochim Acta A Mol Biomol Spectrosc* **191**, 104-110 (2018).

168. Schmitt, S., Castelvetri, L.C. & Simons, M. Metabolism and functions of lipids in myelin. *Biochim Biophys Acta* **1851**, 999-1005 (2015).

169. Zhu, K. *et al.* Electroacupuncture Promotes Remyelination after Cuprizone Treatment by Enhancing Myelin Debris Clearance. *Front Neurosci* **10**, 613 (2016).

170. Monif, M. *et al.* Interleukin-1beta has trophic effects in microglia and its release is mediated by P2X7R pore. *J Neuroinflammation* **13**, 173 (2016).

171. Chen, K.W. *et al.* The neutrophil NLRC4 inflammasome selectively promotes IL-1beta maturation without pyroptosis during acute Salmonella challenge. *Cell Rep* **8**, 570-582 (2014).

172. Sokolovska, A. *et al.* Activation of caspase-1 by the NLRP3 inflammasome regulates the NADPH oxidase NOX2 to control phagosome function. *Nat Immunol* **14**, 543-553 (2013).

173. Lampron, A. *et al.* Inefficient clearance of myelin debris by microglia impairs remyelinating processes. *J Exp Med* **212**, 481-495 (2015).

174. Benardais, K. *et al.* Cuprizone [bis(cyclohexylidenehydrazide)] is selectively toxic for mature oligodendrocytes. *Neurotox Res* **24**, 244-250 (2013).

175. Lee, S. *et al.* A culture system to study oligodendrocyte myelination processes using engineered nanofibers. *Nat Methods* **9**, 917-922 (2012).

Appendix

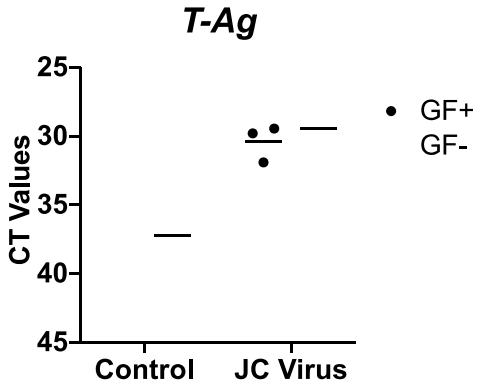

Figure A.1 JC Virus T-Antigen transcript is abundant in PDOs after JC Virus infection. qRT-PCR analysis of *T large antigen* was performed on GF+ (black circles) and GF- (white squares) PDOs infected with 1 MOI of Mad-4 strain of JC Virus for 3 days (n = 3). High levels of T-Ag transcript were detected in PDOs infected with JC virus.

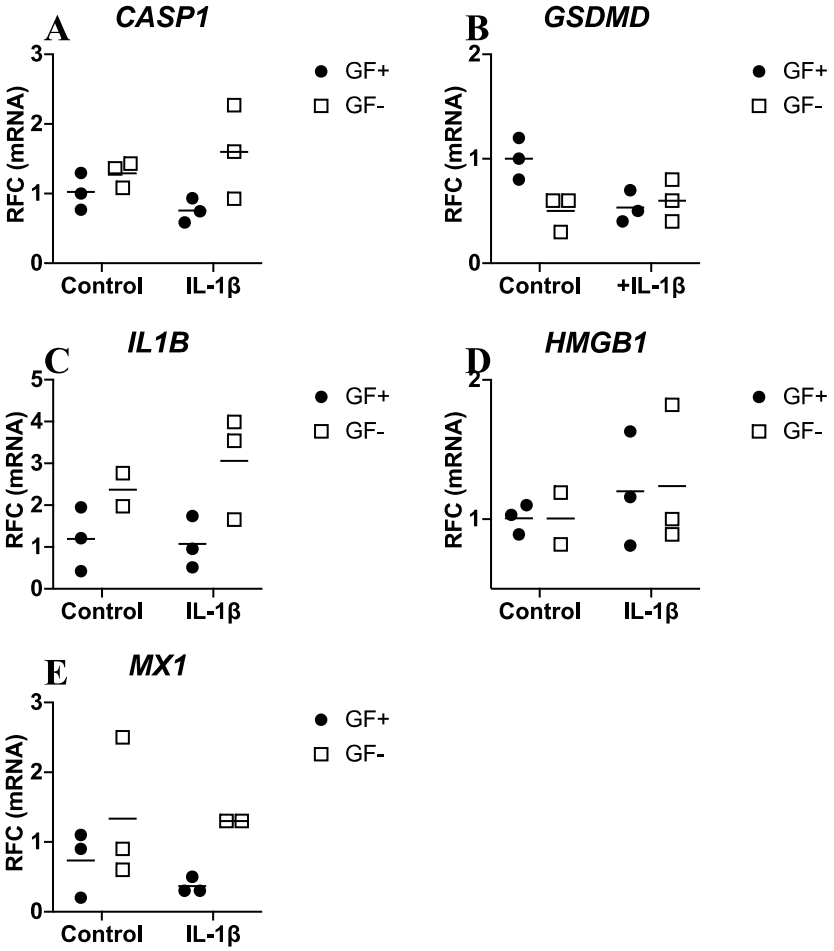

Figure A.2 IL-1β exposure has limited effect on transcriptional changes on PDOs. qRT-PCR analysis of *CASP1* (A), *GSDMD* (B), *IL1B* (C), *HMGB1* (D), and *MX1* (E) were performed on GF+ (black circles) and GF- (white squares) PDOs exposed to 20ng/ml of IL-1β for 24 hours (n = 3). No transcriptional changes in select inflammasome, and antiviral genes were observed in PDOs exposed to IL-1β.

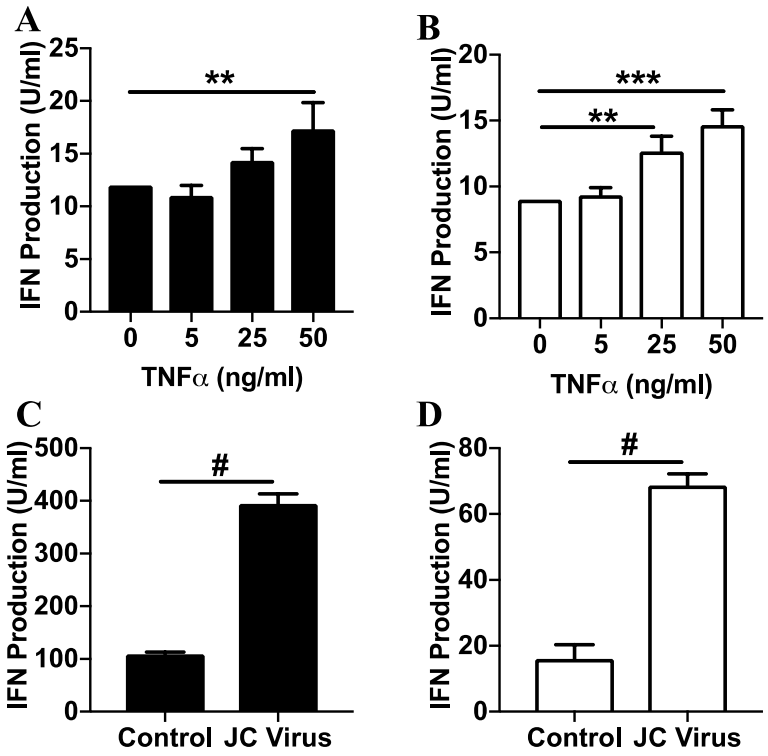

Figure A.3 Type I IFN bioactivity is detected in supernatants from PDOs exposed to TNFα or JC virus. Supernatants of GF+ (black bars) and GF- (white bars) PDOs exposed to increasing concentrations of TNFα for 24 hours (A and B) or injected with 1 MOI of JC virus for 3 days (C and D) were analyzed for Type I IFNs by using a reporter cell line HEK-Blue IFN-α/β (n = 3). Type I IFNs were detected in supernatants of PDOs stimulated with TNFα. **p-value<0.01, ***p-value<0.001 by one-way ANOVA with Tukey's multiple comparison analysis. #p-value<0.0001 by Student t-test.

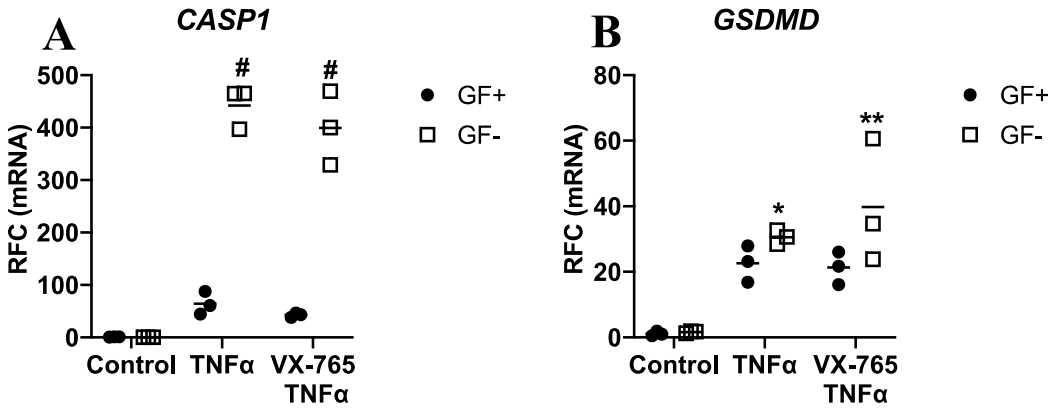

Figure A.4 VX-765 pre-treatment does not prevent TNFα-induced transcript induction in PDOs. qRT-PCR analysis of *CASP1* (A), and *GSDMD* (B) were performed on GF+ (black circles) and GF- (white squares) PDOs exposed to 50ng/ ml TNFα for 24 hours, with or without 4-hour pre-treatment with 50μM VX-765 (n = 3). VX-765 treatment before TNFα had no effect in reducing *CASP1* and *GSDMD* transcript levels. *p-value<0.05, **p-value<0.01, #p-value<0.0001 by two-way ANOVA with Tukey's multiple comparison analysis.

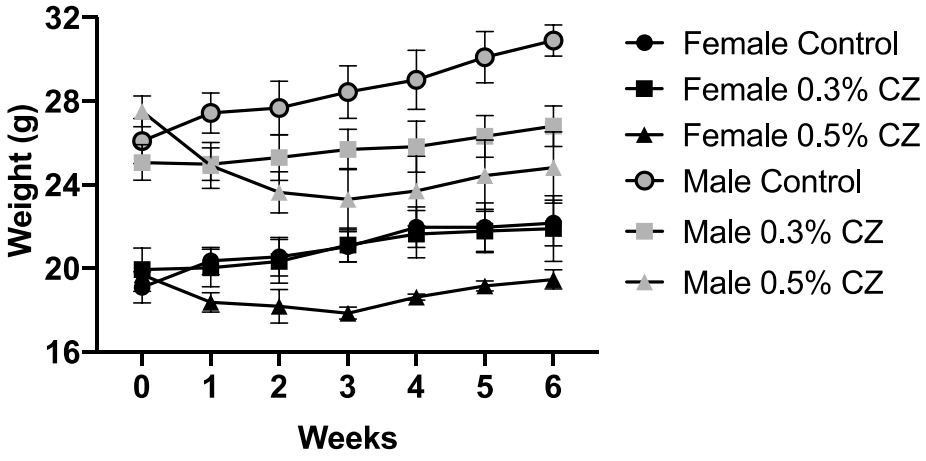

Figure A.5 Mice fed with 0.5% cuprizone diet lost weight compared to mice fed on control or 0.3% diet. Female (black) or male (grey) C57/BL6 mice were either fed with control (circles), 0.3% cuprizone (CZ, boxes), or 0.5% cuprizone (triangles) diet for 6 weeks (n = 6). Weights were recorded once a week for the duration of the experiment. Mice that were fed on 0.5% cuprizone diet lost weight compared to mice that were fed on control diet in both sexes.

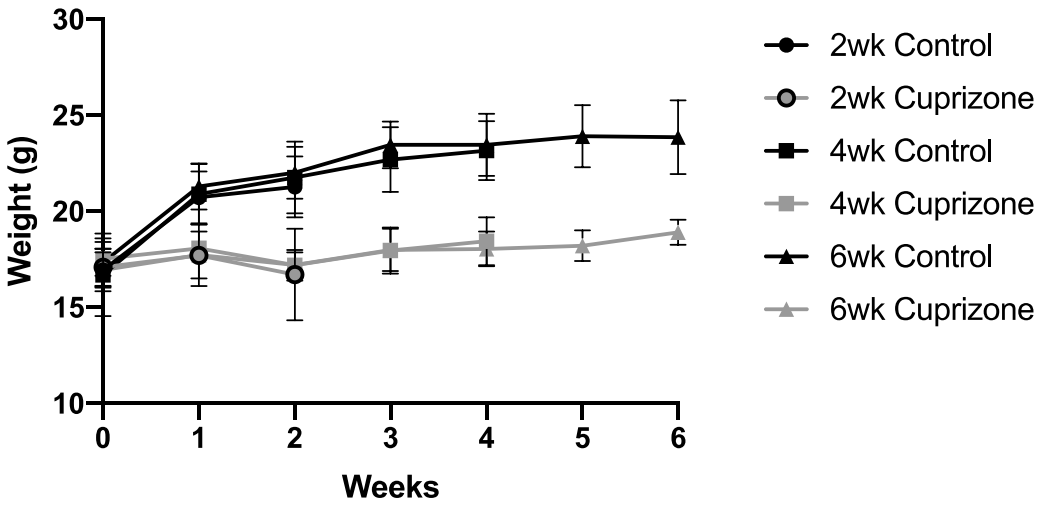

Figure A.6 Mice fed with 0.5% cuprizone diet lost weight compared to mice fed on control diet. Female C57BL/6J mice were fed with 0% (black) or 0.5% (grey) cuprizone (CZ) diet for 2- (circles), 4- (squares), or 6-weeks (triangles) (n = 6). Weights were recorded once a week for the duration of the experiment. Mice that were fed on 0.5% did not gain weight unlike mice that were fed on control diet.

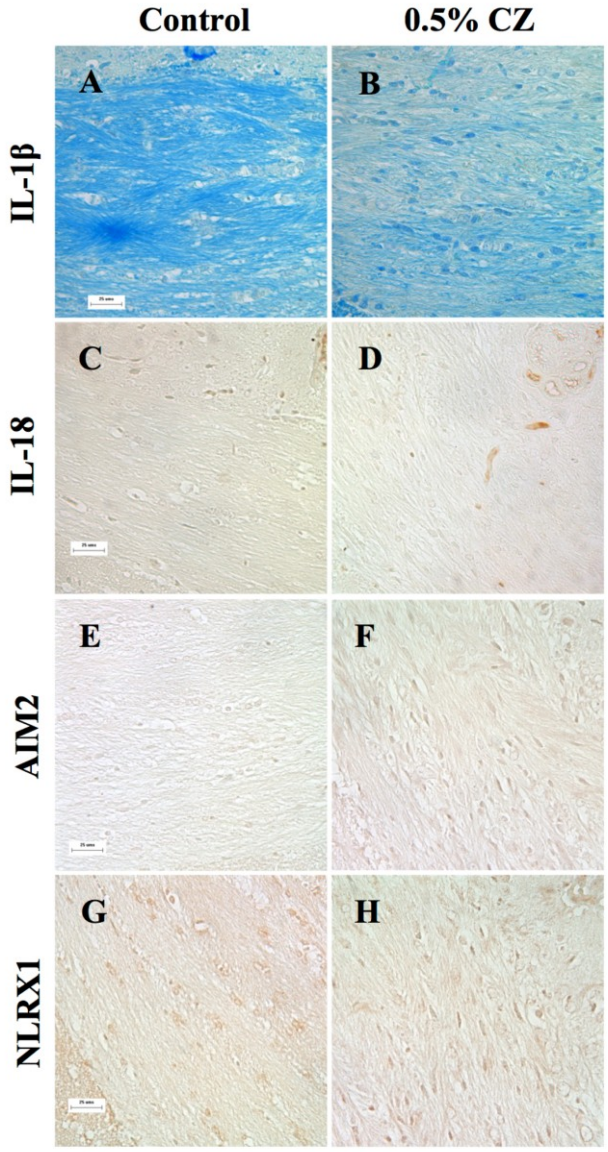

Figure A.7 Other inflammasome-related proteins were not detected in brains of cuprizone-fed mice. Corpus callosum from C57BL/6J mice fed with 0 or 0.5% cuprizone (CZ) diet for 6-weeks were immunolabelled for IL-1β (A, B), IL-18 (C, D), AIM2 (E, F), and NLRX1 (G, H). Images are 40X, size bars are 25μm. Immunolabelling were minimal for all proteins assessed in control and cuprizone-fed mice.

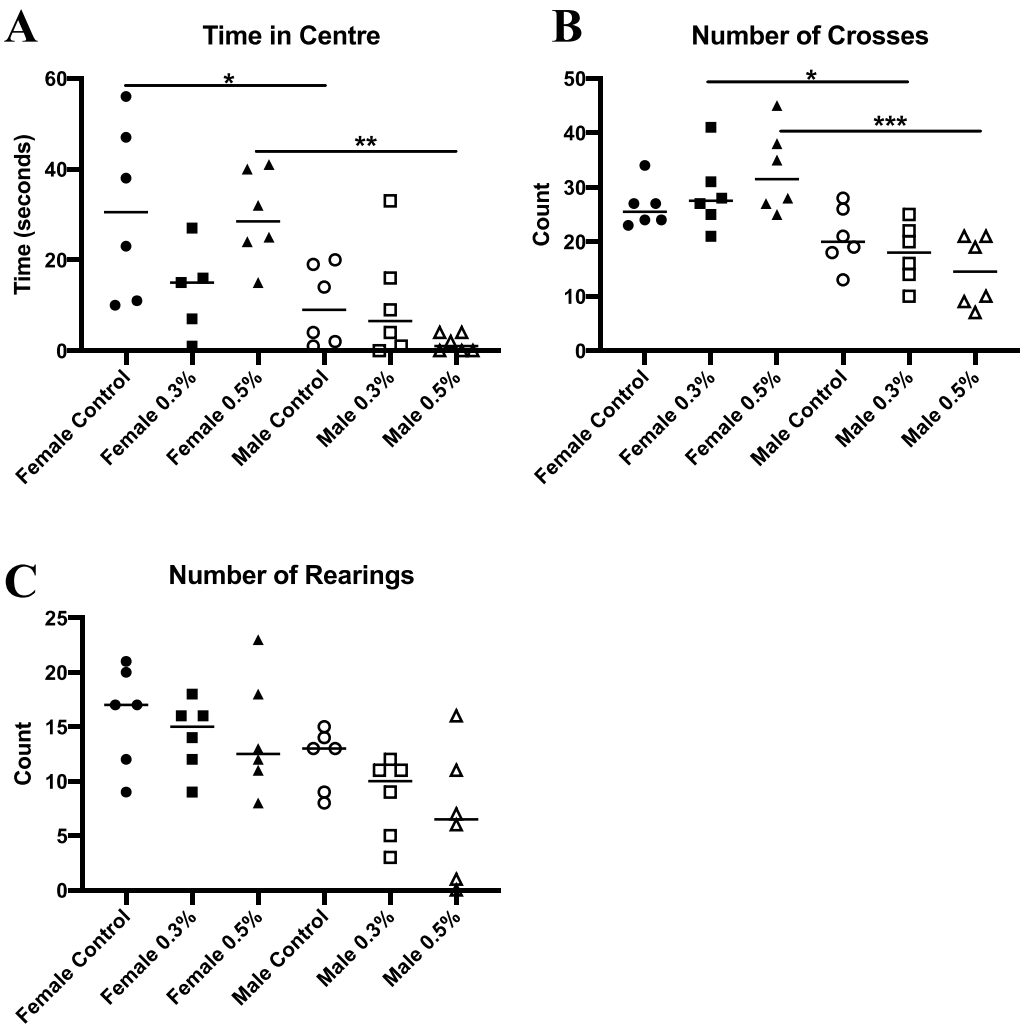

Figure A.8 Cuprizone-fed mice does not display anxiety phenotype. Female and male C57BL/6J mice fed with 0 or 0.3% 0.5% cuprizone (CZ) diet for 6-weeks were assessed by Open Field test (n = 6). Mice were placed in an open field bin for 5 minutes, and the time spent in the centre of open field (A), the number of times it crossed a quadrant of the bin (B), and the number of rearings made (C) were measured. Although differences between female and male mice were observed, there was no effect mediated by cuprizone. *p-value<0.05, **p-value<0.01, ***p-value<0.001 by one-way ANOVA with Tukey's multiple comparison analysis.

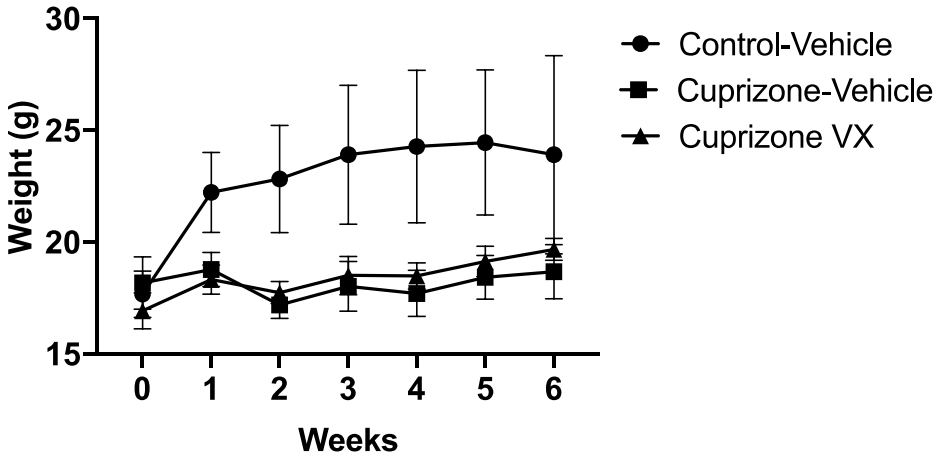

Figure A.9 Cuprizone induced weight loss is not recovered by VX-765 treatment. Female C57BL/6J mice were fed with 0, or 0.5% cuprizone (CZ) diet for 6-weeks, with 4 weeks of daily intranasal VX-765 or vehicle treatment (n = 6). Weights were recorded once a week for the duration of the experiment. VX-765 treatment did not influence the weight loss induced by cuprizone diet.